1995

A study of acoustic emissions in orthogonal cutting operations

Yong-Jin Park
University of Wollongong

A STUDY OF ACOUSTIC EMISSIONS IN ORTHOGONAL CUTTING OPERATIONS

A thesis submitted in fulfilment of the requirements

for the award of the degree of

HONOURS MASTER OF ENGINEERING

from

UNIVERSITY OF WOLLONGONG

by

YONG-JIN PARK

(B.E.)

Department of Mechanical Engineering

JULY 1995

DECLARATION

This is to certify that the research work presented in this thesis was carried out by the author in the Department of Mechanical Engineering of the University of Wollongong, Australia and has not been submitted for a degree to any other university or institution.

Yong-Jin Park

ACKNOWLEDGMENTS

The author is pleased to acknowledge the help of a number of people who assisted in the preparation and publication of this research work. First of all, the author greatly wishes to thank his supervisor, Dr D. P. Saini, for his excellent guidance, supervision and constant encouragement during the period of research study. His insights and understanding of the process have often led me to rethink an old problem with new ideas.

Grateful thanks also go to Mr. J. Abbott, Mr. P. Dunster and Mr. M. Morillas for their operation of machine tools and advice regarding the results of experimental work, and to Mr. Des Jamieson for the valuable assistance in the use of computer hardware and software. The author wishes to extend thanks to all members of the Department of Mechanical Engineering for their assistance and help, and to Dr John Russel and Dr. D. Steel of the Department of Statistical Engineering for helpful discussion and comment.

Appreciation is expressed also to the manager and staff of SAMSUNG Aerospace Pty. Ltd., in Korea, where the author worked for 4 years as a CAD/CAM designer in flexible manufaturing systems, as they greatly assisted me by supplying software packages and the manual.

Finally, to all members of the author's family, especially his wife Yoon-Sook, and two daughters, In-Ah and Jin-Ah whose support and encouragement during this research is deeply appreciated.

ABSTRACT

In recent years, there has been significant growth in the use of unmanned cutting systems, which have been used as a means of improving productivity and quality, reducing product costs and removing the operator from tedious and potentially hazardous environments. Acoustic Emissions (AE) have shown a significant potential for adaptive control processes in many manufacturing areas, especially for the condition monitoring of the tool and workpiece in cutting operations. Attempts have been made to develop some relationship between acoustic emissions and basic cutting parameters in turning operations. These models, however, lack accuracy in the prediction of AE and hence are unsuitable for determination of suitable cutting process parameters and for use in the adaptive control of machining operations. Development of these models is very difficult because the cutting process parameters can affect the geometry as well as the condition of the tool and workpiece.

The objective of this research is to develop mathematical models for the prediction of acoustic emissions with the variation of cutting process parameters, and to study the effects of the cutting process parameters on acoustic emissions and cutting forces generated in Computer Numerical Controlled (CNC) turning operations.

The mathematical models presenting the interrelationship between the cutting process parameters and the AE root mean square (AE_{RMS}) voltage were proposed. The effects of the cutting process parameters on the AE_{RMS} value were investigated using theoretical and empirical mathematical models. An acoustic emission monitor, an oscilloscope and a tool dynamometer were employed for studying the in-process monitoring of cutting tools. A relationship between cutting process parameters and cutting forces was also established to examine the changes in tool condition with the variation of cutting process parameters. A realistic seize ratio and computational

statistical analysis have been employed for improving the accuracy of the developed theoretical models.

The cutting tests were performed under realistic cutting conditions with the workpiece material of ASTM A106-51T and the CVD Tri-phase coated carbide indexable inserts of TPGN 220408. The experimental results were used to verify the validity of the theoretical and empirical models. With the help of a standard statistical package program (SAS) using an IBM-compatible PC, computational statistical analysis was undertaken for developing the regression analysis models of acoustic emissions based on the experimental data. A satisfactory agreement between the AE_{RMS} values predicted by the theoretical and empirical mathematical models and those experimentally measured has been observed.

TABLE OF CONTENTS

LIST OF FIGURES

LIST OF TABLES

NOMENCLATURE

r	chip-thickness ratio
ρ	dislocation density of the undeformed workpiece material
m	mass of workpiece material
U	Volume of work material
t	uncut chip thickness or feed rate (orthogonal cutting)
b	the width of cut or the width of workpiece
d	depth of cut
φ	cutting edge angle
r_n	cutting tool corner radius
ρ_c	dislocation density of the deformed workpiece material
m_c	the mass of the deformed chip
U_c	the volume of chip
t_c	deformed chip thickness
b_c	the width of the deformed chip
l	natural chip contact length on the tool rake face
l_c	the length of the deformed chip
l_{cn}	controlled chip contact length, $l_{cn} = \frac{l}{l_c}$
α	tool rake angle
ϕ	shear plane angle
Δy	the thickness of the shear zone or the layer distance of successive slip planes
ΔS	the deformed distance by the cutting forces
V	cutting velocity of the tool
V_c	chip velocity that moves along the cutting tool
V_s	the shear velocity that moves along the shear plane
ρ_d	dislocation density

b_v	magnitude of the burgers vector
l_{ad}	the average distance of dislocation
γ	shear strain
$\dot{\gamma}$	strain rate
$\dot{\gamma}_{av}$	average strain rate
V_{ad}	average dislocation velocity
β	friction angle
μ_{tc}	friction coefficient in the tool-chip interface
F_s	shear force in the shear plane
F_n	normal force on the shear zone
F	friction force on the tool-chip interface
N	normal force on the tool-chip interface
F_c	cutting force in the shear zone and tool-chip interface
F_t	tangential force in the shear zone and tool-chip interface
F_{tf}	total frictional force in the tool-chip interface
F_{st}	force generated on the sticking region in the tool-chip interface
F_{sl}	force generated on the sliding region in the tool-chip interface
R_s	resultant force on the shear plane
R_{tc}	resultant force on the tool-chip interface
τ_s	shear stress in the shear plane
τ_a	average dynamic shear stress in plastic deformation zones during the metal removing process (or called shear strength of a workpiece)
τ_{st}	frictional stress on the sticking region in the chip-tool interface
τ_{sl}	frictional stress on the sliding region in the chip-tool interface
τ_{fw}	the applied frictional stress between the tool flank and workpiece surface interface
A_c	an undeformed area of cut ($A_c = bt$)
A_s	a cross-sectional area on a shear plane

A_c	the area of cut at shear angle, ϕ
σ_f	normal stress on the tool rake face
$\sigma_{\max}$	maximum normal stress at the tool-tip area
x	the distance from the point at which the chip leaves the rake face of the tool to the end of the cutting tool edge
n	parabolic constant (the exponent of the seize rate of two regions divided on the tool face)
l_{st}	the contact length of the sticking region in the tool rake face
l_{sl}	the contact length of the sliding region in the tool rake face
A_{tc}	the contact area of the chip-tool interface ($A_{tc}=b_c l$)
V_{fw}	sliding speed between the tool flank and workpiece surface
$A_{r_{fw}}$	the real area of sliding contact interface between the tool flank and workpiece surface
A_a	the apparent area of sliding contact interface between the tool flank and workpiece surface
P_a	the apparent contact pressure
μ_{fw}	the coefficient of sliding friction in the tertiary zone
η	the ratio of the real and apparent contact area between the tool flank and workpiece surface
$F_{c_{fw}}$	cutting force between the tool flank and workpiece surface
$F_{t_{fw}}$	tangential force between the tool flank and workpiece surface
R_{fw}	resultant force between the tool flank and workpiece surface
R_t	total resultant force generated in the tool flank and workpiece interface
l_{fw}	the average wear length of the tool-flank (VB)
E_t	total energy power consumption rate generated per unit time
E_s	the energy rate of shear deformation per unit time
E_{tc}	the energy rate of the sticking and sliding deformation per unit time

E_{fw}	the energy rate of the sliding deformation per unit time
AE_{RMS}	the RMS of acoustic emission signals
AE_{RS}	digitised raw AE signal
AE_C	AE generated from the cutting operation
R_S	the transmission response of sensor location
AE_N	background noise during cutting
V_{RMS}	the AE signal voltage of root mean square
$V_{\max}$	the maximum voltage value of AE signals
k	damping constant
ϖ	angular frequency ($\varpi = 2\pi f_a$)
f_a	being measured frequency in the oscilloscope per unit time($f_a = \frac{1}{\Delta T}$)
V_{th}	threshold voltage
t_{lp}	instant time as the last peak reaches the established threshold value
N_c	the number of counts measured for a single event which is over the threshold value
ΔE	energy expenditure
ΔT	the period of interval time
C	the constant of proportionality
C_1	AE signal attenuation constant corresponding to the signal transmission losses in the primary deformation zone
C_2	AE signal attenuation constant corresponding to the signal transmission losses in the secondary deformation zone
C_3	AE signal attenuation constant corresponding to the signal transmission losses in the tertiary deformation zones
m	the proportionality constant of the tool-chip contact length
$(V_{RMS})_{Expt}$	the measured RMS voltage of acoustic emission signals
$(V_{RMS})_{Theo}$	the computed RMS voltage of acoustic emission signals
$(V_{RMS})_{ave}$	the average RMS voltage of acoustic emission signals

$(V_{RMS})_i$	initial voltage obtained at the initial cutting stage using fresh tools
$(F_c)_{ave}$	the average cutting force in turning operations
$(F_c)_i$	initial cutting force obtained at the initial cutting stage using fresh tools
ε	the gradient of the plotted function
VB	the wear land of tool flank
Y	dependent variable (response parameter)
K	statistically fitted constant
a	statistically fitted constant
b	statistically fitted constant
c	statistically fitted constant
D	offset value
F_x	cutting force for an empirical model fit
F_y	tangential force for an empirical model fit
F_z	radial force for an empirical model fit
a_1	statistically fitted constant
a_2	statistically fitted constant
a_3	statistically fitted constant
a_4	statistically fitted constant
a_5	statistically fitted constant
a_6	statistically fitted constant
a_7	statistically fitted constant
T	machining time in seconds
b_1	statistically fitted constant
b_2	statistically fitted constant
b_3	statistically fitted constant
b_4	statistically fitted constant

$V_{RMS(Log)}$ the RMS voltage of acoustic emission signals for a curvilinear regression analysis

$V_{RMS(Pol)}$ the RMS voltage of acoustic emission signals for a polynomial regression analysis

$V_{RMS(Lin)}$ the RMS voltage of acoustic emission signals for a linear regression analysis

PUBLICATIONS

I. Papers in International Conference Proceedings and Journals :

[1] Y. J. Park and D. P. Saini, *"A New Model for Prediction of Acoustic Emissions in Orthogonal Cutting Operations"*, 3rd International Conference on Computer Integrated Manufacturing, **ICCM/AUTOFACT-ASIA'95**, July 1995, pp. 1077-1088.

[2] Y. J. Park and D. P. Saini, *"A Quantitative Model of Acoustic Emissions in Orthogonal Cutting Operations"*, Accepted for Publication in the **Journal of Materials Proceeding Technology**.

II. Papers to be Submitted :

[3] Y. J. Park and D. P. Saini, *"A Study of Tool Flank Wear and Acoustic Emissions in Orthogonal Cutting Operations"*, to be Submitted to **International Journal of Machine Tools and Manufacture**.

[4] Y. J. Park and D. P. Saini, *"Empirical Modelling of Acoustic Emissions in Two-Dimensional Cutting Operations"*, to be Submitted to **Wear**.

CHAPTER ONE

INTRODUCTION

1.1 MOTIVATION

The fast increasing competition for selling manufactured products on global markets has resulted in greater demands on product quality and production costs. The shortage of skilled labour, the level of safety requirements and the need for product liability together with the increasing demand for metal products, have brought a need for the development of an automated cutting process to cope with many of the present problems in turning operations. The untended manufacturing operations including CNC machining, need to operate at optimum efficiency, necessitating on-line tool condition monitoring and improved adaptive control. Sensing the condition of tools and recognising when they require changing, is an important aspect of unmanned machining operations.

In recent decades, several effective and reliable machining processes have developed using modern computerised cutting machines such as computer numeric control machines. However, totally adequate process control systems have not been developed, due to a lack of intelligent sensors and mathematical models that correlate the variation of cutting process parameters, the cutting geometry and the AE_{RMS} output for the automated cutting process. Researchers have recently recognised the

effectiveness of acoustic emission (AE), for tool condition monitoring in machining operations, but not much effort has been directed towards understanding the generation of AE from various sources in those operations.

The development of a mathematical model which can be programmed readily and fed to the CNC machine is essential, to make effective use of the automated cutting process. It should have a high degree of reliability in predicting the acoustic emission signal, which is closely related to cutting variables such as the tool and workpiece material, and the product quality determined by the condition of the cutting tool edge. Such a model should also be able to apply to a wide range of cutting process parameters. The basic cutting process parameters such as feed rate, cutting speed, rake angle, flank wear land and cut width are interdependent, so one parameter affects the others. The relationships between the cutting process parameters and the generated AE_{RMS} voltage are very complex.

A feedback control in the machining operation should be able to work on the basis of a practical mathematical model, and therefore the machining operation system should be composed of three principal components :

(1) transducers which produce a signal for the purpose of detecting or measuring the condition of the cutting process,

(2) a mathematical process model which analyses the relationship between the cutting process parameters and the cutting geometry,

(3) computer control of machines and systems which evaluates the sensor data and changes the best fit of cutting process parameters as recognised by the abnormalities process.

This research mainly concentrates on the study of the generation of AE_{RMS} voltages in the variation of cutting process parameters during machining operations. The development of new models and the methodology for the derivation of the equations

will play an important role in the improvement of the unmanned cutting system. In the recent past several techniques for tool wear detection have been proposed and evaluated to optimise cutting processes, from the theoretical mathematical models based on physical principles and empirical mathematical models based on experiments. None of these approaches however, meets the requirements of an ideal technique. Each has its own advantages and limitations. This study presents a review of the various sources of AE and then attempts to develop new theoretical and empirical models for prediction of AE during two-dimensional cutting operations. The developed models have also been verified with the AE generated under realistic cutting operations.

1.2 SCOPE OF THE RESEARCH WORK

In-process sensing systems and adaptive control in automated cutting operations which can promptly rectify process abnormalities and failures are highly significant to the product quality and in determining the extent of the deterioration of the cutting tool.

The major part of this research work is devoted to developing the analytical and empirical mathematical models that correlate the basic cutting process variables and the generated AE signal that is proportional to the measured quantity.

To depict a blueprint for advanced metal cutting, the research will be thoroughly investigated and improved in the following aspects :

1. The major limitations in irreversible deformation zones (called primary, secondary and tertiary deformation zones) are generated as soon as the cutting tool engages the workpiece material. The limitations such as tool wear and AE signal losses in each cutting zone, are examined for better understanding, and for improving the knowledge base of the cutting mechanism.

2. The concept of a tool condition monitoring method using the acoustic emission technique is identified by interrelationships between the condition of the tool in each cutting zone, the fundamental cutting process parameters and the variation of AE_{RMS} voltages.
3. The geometrical and empirical theories are investigated for the development of theoretical models. On the basis of these theories, new theoretical mathematical models are established for the prediction of acoustic emission signals in orthogonal cutting operations. With the help of the computational work, the AE signal attenuation constants in each cutting zone which have not been found a solution in the previous developed theoretical models are statistically fitted.
4. The advanced empirical mathematical models which study the influence of the basic cutting process parameters on the detected AE_{RMS} outputs, are developed by experimental results using both fresh tools and worn tools. For determination of the most effective cutting process parameter, the effective interactions of each cutting process parameter are investigated using multiple regression analysis techniques with a standard statistical package program (SAS).
5. New mathematical models are compared to the published theoretical and empirical formulae relating cutting process parameters and the AE_{RMS} voltage produced during orthogonal cutting operations.
6. The validity of the developed models verified by showing a close agreement in comparison of the experimental results and the predicted values calculated using the new models.

1.3 SUMMARY OF CONTRIBUTIONS

The approaches to the theoretical and practical work which form part of this thesis, as listed below, are considered to have had an important bearing on the major results and conclusions developed :

1. Development of fundamental mathematical models for prediction of theoretical AE_{RMS} function value. (Chapter Three)
2. Development of theoretical mathematical models which can predict the AE_{RMS} voltage level according to the variation of basic cutting process parameters. (Chapter Four)
3. Development of the seize ratio model based on the definition of parabolic constant and empirical theories, which can predict the ratio of the sticking and sliding zones' contact length in the tool-chip interface. (Chapter Four)
4. Estimation of AE signal attenuation values generated in plastic deformation zones using the statistical analysis techniques. (Chapter Four)
5. Development of empirical mathematical models for prediction of the AE_{RMS} voltage level using a detailed experimental study on the effects of interaction of cutting process parameters. (Chapter Five)
6. Determination of the best equation in the three types of empirical mathematical models developed using multiple regression analysis techniques. (Chapter Five)

1.4 ORGANISATION OF THE THESIS

The thesis begins with a general introduction which discusses the present problems and some methods of improvements in machining operations. It is divided into 6 chapters, each consisting of an introduction and a number of sections. Each of the chapters contains a large number of themes.

Chapter One presents the outline of the thesis describing the importance, scope and contributions of the current research work.

Chapter Two deals with a comprehensive literature survey relating all aspects of the basic cutting operation, sensor and sensing methods for control of the cutting process, acoustic emission techniques and AE models representing the relationship between the

cutting mechanism and the major sources of AE signal, as well as a review of previous studies on theoretical and experimental techniques accomplished by a number of researchers.

Chapter Three highlights the application of theoretical and empirical theories for development of analytical models which can predict the plastic deformation energy converted to acoustic emission energy in orthogonal cutting operations. The development of new theoretical models is based on physical principles and experimental results, for better understanding the relationships between cutting process parameters, cutting geometry and the cutting mechanism.

Chapter Four introduces the analysis of acoustic emission signals using the RMS voltage technique and presents the development of theoretical models which are derived from the quantitative relationship between the energy rate consumed in various cutting zones and the AE_{RMS} voltage. The deviation of a realistic seize ratio and parabolic constant in the tool-chip interface is constructed for improving the accuracy of the developed models. The attenuation values of acoustic emission signals generated in various cutting zones are expressed by the results of computational work. In addition, experimental results which point out the effects of the variation of basic cutting process parameters on the AE_{RMS} voltage will be discussed. The experimental results are critically compared with previous researchers' experimental outputs, and present the important trends and differences in various outputs which are obtained from the experimental tests. The verification of the validity of the developed theoretical models is based on the experimental investigations.

Chapter Five is concerned with the experimental procedures and aspects in the development of empirical mathematical models. New empirical models such as curvilinear, polynomial and linear models are proposed, to be formed by statistically fitted constants, which are computed by using multiple regression analysis techniques.

The effects of interaction between the cutting process parameters and the AE_{RMS} outputs, is discussed using the results of the polynomial regression analysis technique.

Chapter Six summaries the conclusions of the research work and recommends directions for further study.

CHAPTER TWO

LITERATURE SURVEY

2.1 INTRODUCTION

The yearly cost associated with material removal operations in the USA has been estimated at about 10 percent of the gross national product [1]. Adaptive control in manufacturing processes plays a major role in effecting reduced cost and producing a higher product quality. For optimisation of cutting processes, present methods of production must be improved, in order to establish radically new production methods. However, it is impossible to improve the feedback control in machining operations without a basic knowledge of the cutting mechanism and the concepts of automated control.

In this chapter, the basic mechanics of the machining process are first discussed so as to properly understand the cutting mechanism as it occurres in various cutting zones. Variables such as chip ratio, shear angle, shear strain, strain rate, and tool-chip contact length are identified, and the study of acoustic emissions, one of the promising sensing and adaptive control techniques in the cutting process, is presented. A comprehensive literature survey, with the specific topics covering the fundamentals of the machining process, sensing and adaptive control for the machining process, and

acoustic emissions in the machining process, are presented in this chapter. The basic definitions and concepts of work carried out and published by many different researchers will be reported and critically examined.

2.2 FUNDAMENTALS OF THE MACHINING PROCESS

2.2.1 History of the Machining Process

Early studies in the field of metal cutting mechanics were made to explain the fundamentals of the cutting process by Zovorykin in the nineteenth century [2]. Some of this early work has been reviewed and the basic theories by Finnie in 1956 [3] have been pointed out. However, active studies for the major mechanics of metal cutting which have resulted in present day understanding of the area, were started after the work of Piispanen [4], Ernst [5], Merchant [6], Zorev [7] and Shaw [8].

The previous approach has been extensively used in metal cutting fields for development of the ability to apply fundamental concepts and the improvement of cutting techniques. The wide scope of material removal is still an area of very intense and interesting study in that field, together with its relation to other fields of science and engineering. The current direction of research in machining processes is in the development of predictive machining theories in knowledge base systems and condition monitoring techniques for unmanned cutting operations.

2.2.2 Cutting Models of the Machining Process

The fundamental nature of metal deformation and the geometry of machining need to be explained so as to better understand the cutting mechanism. Machining geometry is generally divided into two cutting operations : orthogonal (two-dimensional) cutting and oblique (three-dimensional) cutting. Figure 2.1 shows the two types of cutting

models. In research over the past few years, orthogonal cutting models [5-10] have been used so that the oblique cutting model may be understood more easily without any complication of the three dimensions. Orthogonal cutting is represented as an ideal cutting process because it is more useful in improving and understanding the basic mechanism of the metal removal process. As can be seen in Figure 2.1, the orthogonal geometry that has a single cutting tool edge, is perpendicular to the feed direction of the workpiece turning by spindle and parallel to the workpiece surface, and the cutting force is in the same direction as the cutting velocity. The oblique cutting model [11-14], which typifies the most common cutting method being employed in industry, is a real cutting process since it can alter the chip flow direction from cutting zones according to the extent of the inclined angle.

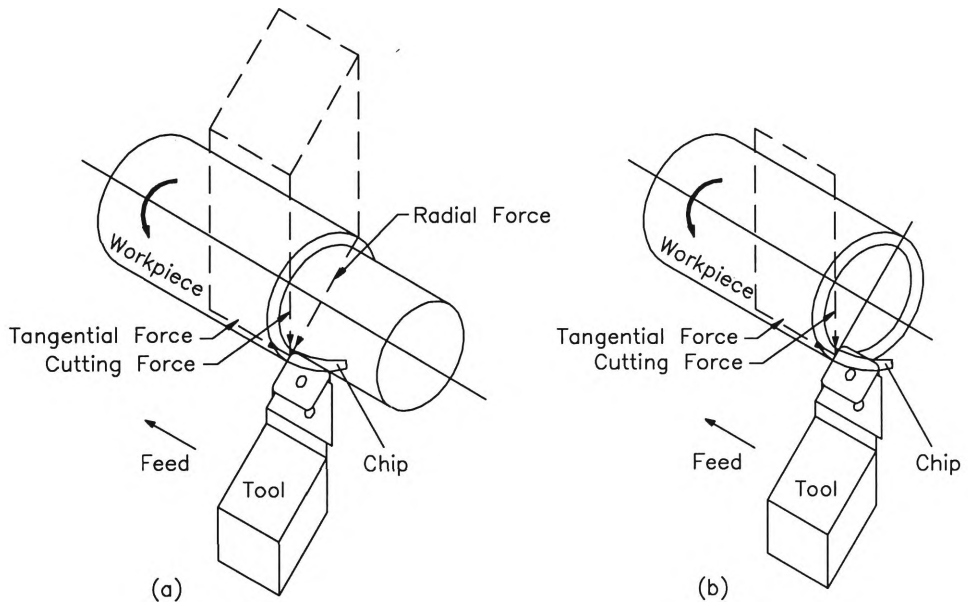

Figure 2.1 Comparison of oblique and orthogonal machining geometry

(a) oblique cutting (b) orthogonal cutting

2.2.3 Plastic Deformation in Metal Cutting Zones

Plastic deformation in the workpiece material is due to the slip and twining mechanisms on the grain boundaries in micro-areas with high stress around the plasticity limit of the metal structure [15]. It results from the movement of vacancies

and dislocations in the metal structure and the heat generated by the friction between the cutting tool edge and the workpiece material, or between the tool-flank and the workpiece surface being machined. Dislocation occurs by the action of tensile stress and causes the growth of a crack in the workpiece material [16]. As shown in Figure 2.2, all plastic deformations in the radial compression area are first produced by elastic compressions, which occur at a distance fairly remote from the cutting tool edge. After that, they are changed into plastic compressions by the cutting forces as the workpiece material approaches the cutting edge of the tool [17]. The elastic and plastic deformation boundaries of all workpiece materials are absolutely related to the inherent material hardness of the workpiece.

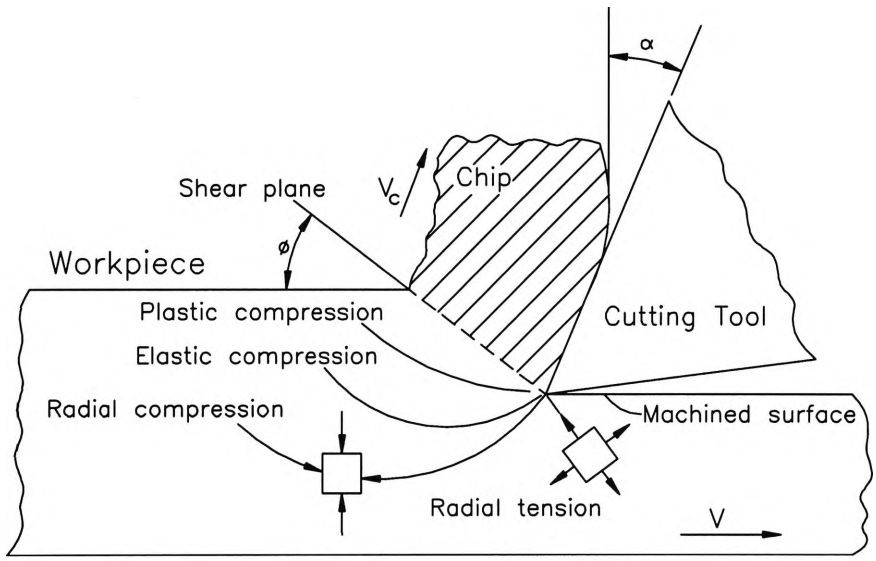

Fig. 2.2 The state of plastic deformation zones in metal cutting.

During the metal removal process, localised plastic deformation between the work material and the cutting tool edge is typically composed of three basic deformation zones : primary, secondary and tertiary. Without exception, each deformation zone begins with chip formation, the deformation zone depending largely on the property of workpiece material being machined, and the cutting process parameters being used.

The nature of the primary deformation zone, called shear deformation zone or shear plane, is closely related to the situation in which it occurs as a result of the fracture of the workpiece material, when the workpiece material is compressed by the cutting tool edge. The chip formation is especially affected by shear direction and shear stress. These have an effect on heating and straining of the material and the chip, both of which inevitably result from dislocation of the metal structure [18].

The secondary deformation zone, is separated into two deformation regions, in terms of the sticking and sliding of the chip against the cutting tool as the chip passes over the tool rake face [19]. While the chip moves along the tool face from the cutting tool edge to the point at which the chip leaves the tool face, sticking and sliding between the chip and the tool face become one of the major sources of crater wear. The influence of cutting temperature generated in the sticking and sliding zones accelerates the wear of tool flank by heat transformation in the tool flank and workpiece interface [20].

The tertiary deformation zone, known as the tool flank and workpiece surface interface, is defined by the rubbing action between the tool flank and the surface of the workpiece. Sliding friction between the two contact faces weakens the cutting tool edge, causing deterioration of the workpiece surfaces [21], and increasing the cutting forces and cutting temperatures [22]. The measurement of wear land on tool flank is of great concern since the tool life is determined by the amount of flank wear.

2.2.4 Important Variables in the Machining Process

Various factors influencing the machining process are generally classified into two groups : -

(1) **independent input variables** such as cutting process parameters, tool and workpiece material and their condition, tool geometry (ie, rake angle, clearance

angle, nose radius, and its surface characteristics), cutting parameters (ie, feed rate or depth of cut, cutting speed, and width of cut), workpiece temperature, cutting fluid and the characteristics of the machine tool (ie, stiffness, power and damping),

(2) **dependent output variables** such as the shear plane angle, cutting forces, stresses, energy dissipated in the cutting process, natural tool-chip contact length, tool temperature rise, wear of the tool, the surface finish and surface texture, tool life, chip formation and tool stability. The establishment of quantitative relationships between all the independent input and dependent output variables is an important requirement for complete analysis of the cutting operation.

The most important factors in metal cutting relative to the development of mathematical models for the condition monitoring of the cutting process, are the shear strain rate [23], the shear angle created on the shear plane and the tool-chip contact length generated with chip formation in the tool-chip interface [24]. The importance and effect of the shear strain rate, shear plane angle and tool-chip contact length have been proven through the analysis of the developed theoretical equations and practical cutting tests.

A survey of the metal cutting literature investigates the several equations published on the shear strain and strain rate, chip-thickness ratio, shear plane angle and tool-chip contact length, these being determined under the reasonable assumptions associated with metal deformation zones. Additionaly, the determined equations have been applied to the development of theoretical models, due to the current lack of a suitable and reliable theoretical approach in order to optimise the automated cutting operation.

2.2.5 *Chip-Thickness Ratio in Cutting Zones*

The chip-thickness ratio (r) is basically determined by the undeformed chip thickness (t) and deformed chip thickness (t_c). The definition of the chip thickness ratio is based on a number of assumptions, including that : -

- the shear process is a plane.
- the cutting edge is perfectly sharp and straight.
- there is friction between the tool flank and the workpiece surface due to the assumption that the deformed chips have no side flow, (namely, $b = b_c$).
- the cutting velocity and depth of cut are constant.
- a continuous chip is produced without built-up edge.

On the assumption that the dislocation density (ρ) of workpiece material does not change while the metal is removed, the volume of the unit area and the chip thickness ratio can be defined from the relationship between the volume of the chip and the volume of the workpiece [5,6] :

$$r = \frac{t}{t_c} = \frac{l_c}{l} = \frac{b}{b_c} = \frac{V_c}{V} \qquad \text{(from } \rho = \rho_c \text{, viz. } btl = b_c t_c l_c\text{)} \qquad (2.1)$$

However, to measure a deformed chip thickness is actually difficult because of the roughness on the back surface of the chip. Derivation of theoretical equations for the realistic chip thickness plays a valuable role in prediction of the chip thickness ratio which can affect the shear angle in the shear zone. The equation of chip thickness which can be employed in the three-dimensional cutting operation has been proposed, using the relationships of the feed rate, depth of cut, cutting edge angle and nose radius of the cutting tool by T. Hodgson [25].

$$t_c = fd\{\sin\varphi[d - r_n(1-\cos\varphi)] + \frac{\pi\varphi r_n}{180} + \frac{f}{2}\} \qquad (2.2)$$

The formula for prediction of chip thickness in two-dimensional cutting operations was constructed in this research work using the relationships between the deformed chip thickness and the basic input parameters such as feed rate, rake angle and cutting speed. As described later in chapter 5, a detailed derivation method of the chip thickness equation for the orthogonal cutting can be expressed using the regression analysis technique as follows :

$$t_c = 140 f^{0.7776} (90 + \alpha)^{-0.6612} V^{-0.2506} \tag{2.3}$$

From the relationship between the geometry of the cutting tool and deformed chip thickness, the ratio of chip thickness could be expressed as a function of a shear angle and a rake angle, as formula (2.4) derived using the mechanism in Figure 2.3 [5,6].

$$r = \frac{t}{t_c} = \frac{AB \sin \phi}{AB \cos(\phi - \alpha)} \tag{2.4}$$

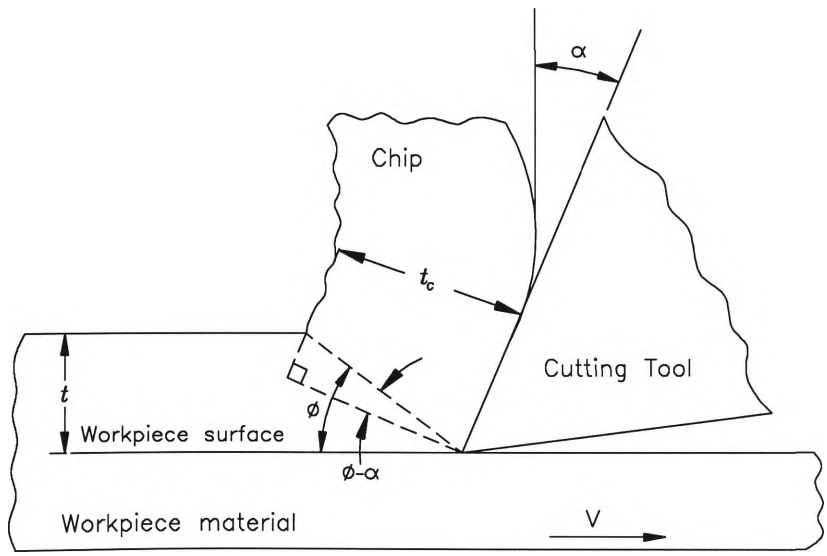

Figure 2.3 Relationship between chip thickness ratio(r) and shear angle(ϕ)

De Chiffre [26], who developed the chip thickness ratio formula, considered the influence of the crater wear in the tool-chip interface by the effect of the controlled chip contact length and rake angle.

$$r = \frac{t}{t_c} = (1 + l_{cn} \cos\alpha)^{-\frac{1}{2}} \tag{2.5}$$

2.2.6 Shear Strain and Strain Rate

The amount of plastic deformation in the shear deformation zone is depicted as a card model in Figure 2.4, and the chip which undergoes the shear strain (γ) is closely related to the shear angle and rake angle [4-6].

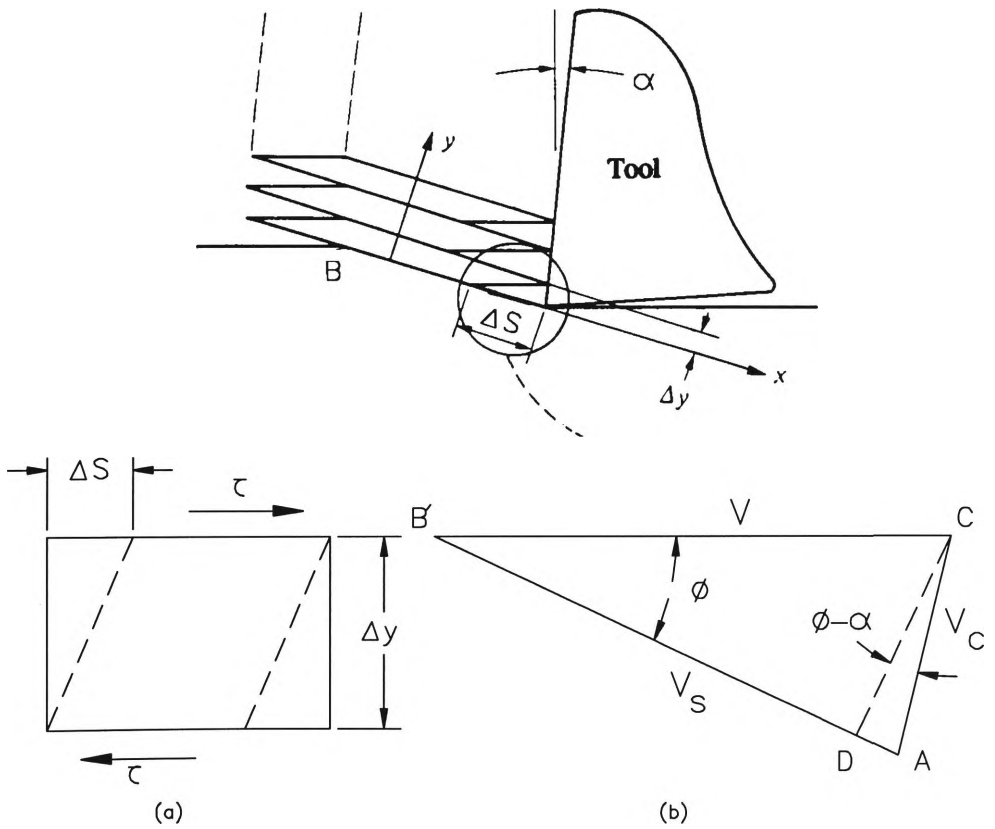

Figure 2.4 Formation of shear strain.

(a) General shear strain. (b) Shear strain in cutting.

The measurement of a large plastic deformation in a shear plane is estimated from the shear strain which is directly formed as soon as the cutting tool edge approaches the workpiece material. As shown in Figure 2.4 (b), the geometry of the shear strain is defined from the sum and difference equations of the sine and cosine function as given by :

$$\gamma = \frac{\Delta S}{\Delta y} = \frac{AD}{CD} + \frac{DB'}{CD} = \tan(\phi - \alpha) + \cot\phi = \frac{\cos\alpha}{\sin\phi\cos(\phi - \alpha)} \tag{2.6}$$

The relationship between the strain rate and three velocity vectors which takes place during the metal removal process is predicted from the principles of kinematics as presented in Figure 2.5. The chip velocity (V_c) and the shear velocity (V_s) can be expressed by substituting the chip thickness ratio and the cutting velocity, respectively [5,6].

$$V_c = \frac{\sin\phi}{\cos(\phi - \alpha)} V = rV \tag{2.7}$$

$$V_s = \frac{\cos\alpha}{\cos(\phi - \alpha)} V = \gamma \sin\phi V \tag{2.8}$$

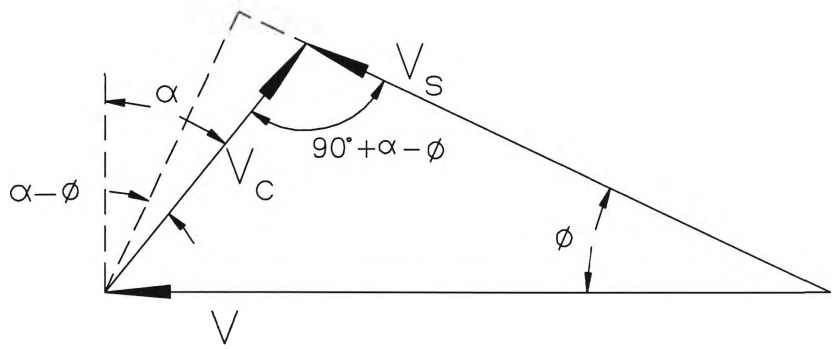

Figure 2.5 Relationship of velocities and angles in the shear zone and tool-chip interface.

The rate of shear strain (γ) in cutting, can be extended by three types of parameters, $\gamma = \psi(\Delta y, \Delta S, \Delta T)$: the deformed distance (ΔS) of the workpiece material along the

shear plane per the elapsed time(ΔT) and the thickness(Δy) of a slip plane in the shear zone. The shear strain rate is defined as a function of cutting speed and the thickness of shear layer, $\dot{\gamma} = \psi(V, \Delta y)$ [27].

$$\dot{\gamma} = \frac{\Delta S}{\Delta y} \cdot \frac{1}{\Delta T} = \frac{V_s}{\Delta y} or \frac{\cos\alpha}{\cos(\phi - \alpha)} \cdot \frac{V}{\Delta y} \tag{2.9}$$

As in the experiment of Kececioglu [28], the reasonable mean value for Δy generally takes the range of 0.0025 mm< Δy <0.025 mm for carbon steel.

Turkovich [29] presented that the rate of the shear strain was as a function of the dislocation rate generated by the alteration rate of the dislocation density of workpiece material.

$$\dot{\gamma} = \rho_d b_v l_{ad} \tag{2.10}$$

Cottrel [15], also described the average strain rate as a function of the dislocation density, magnitude of the bugers vector and the average dislocation velocity.

$$\dot{\gamma}_{av} = \rho_d b_v V_{ad} \tag{2.12}$$

As briefly discussed for the strain and the strain rate, among the developed formulae, the most useful and simplified equations are the equations of (2.6) and (2.9) analysed using the fundamental theory of the metal structure deformation .

2.2.7 Shear Plane and Shear Plane Angle

Piispanen [4] proposed a shear plane model describing the shearing process as a deck of cards, using a graphical analysis for shear plane angle (ϕ) and shear strain (γ).

However, this early work did not consider a theoretical expression. Many solutions for shear plane angle in orthogonal cutting operations were expanded later by Merchant, and Lee and Shaffer. The concept of the derived equations was employed in the quantitative analysis of the cutting forces and shear stress on the shear plane.

The formula developed by Merchant [6] derived from the relationships between the resultant force on the shear plane(R_s), the friction angle (β) and rake angle (α). Lee and Shaffer [30] expressed a derivation using the relationships between a direction of maximum shear stress, the friction angle, the angle of the built-up edge size (θ) and rake angle. H$\ddot{u}$cks [31] also extended a derivation using the influence of the normal stress on the shear plane as in similar work done by Merchant, and Lee and Shaffer. On the other hand, Stabler [32] presented an analysis for shear plane angle in oblique cutting operations, on the assumption that the maximum shear stress on the shear plane and the resultant shear strain were collinear. Oxley in 1962 [33] critically reviewed some of the assumptions made for the development of equations (2.20), and expressed a new model for calculating the shear plane angle by considering the angle of inclination of resultant cutting force to the shear plane (φ).

Several equations concerned with the shear plane angle available in two-dimensional [5, 6, 30-31, 33-37] and three-dimensional cutting operations [32, 38, 39], have been developed with many assumptions as listed in table 2.1. Those equations were expressed by two types of models taking into account the effect of built-up edge(BUE), and without considering BUE. The shear plane angle, one of the most important and persistent problems in the metal cutting, appeared as a function of the rake angle and the friction angle ; so, $\phi = \psi(\alpha,\beta)$ when a dimensional analysis is performed using the quantitative relationship. However, equations (2.14) (2.16) (2.18) and (2.21) include the effect of BUE or normal and shear stress generated on the shear plane, which were not included in the dimensional analysis.

Table 2.1 Developed model for shear angle.

Researcher	Developed Model	Year	No	Remarks
Ernst and Merchant [5]	$\phi = \frac{\pi}{2} - \frac{\beta}{2} + \frac{\alpha}{2}$	1941	2.13	$\phi = \psi(\alpha,\beta)$
Merchant [6]	$\phi = \frac{C_m}{2} - \frac{\beta}{2} + \frac{\alpha}{2}$	1945	2.14	$C_m = Cot^{-1}k$, BUE
	$\phi = \tan^{-1}\frac{r\cos\alpha}{1-r\sin\alpha}$	1945	2.15	$\phi = \psi(\alpha,r)$
Lee and Shaffer [30]	$\phi = \frac{\pi}{2} + \theta - \beta + \alpha$	1951	2.16	No BUE when $\theta = 0$
Hücks [34]	$\phi = \frac{\pi}{2} - \frac{C_t}{2} + \alpha$	1951	2.17	$C_t = \tan^{-1} 2\mu$
	$\phi = \frac{C_m}{2} - \frac{C_t}{2} + \alpha$	1951	2.18	$C_m = Cot^{-1}k$, BUE
Stabler [35]	$\phi = \frac{\pi}{2} - \beta + \frac{\alpha}{2}$	1951	2.19	$C_t = \tan^{-1} 2\mu$
Oxley [36]	$\phi = \varphi - \beta + \alpha$	1962	2.20	$\psi = (\alpha,\beta,\varphi)$
Sata [34]	$\phi = \theta - \beta + \alpha$	1963	2.21	$\phi = \psi(\alpha,\beta,\theta)$,BUE
Boothroyd [35]	$\phi = \phi_\circ + e\delta$	1970	2.22	0.75<e<1
Mittal and Juneja [36]	$\cos\phi' = -\tan\alpha + \frac{1}{\cos}\left[1 + \frac{l_{cl}\cos\alpha\sin 2\beta}{t\sin 2(\phi+\beta-\alpha)}\right]$	1982	2.23	used controlled contact length (l_{cl})
Robert [37]	$\phi = 0.048V + 15.738$ $\phi = 28.56t + 14.93$	1987	2.24-2.25	$\alpha = +6^\circ$
Albrecht [38]	$\phi = \frac{1}{2}(\pi + \alpha - \tau_Q) + \tan^{-1}\left\{\frac{\%_b - 1}{\%_b + 1}\tan\left[\frac{\pi}{4} - \frac{1}{2}(\alpha - \tau_Q)\right]\right\}$	1987	2.26	Oblique cutting
Lin [39]	$\phi = \phi_\circ + \tan^{-1}(\frac{dt}{dy})$	1991	2.27	Oblique cutting

Lee and Shaffer [30] and Oxley [33] presented a slip line field (SLF) solution, including the strain hardening and variation of shear stress on the tool rake face. Sata [34] derived a shear plane angle equation using the relationships between resultant forces, the ratio of tool-chip contact length versus the undeformed chip thickness, and

rake angle. Oxley [33] and Mittal and Juneja [36] also presented a SLF solution based on the effect of stress distribution, using tools of controlled contact length. Since 1970, empirical equations [35, 37] based on the experimental data have been developed in the shear plane angle, but these were limited to apply to all cutting tool and workpiece materials with the variation of cutting process parameters.

Rowe and Spick [40] and De Chiffre [26] suggested a simple upper bound approach using the dependent out variables, such as the distribution of stresses and the chip-thickness ratio related to the controlled contact length, instead of using the friction angle.

None of these analytical and empirical models are still found to be really satisfactory when the various equations are tested against a wide range of experimental data [1]. Much research preceded development of the shear angle formula, and some equations resulted from the assumption of uncertain hypothesis in their development. Subsequently, among the developed or modified mathematical models, for the most conveniently solved in prediction of a shear angle without any complicated assumptions, a formula 2.15 was arrived at. This took into account the chip-thickness ratio obtained by measuring the deformed chip thickness. From the equation 2.15, it can be predicted that the shear plane angle increases with the increasing chip-thickness ratio when the rake angle remains constant.

2.2.8 Investigation of Tool-Chip Contact Length

2.2.8.1 Influences of Tool-Chip Contact Length in Machining Process

The role of tool-chip contact length in the cutting process is quite important in various aspects of machining processes, because the natural tool-chip contact length is not only affected by a great number of cutting parameters, but also it affects some

dependent output parameters generated during the machining. The effective and controlled tool-chip contact length can reduce the maximum crater wear on the tool rake face [41], which results from the chip thickness, size and shape. These can be changed according to the variation of cutting process parameters and the geometry of the cutting tool. Furthermore, both residual stresses and plastic strains decrease and the quality of the machined surface improves with tools having controlled tool-chip contact lengths [42].

Prediction of the tool-chip contact length is capable of improving the tool-life and product quality when the interrelationships of the correlated variables are taken into consideration. These variables include cutting forces, stress distributions, chip thickness and formation, tool geometry and cutting process parameters. A large number of models and theories derived for prediction of the contact length are reviewed and estimated. The theoretically unpredictable and limited accuracy of the models developed in the tool-chip contact length can be a major problem in the automated cutting process and in achieving the desired cutting productivity. Determination of the most adequate equation of the contact length estimation has a strong influence on the analysis of the experimental and theoretical data in the present research.

2.2.8.2 Developed Models for Prediction of Tool-Chip Contact Length

In the past decade, many of the theoretical solutions for the contact length in orthogonal cutting operations have been made to predict a comprehensive database for the quantitative analysis of machining performance. These developed models were based on the geometry of the shear plane model which was initially proposed by Ernst and Merchant [5, 6].

Hahn in 1953 [43], derived a analytical equation from the relationships of the uniformly-distributed shear and normal stress on the shear plane and tool rake face, respectively. It was based on the fundamental mechanics of cutting operations proposed by Merchant.

$$l = \frac{t\sin(\phi + \beta - \alpha)}{\sin\phi\cos\beta} \tag{2.28}$$

Klushin [44] has applied the resultant forces equilibrium in which the resultant force (R_s) in the shear plane is equal to the resultant force (R_{tc}) on the rake face of the tool, but has not considered rotational equilibrium. This model has also assumed that the normal stress on the shear plane and tool rake face is uniformly distributed, and it is dependent on the deformed chip thickness. The model was derived from the constant of proportionality (m) to define the offset value between the measured contact length and the predicted contacted length, and the range of m was as $1 \le m \le 2$.

$$l = m\frac{t\cos\beta}{\sin\phi\cos(\phi + \beta - \alpha)} \tag{2.29}$$

Oxley [45] investigated the equilibrium of the shear stress in the shear plane and the normal stress on the rake face using the Mohr's stress diagram, and assumed that the shear and normal stress distributions on the rake face are to be constant.

$$l = \frac{t\sin\beta}{\sin\phi\cos(\phi + \beta - \alpha)\cos 2(\phi - \alpha)} \tag{2.30}$$

Rubenstein [46] has presented a deviation based on Hahn's formula, but has considered that the deformed chip is in linear and rotational force equilibrium. The application of the deformed chip equilibrium also derived from the constant of proportionality (m). This application between the normal stress distributions on the rake face and the contact length was proposed in three particular cases :

(1) uniform

(2) triangular

(3) exponential

The theoretically predicted value of the proportionality constant was fitted by comparing of the measured value and theoretical value calculated, using experimental data such as the measured value of the cutting force, tangential force and chip thickness. The estimated values for m were 1.5 to 2.6, with mostly around 2 for carbon steel.

$$l = m\frac{t\sin(\phi+\beta-\alpha)}{\sin\phi\cos\beta} \tag{2.31}$$

Zorev [47] has also obtained an expression for the contact length on the basis of the rotational force equilibrium of the deformed chip using the action of moment arms about a point on the cutting edge. The theoretically developed equation also took into account the ratio (m) of the moment arms for the normal force on the shear plane and rake face, and the value of m was experimentally estimated around 4.

$$l = mt[\tan\beta+\tan(\phi-\alpha)] \approx mt\tan\beta \tag{2.32}$$

So far, the briefly explained theoretical approaches as above, have taken into consideration a specific normal stress distribution for the shear plane and tool rake face based on the relationship of the deformation geometry and chip equilibrium, such as major process parameters (depth of cut, shear angle, rake angle and friction angle). However, Abuladze in 1982 [48], established a simplified equation which only included the depth of cut, rake angle and shear angle, without considering the friction angle. This model analysed the geometry of plastic deformation zones and the shear stress field in the deformed chip generated during cutting operations.

$$l = t[\cos\alpha(\cot\phi + 1) - \sin\alpha(\cot\phi - 1)] \tag{2.33}$$

Gad in 1992 [49], empirically developed a new model for the contact length using the statistical curve fitting technique. In the study, the accuracy of the empirical equation derived from the quantitative relationship between the basic cutting process parameters and the contact length, was estimated by comparing the assessment of the various models, and emphasised the importance of fundamental cutting parameters such as depth of cut (feed rate in orthogonal cutting), rake angle and cutting speed.

$$l = 9.980t^{0.674}(90 + \alpha)^{-1.70}V^{-0.353} \tag{2.34}$$

Through the survey of the tool-chip contact length literature, it was noted that the values of the tool-chip contact length predicted using the various formulae developed do not completely satisfy the agreement for all material combinations [49]. This agreement can be found from the measurement of realistic cutting tests using different workpiece and tool materials.

2.3 SENSING AND ADAPTIVE CONTROL FOR MACHINING PROCESS

2.3.1 Sensing for Machining Process

The role of the sensors has become more important with an increasing demand for automated cutting systems, since sensors have been employed widely in industrial and engineering areas. Poor quality in cutting production becomes apparent in dimensional and surface roughness when the cutting process parameters are not controlled [50]. Sensors employed in automated cutting processes must detect the variations of the tool wear and tool failure, and produce an output that is in some way

related to the change being detected. Complete cutting requires the qualities of dimensional accuracy, surface finish, and an undamaged workpiece and tool.

The requirements of cutting senors are that they should be universal, durable, reliable, compact, non-wearing and maintenance-free. However, cutting sensors that satisfy all of these demands are not available yet, because each sensor has limitations either in its design or in machining applications. For this reason, some cutting tests may result in the need for use of multi-sensors in automated cutting operations [23, 51].

2.3.2 Classification of Sensing Methods and Sensors

Since tool wear or tool failure affects the behaviour of cutting operations, a sensor can detect the signal that converts one type of physical energy into another type of electrical energy, either directly from the tool or the workpiece or from the process machine through the way of continuous or intermittent cutting operations [52]. The sensor will provide the information for control of cutting operations, and employ various techniques to control cutting processes. Sensing methods for adaptive control technologies can be divided into two types of measurements with or without contact :

(1) direct measurement methods which evaluate the volumetric loss of the cutting tool such as crater wear, flank wear land or both together,
(2) and indirect measurement methods which examine the correlations between the tool wear or failure and the cutting process parameters.

The measurement of the direct sensing method is the most common and reliable method. However, it is limited to interrupted cutting in which the cutting tool is observed directly using particular optical methods. In all, the direct sensing method has an influence on the economic loss of the operation, when the machine is stopped.

On the other hand, indirect sensing methods are commonly used to estimate the condition of the tool from the signals detected for the continuous cutting or, for most of the interrupted cutting.

The sensing methods and sensors developed and classified by several researchers for the on-line tool condition monitoring process, are listed in Table 2.2 (a) and (b).

Table 2.2 Classification of sensing methods and sensors for tool wear estimations.

(a) Direct measurement

Mothods	Application	Measurement	Sensors
Direct sensing	Optical	Shape or existence of cutting tool edge	Fibre optic [54], TV camera [55]
	Electrical resistance	Reduction of electrical resistance in tool/work junction	Voltmeter [56-57]
	Radioactive particle	Volumetric loss of the tool	Radioactive[58-60]

The indirect sensing methods have many advantages in sensing signals, but those signals are affected by other factors that reduce the reliability of tool condition monitoring [53]. Some of these other factors are :

(1) the indirect measurement sensors such as the AE sensor and the force transducers of strain gauge or semi-conductor type are restricted from the location of the sensor,

(2) the vibration and sound measurement methods are much affected by external noises from the ambient or the adjacent machines.

Reliable and effective sensing technologies must be developed to guarantee the reliability of the system and the quality of the products.

(b) Indirect measurement.

Mothods	Application	Measurement	Sensors
Indirect sensing	Workpiece dimension	Changes of workpiece size	Laser beam[61-62] Electromagnetic[63]
	Difference of distance	Variations of the distance between the tool post and the workpiece	Micrometer [64] Ultrasonic [65] Pneumatic [66] Displacement [67]
	Cutting force or torque	Variations, increments and differences of cutting force or torque	Tool Dynamometer [68-71]
	Vibration	Vibration levels of tool or tool post	Piezoelectric sensor [72-73]
	Ultrasonic	Changes of acoustic waves	Microphone [74]
	Surface roughness	variations in surface roughness of workpiece	Optical fibre [75] Laser beam [76] Electric micrometer [77],Ultrasonic[78]
	Cutting temperature	Variations of temperature on the cutting tool edge	Thermocouple [79] Infrared [80-81]
	Electrical power	Variations of the electrical power consumption	Current meter, Watt meter [82]
	Acoustic emission	Variations of the level of acoustic emission signals	AE sensor [83-85]

2.3.3 Adaptive Control

The main contribution of adaptive control, defined as automatic on-line adjustment of process parameters in manufacturing operations, is to obtain high efficiency, high quality, high productivity, minimal cost, and to result in a need for fewer and less skilled machinists. A large amount of research in manufacturing has been dedicated to adaptive control techniques for adaptation of input parameters in actual cutting conditions [72, 85, 86]. For adaptive control to be effective in automated cutting

operations, quantitative relationships are employed to monitor information about cutting characteristics and cutting process parameters. These quantitative relationships are used also (1) to determine whether or not a particular measurement is exceeding the preset thresholds, and (2) to modify those process parameters through the system controller, (3) to manage the quality of cutting within acceptable limits. Good quality cutting must have the characteristics of dimensional accuracy and good surface finish without any processing difficulties. The systems for adaptive control can be compared with two types of control techniques as set out in sections 2.3.3.1 and 2.3.3.2.

2.3.3.1 Open-Loop Machining Control

A significant improvement on the cumbersome early conventional cutting systems has been achieved with the development of open-loop adaptive control, called manual adaptive control (MAC) [87]. This development allowed set-up times to be reduced, more tasks to be performed and routines to be stored for later use. However, in the MAC systemt, to enable problems in the cutting process to be corrected, it is essential that the operator stops the operation immediately and modifies the performance of the program in the machine controller. Therefore, the MAC is definitely inferior to the more sophisticated closed-loop adaptive control, called automatic adaptive control (AAC). In MAC, an operator takes the place of automatic sensors, and serves as the interface between an inexpensive programmable computer and the machine [88]. Because operators make use of their senses of sound and sight to collect cutting information after processing and interpretation, MAC will be much less effective in controlling the cutting process than AAC. Therefore, the MAC system will not always produce consistent results of dimensional accuracy and high surface quality over the cutting tool life, since operators are limited in experience or modelling to enable selection of the necessary input parameters to achieve the desired output parameters. Due to these shortcomings, much research and development work has concentrated on sensing and control methods to enhance the automated cutting process.

2.3.3.2 Closed-Loop Machining Control

The closed-loop adaptive control system, AAC system, receives the measured or calculated actual output parameters and selects the necessary cutting input parameters based on these output parameters, and then initiates the cutting process while simultaneously monitoring the cutting conditions to determine the success of the cutting operation. On the basis of sensed outputs, the machine must be able to interpret and adjust stepwise for optimisation of the cutting process.

Automatic adaptive control (AAC) was first achieved by Gall [89] for control of an abrasive cut-off machine to a minimum cost per cut. A more effective approach for AAC process in cutting operations was achieved using a fully integrated machining structure having an CNC lathe, a part feeder, robotics work handling and scheduling, and a sensor and central computer [90]. With the combination of sensors and mathematical models, increased effectiveness for adaptive control in turning operations such as rate of surface finish [86, 90, 91], tool wear [92-94] and tool fracture [95, 96] was shown in many studies.

Mathematical models based on the control system are not suited to totally real-time adaptive control, because of their inability to isolate the process input parameters, thereby resulting in excessive processing times. These systems are not capable of taking account of the relative effectiveness of each input parameter. Mathematical systems are also inflexible to changes in hardware, due to their rigid control laws, and unlike humans are unable to learn from success or failure. Development of practical models is still continuing in this area because development is extremely difficult and each cutting parameter has at least some effect on the others.

2.4 ACOUSTIC EMISSIONS IN THE MACHINING PROCESS

2.4.1 Background and Application of Acoustic Emissions

In early times, acoustic emissions (AE) in metals were observed in terms of "tin cry" generated during twining deformations of tin and "audible sounds or clicks" generated in the heat treatment of metals [97]. The earliest use of electronic instrumentation for AE analysis was initiated by Kaiser [98], to detect audible sounds created in the metal deformation. In the studies, it was identified that the irrecoverable deformation in the metal cutting process occurred as the level of stress waves exceeded the plastic limitation of workpiece materials. A couple of years later, Schofield [99] and Tatro [100] improved the instrumentation for measurement of acoustic emission, and reviewed the deformation of the plastic work to clarify the proposal in Kaiser's theory that major sources of AE signals result from dislocation by slip and twining of the grain boundary in the internal metal structure.

The advance of AE technology was made by minimising the background noise [101], which for early workers resulted in many limitations in the wide frequency range of the AE. With the improvement of AE analysis using a more modern AE monitoring system, it was possible to ignore almost all background noise from the cutting process by using filtering devices and transducers sensitive enough to detect flaws in the cutting process. Sounds and stress waves generated in the metal cutting operation were mainly utilised to estimate materials characterisation and structural evaluation as a form of non-destructive testing (NDT).

Acoustic emission techniques have been generally accepted in the two groups of studies : deformation or fracture in geological materials [102] and the assessment of structural integrity [103]. Recently, most AE techniques have been used to assess the transient nature of the mechanistic processes involved in deformation, fracture and

flaws of structures, and to verify the qualitative relationships for a wide variety of materials and structures.

Over a number of years many investigations into the AE monitoring system have shown a significant potential, and several of these have been recorded in the publication "Acoustic Emission, ASTM STP 505", and applied in modern industry and many engineering research areas. These areas of application include : monitoring of earth slopes and dams, vibration analysis, pipe-line condition monitoring, leakage monitoring, delamination and fracture of fibre reinforced plastics, dynamic monitoring of crack growth, and the determination of location and size of cracks in pressure and nuclear vessels without emptying. Other areas of application have been found in structural integrity of bridges, buildings, and wooden beams, bearing condition monitoring, in-process monitoring of welding, tool wear and fracture, and observing chemical (oxidation) reactions. Various other applications also have been found.

2.4.2 Statistical Analysis Techniques of AE signals

In analysis and interpretation of the detected AE signals, the application of AE techniques is restricted by limitations in accurate assessment of the cutting process. The limitations may occur through such problems as :

(1) the randomness and non-periodic nature of the AE signal amplitude,

(2) the wide range of frequencies of the detected AE signals,

(3) a lack of database and mathematical models for prediction of the AE signal generation all of which can affect decisions about the cutting conditions before machining.

Since these limitations, AE analysis techniques have continued to be developed, in order to establish the most suitable modelling for adaptive control of cutting processes using the AE monitoring system.

AE testing is a very versatile non-destructive testing method for the analysis of flaws and defects in materials or structures. The commonly employed statistical techniques for analysis of AE data can be classified as follows :

- RMS voltage analysis technique is used to measure the changing amplitudes of the AE signal due to the vibration created between the tool and workpiece during metal cutting [104-114].
- Count and count rate analysis technique is used to record the rate of AE events for each cut as the detected AE signals exceed a preset threshold voltage [115-118].
- Frequency spectrum is used to indicate the contribution of predominantly detected signals of each frequency component to the total power using a high speed spectrum analyser [119].
- Amplitude distribution analysis gives an indication of the number of AE signals whose the amplitude falls within a predefined range [120].
- Autocorrelation function enables comparison of a signal waveform against a delayed version of the same waveform [121].
- Homographic processing of detected AE signals is used as a means of separating the AE source characterisation and signal path transmission effects [122, 123].

Among the several AE techniques developed in machining processes, the most promising technique is to analyse the RMS voltage of AE signals (AE_{RMS}) converting the raw AE analogue signals to electric digital voltage values. In recent times, analysis of the AE_{RMS} is the most commonly used technique for condition monitoring of the tool wear, fracture, failure and the surface roughness of the newly machined workpiece.

Based upon the discussed AE analysis techniques above, several modelling techniques for intelligent machining have been applied to the process state representation. These techniques are used to completely understand and adequately describe the process mechanisms in the form of a knowledge base. The different modelling techniques for

statistical and artificial intelligent (AI) approaches in cutting operations have been defined and evaluated in the technical papers, such as :

- Pattern recognition, is used to classify significant process effects, such as the categorisation of input data into identifiable classes via the extracted some given attributes, derived from the frequency spectra of AE signals [124-126]
- Autoregressive time series (AR) is used to derive the mathematical model for a dynamic system based on physical laws which can calculate the value of some time-varying quantity at any particular instant of time [121, 127].
- Autoregressive moving average (ARMA) time series is used to quantify the process dynamics embedded in the AE signals [128].
- Multiple regression analysis is used to construct a model which presents the variability in a dependent variables using several independent variables [107].
- Group method of data handling (GMDH) is used to offer a self-organising modelling and a large selection of cutting parameters and strategies that can affect on the model of provided best results [129].
- Neural network is used to make a final decision on the state of the cutting tool from the output training set based on the input and output interrelationship [130-134].
- Fuzzy logic is used to derive optimised control algorithms to obtain a prescribed quality of cutting, using other analysis modelling such as time AR series and pattern recognition [135, 136].

2.4.3 Developed Models for Prediction of AE_{RMS}

A derivation of the energy rate consumed in the cutting process was presented by Merchant [6], and an expression for the total power consumption in the total cutting zone was first described as :

$$E_t = F_c V = \tau A V \frac{\cos(\beta - \alpha)}{\sin\phi \cos(\phi + \beta - \alpha)} \tag{2.35}$$

The derived formula 2.35 which can compute the total amount of the energy rate consumed in cutting operations, is not widely adaptable in the theory of various cutting zones. However, based on the basic mechanics of two-dimensional cutting operations proposed by Ernst and Merchant and the developed model of the total power consumption by Merchant, many models for prediction of the AE_{RMS} or cutting forces relating to cutting process parameters, using specified techniques such as acoustic emission or cutting force techniques, have been applied for adaptive control systems in automated cutting processes.

As indicated in Figure 2.6, AE models [23, 24, 138, 139] have been derived from the quantitative relationship between the AE_{RMS} voltage levels and the energy rate consumed in various (primary, secondary and tertiary) deformation zones during the two dimensional cutting operation.

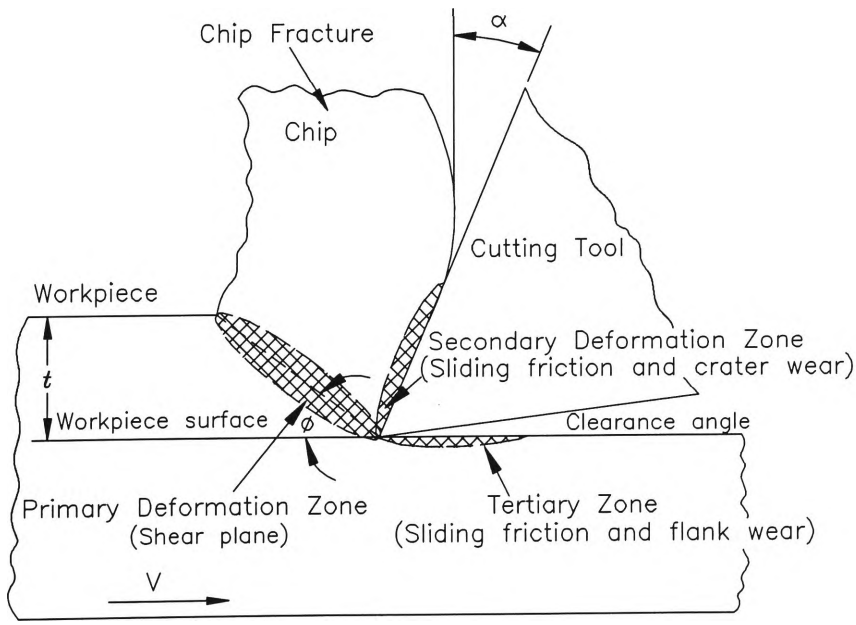

Figure 2.6 Cutting mechanism and generation of acoustic emissions on the irreversible deformation zones.

Dornfeld and Asibu [23] first derived a theoretical relationship from the theory of acoustic emission and the analysis of emission signals. The analytical model was suggested by the basic mechanics of orthogonal cutting operations. This model applied the relationship between the energy expenditure based upon the dislocation of workpiece material in the primary deformation zone and the AE_{RMS} voltage according to variations in cutting process parameters such as feed rate, cutting speed and rake angle. In the studies, the dependency of emission energy on the cutting speed and strain rate were verified. Furthermore, in the theoretical equation 2.35, the constant of proportionality (C) was suggested to fit the difference between the measured AE_{RMS} voltage and the energy rate calculated theoretically on the basis of the experimental data

$$V_{RMS} = C(\tau_s \frac{r_c \cos\alpha}{\sin\phi} \frac{V}{\Delta Y} U)^{\frac{1}{2}} \tag{2.36}$$

Asibu and Dornfeld [24], extended the quantitative relationship of the previous model by considering the influence of the acoustic emission signal at the tool-chip interface, rather than stress distributions in the shear zone predicted by the slip line field (SLF) theory. A comprehensive analytical relationship between the acoustic emissions and cutting process parameters, was based on the experimental theory of Zorev [19] and Trigger [137], and compared the level of the experimentally measured AE_{RMS} voltage with the value of the theoretically predicted AE_{RMS} voltage. The developed model was derived from the theory of power law and applied stress distributions in the tool-chip interface, using the relationship of the normal load and friction force. However, the constants of powers (a and b) and the seize ratio (the ratio of the sticking and sliding regions separated in the tool-chip contact zone proposed by Zorev) in the tool-chip interface, were not clearly defined. The value of the power constant was assumed to be equal to 1, viz ; a=b=1, and the lengths of the sticking (l_{st}) and sliding (l_{st}) zones, were assumed as half of the total natural chip contact length (l), viz $l_{st} = l_{sl} = 0.5l$.

The effects of the tool-chip contact length and rake angle were significant for the theoretical model and were identified in experiments by measuring.

$$V_{RMS} = C\sin\alpha\{\tau_a bV[\frac{t\cos\alpha}{\sin\phi\cos(\phi-\alpha)} + \frac{1}{3}(l+2l_{st})\frac{\sin\phi}{\cos(\phi-\alpha)}]\}^{\frac{1}{2}} \quad (2.37)$$

Schmenk [138], modified the formula of Asiu and Dornfeld as a result of data obtained from experiments, which employed both sharp and artificially worn tools. Some assumptions considering the relationship between the tool-chip contact length (l) and the uncut chip thickness (t) on the change of rake angle, were derived from the experimental result. It has been assumed that the seize ratio of the sticking zone was the same as the uncut chip thickness ($l_{st} = t$), and the total natural chip contact length was the twice of the uncut chip thickness ($l = 2t$) at zero rake angle in the tool-chip interface. The size effect of the chip load was described in the tool-chip contact interface, and it showed an increased influence on the AE_{RMS} output at the small chip loads formed by the low range of feed rate.

$$V_{RMS} = C\{\frac{\tau_s bV}{\cos\phi}[\frac{1}{\sin\phi} + \frac{(l+2l_{st})\sin\phi}{3t}]\}^{\frac{1}{2}} \quad (2.38)$$

Lan and Dornfeld [139] presented a derivation by including the effects of the AE signal created in the tool flank and workpiece interface, which took into account the influence of the AE_{RMS} voltage increased linearly with increase of wear land on the tool flank [140]. The frictional stress (τ_{fw}) and sliding speed (V_{fw}) in the tool flank-workpiece interface were assumed as reasonable. The derived model was also assumed a little differently from the model of Asibu and Dornfeld. It was proposed that the AE signal attenuations (C_1, C_2 and C_3) occur in the three plastic deformation zones by signal transmission losses. In all, it applied the law of power in order to approach realistic values according to the change of materials. The constant of

proportionality (C) indicates the AE signal loss in the cutting tool itself. The constant of power (m) is dependent on the tool and workpiece materials.

$$V_{RMS} = C\{\tau_a bV[C_1 \frac{f\cos\alpha}{\sin\phi\cos(\phi-\alpha)} + C_2 \frac{1}{3}(l+2l_{st})\frac{\sin\phi}{\cos(\phi-\alpha)} + C_3 l_w]\}^m \qquad (2.39)$$

As briefly summarised above, the models developed for prediction of the AE_{RMS} voltage were well defined using some assumptions and experimental results. However, the theoretical models were limited in determining the feasibility of adaptive control because some of the assumptions were not reasonable, as follows : -

(1) the values of the seize ratio in the tool-chip contact lengths in the tool-chip interface were not correctly estimated.

(2) the values of acoustic emission signal attenuation constants (C_1, C_2 and C_3) in various cutting zones were not determined reliably.

(3) the constants of proportionality (C and $C\sin\alpha$) were not estimated.

(4) the value of $C\sin\alpha$ is equal to zero when the rake angle (α) is zero.

Even though Lan and Dornfeld [139] obtained the acoustic emission signal attenuation value in the primary cutting zone (C_1) using the lead break test, they assumed that the values of the secondary and tertiary cutting zones are equal to be 1 (viz $C_2 = C_3 = 1$) without some reasonable reasons. In addition to, the proportionality constants (C and m) have not been determined.

In this research work, a realistic seize ratio indicates that the ratio of the sticking and sliding zones are not half of the total natural chip contact length. The constants of acoustic emission signals generated in each cutting zones which includes the proportionality constant, will be estimated with the help of the computational work. As described later in chapter four, the values of the constants shows a big difference when compared with the constant values of Lan and Dornfeld.

CHAPTER THREE

THEORIES FOR DEVELOPMENT OF MATHEMATICAL MODELS

3.1 INTRODUCTION

A knowledge of material behaviour with chip formation is of great significance, since it gives an illustration of how tool and workpiece material properties and cutting conditions influence the important process parameters, such as cutting forces, tool wear and power consumption. So as to put the analysis of the metal cutting operation on a qualitative basis, certain observations must be made before and after a cut. Definition of the physically consistent relationships of cutting forces, stress distributions and energy expenditure in various cutting zones, is essential to the analysis of the mechanics associated with the cutting process.

In this chapter, a wide variety of factors in each cutting zone which produce cutting forces, stress distributions and energy consumption will be discussed first, and the significant variables which lead to the practical cutting action will be identified, so as to develop theoretical models. Application of theoretical and empirical theories were described for development of theoretical models. Finally, acoustic emission analysis technique, one of the most promising and useful techniques for the monitoring of

cutting conditions will be described, and the fundamental formula developed for prediction of AE signal generation, will be presented.

3.2 MECHANICS OF THE ORTHOGONAL CUTTING PROCESS

3.2.1 Cutting Forces

In accordance with the cutting models, the orthogonal cutting operation has been defined as a two-component force system, while the oblique cutting operation is a three-component force system. The number of observations that can be made of the cutting process is rather limited. One of the more important of those observations, is the determination of the cutting force components. An ability to predict the forces generated in various cutting zones is necessary in the design of machine tool structures and cutting tools, as well as for the determination of appropriate cutting conditions.

The magnitude of cutting forces is directly related to the material properties of the workpiece and cutting tool, the cutting conditions, the structural rigidity of the machine and the status of lubrication [72]. Among the tool and work material characteristics, material hardness plays a significant role in the cutting forces. For instance, the cutting force for ceramic tools is invariably much smaller than for high speed steel or the cemented carbide tool, by virtue of its lower value of the coefficient of friction [17, 141]. Furthermore, the cutting and tangential forces which have an influence on other forces, depend predominantly on the cutting process parameters, such as the feed rate, the depth of cut, the width of cut, the cutting speed, the tool rake angle and the wear land of tool flank [9, 14, 72, 109, 137]. According to the experimental data by Sadik [142], the cutting force increases with increasing tool-chip contact length and cutting time and decreasing cutting speed.

As can be seen in Figure 3.1 (a force diagram of geometric relationships), the cutting forces have been differently estimated in the two cutting zones. When the deformed chip is isolated in the two irrecoverable deformation zones, it can be considered as two resultant forces : the resultant force (R_s) in Figure 3.1 (b) between the workpiece and the chip that moves along the shear plane, and the resultant force (R_{tc}) in Figure 3.1 (c) between the back surface of the deformed chip and the tool rake face in the chip-tool interface. These kinematic forces associated with orthogonal metal cutting operation were developed by Ernst and Merchant [5, 6].

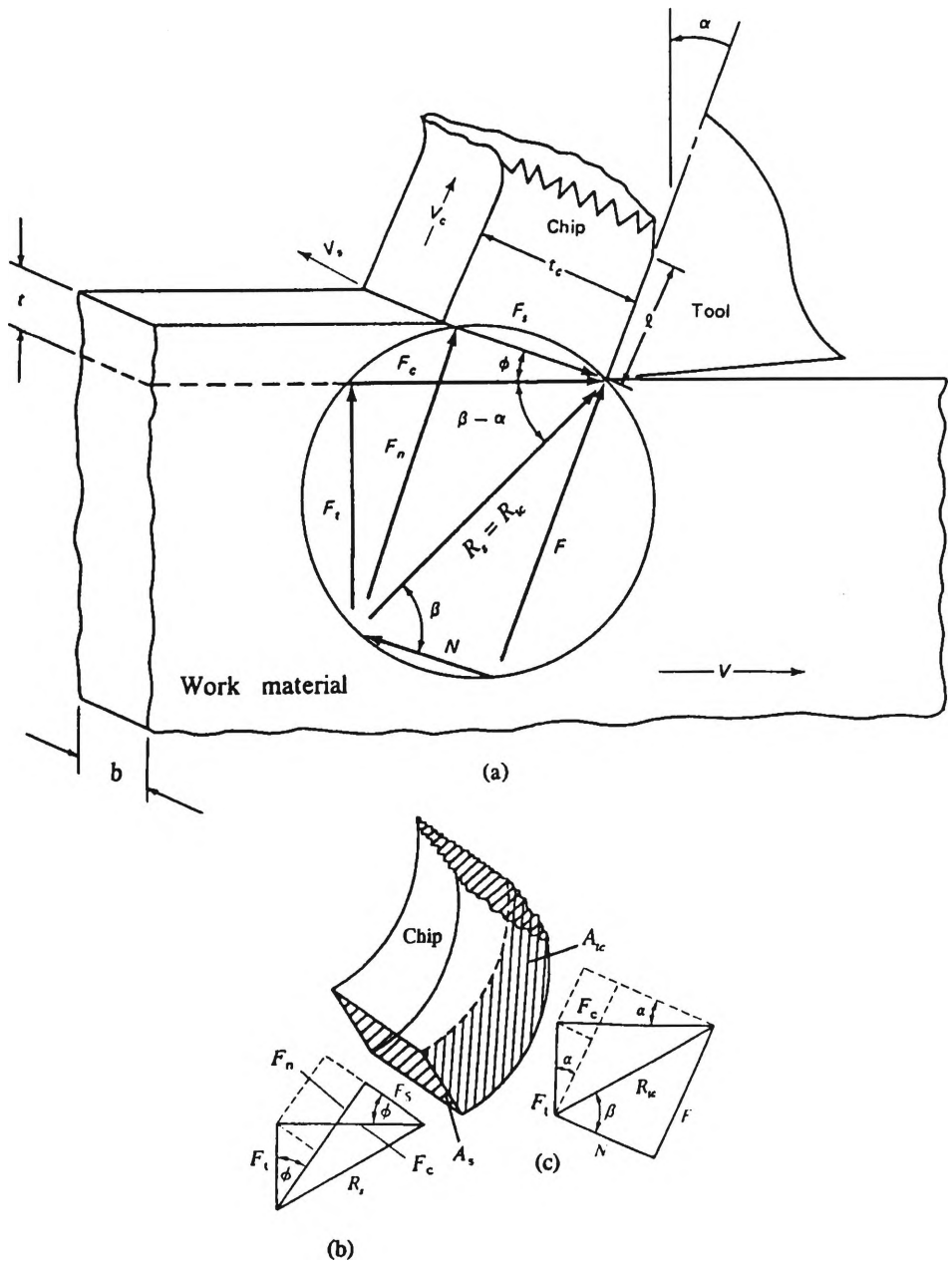

Figure 3.1 The geometry of machining.

(a) cutting forces diagram. (b) shear plane. (c) Tool face.

The cutting forces, generated between the tool face and the chip, have been separated at the shear plane and can be expressed in the chip equivalent form.

- Forces generated on the shear plane

$$F_s = F_c \cos\phi - F_t \sin\phi \qquad \text{(from Figure 3.1(b))} \qquad (3.1)$$

$$F_n = F_t \cos\phi + F_c \sin\phi \qquad \text{(from Figure 3.1(b))} \qquad (3.2)$$

- Forces acting on the tool-chip interface

$$F = F_c \sin\alpha + F_t \cos\alpha \qquad \text{(from Figure 3.1(c))} \qquad (3.3)$$

$$N = F_c \cos\alpha - F_t \sin\alpha \qquad \text{(from Figure 3.1(c))} \qquad (3.4)$$

Analysis of the Coulombic sliding friction on the tool rake face is defined by the cutting and tangential forces generated with the tool rake angle. The coefficient of sliding friction in the tool-chip interface, μ_{tc} is presented by the ratio of friction force, F and normal force, N and can also be expressed as the friction angle, β. The friction coefficient is dependent on the cutting velocity as an increase in cutting speed produces lower sliding friction.

$$\mu_{tc} = \tan\beta = \frac{F}{N}$$

$$\mu_{tc} = \frac{F_c \sin\alpha + F_t \cos\alpha}{F_c \cos\alpha - F_t \sin\alpha} \qquad \text{(from Figure 3.1(c))} \qquad (3.5)$$

In orthogonal machining, the resultant cutting force is a composition of the pressure and the friction acting on the rake face and the flank of the cutting tool. The two resultant forces, R_s, R_{tc}, can be defined by the vector sum of the forces generated in

the shear plane and the tool-chip interface respectively, as shown Figure 3.1(b). However, the resultant forces are obtained on the assumptions that :

(1) the resultant force in the shear plane is equal to the resultant force in the tool-chip interface, viz. $R_s = R_{tc}$,

(2) R_s is opposite to R_{tc},

(3) R_s is collinear to R_{tc}.

The resultant forces on the shear plane can be presented with two components : a shear force F_s acting along the shear plane, and a normal force F_n acting perpendicular to the shear plane.

$$R_s = \sqrt{F_s^2 + F_n^2} = \sqrt{F_c^2 + F_t^2} \tag{3.6}$$

The resultant force on the tool rake face can also be expressed by a friction force F, and normal force N at the tool-chip sliding interface.

$$R_{tc} = \sqrt{F^2 + N^2} = \sqrt{F_c^2 + F_t^2} \tag{3.7}$$

From the above defined equations of the forces, it can be seen that the forces are a function of the cutting force (F_c) and the tangential force (F_t). The cutting force which is in the direction of the cutting velocity and the tangential force which is in the direction perpendicular of the cutting velocity or the machined surface, can be measured by experiment, using a tool dynamometer mounted in the workholder or toolholder. On the basis of the measured values of the cutting and tangential forces, other forces generated in each plastic deformation zone can be resolved using the theoretical equations above mentioned.

3.2.2 Stress Distributions in Cutting Zones

Shear and normal stresses in the metal removal process take place in the shear plane and on the tool rake face. The stresses generated in the shear plane are analysed on the assumption that they are uniformly distributed. On the other hand, the stresses in the tool-chip interface provide a different derivation, assuming that they are non-uniformly distributed, based on the experimental evidence of Zorev [19]. The magnitude of the stresses depends largely on the elastic and plastic boundary in workpiece materials, and is determined by cutting conditions and strain hardening [16, 17, 141]. An understanding of the stress distribution gives an improved knowledge of the process mechanics and the cutting tool wear mechanisms.

3.2.2.1 Uniform Stress distribution in the shear plane

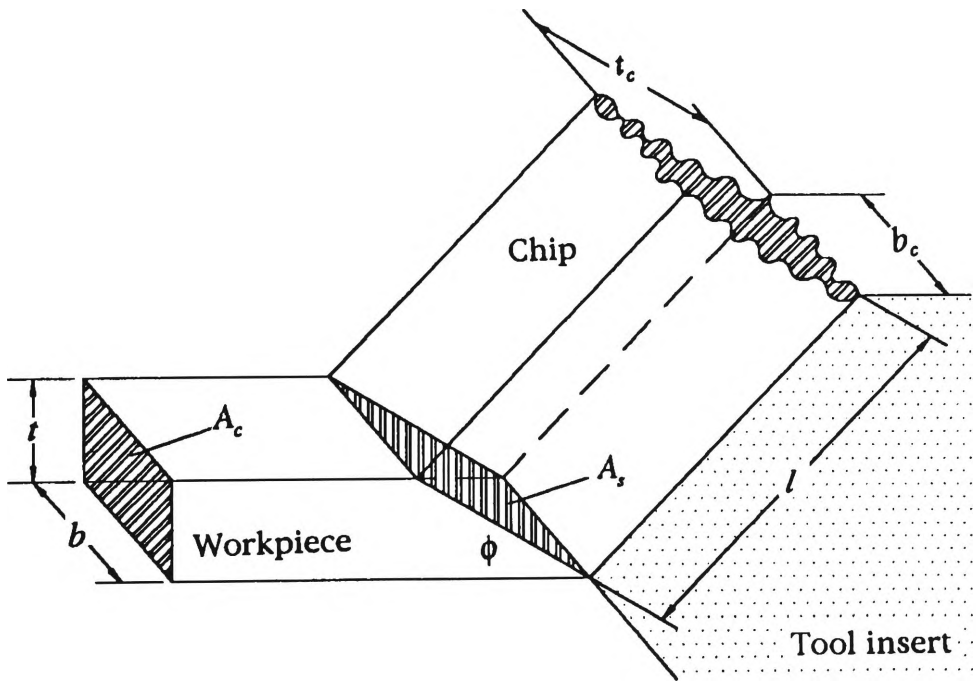

Figure 3.2 A cross-sectional area between the shear plane and tool-chip interface.

Shear stress and normal stress distribution in the primary shear deformation zone can be determined by the effects of forces acting on the shear plane. These forces (shear

and normal forces) are based on the dislocation motion of the internal metal structure of the workpiece material when the cutting tool engages the workpiece. The shear stress τ_s, can be derived from the shear force which exists on the shear plane and an area of shear plane, A_s formed by cutting the metal structure, as depicted in Figure 3.2.

$$\tau_S = \frac{F_S}{A_S} = \frac{F_c \cos\phi \sin\phi - F_t \sin^2\phi}{bt} \tag{3.8}$$

The cross-sectional area of chip before workpiece removal (A_c) is computed from the undeformed area of cut (bt) inclined at the shear angle.

$$A_s = \frac{A_c}{\sin\phi} = \frac{bt}{\sin\phi} \tag{3.9}$$

The normal stress σ_s, is similarly extended, using the equation of the normal force on the shear plane, because it is in units of force per unit area. Therefore, the normal stress is :

$$\sigma_s = \frac{F_n}{A_s} = \frac{F_t \cos\phi \sin\phi + F_c \sin^2\phi}{bt} \tag{3.10}$$

From the equation 3.10, it can be seen that the theoretical correlation of the stresses (τ_s and σ_s), that are generated by the actual dislocation state of a cutting metal, relies largely on the input and output variables such as the geometry of cut (b and t), the shear angle (ϕ), and the measured cutting forces (the cutting force, F_c and tangential force, F_t). The normal stress on the shear plane has no effect on the shear flow stress of the workpiece material, and it is assumed that σ_s is independent of τ_s [143]. However, the shear stress in the shear plane was estimated as a constant in particular

workpiece materials and the variations of cutting process parameters without respect to the magnitude of the normal stress [137, 144].

3.2.2.2 Average Dynamic Shear Stress in the Plastic Deformation Zones

The average dynamic shear stress (τ_a) of metal, called a maximum resisting shear strength [1] of workpiece material, or shear strength [24], can be regarded as a basic physical theory used to predict the fundamental theoretical model which applies in the plastic deformation zones. It might be expected to be a constant regardless of the variation of the cutting process parameters, tool and workpiece materials.

Chao [137] and Ramalingham [144] proposed the constancy of dynamic shear stress of workpiece material under high-speed machining conditions. The average dynamic shear stress in the experimental result of Chao, has proved that it shows no change under the same cutting condition of feed rate with variations in cutting speed, tool-chip contact length and some workpiece materials (carbon steel and copper). Ramalingham has established that the average shear stress takes on a constant value for a variety of metals.

Mesquita [9], also presented a method of determining the dynamic shear stress using the effect of crater and flank wear, and the indentation force on the distribution of the shear stress in the metal cutting process. In comparison with the shear stress values obtained using the models proposed by other researchers, the dynamic shear stress in this experiment was essentially constant.

From the view point of these experimental results, it can be summarised that the average dynamic shear stress of a metal shows invariant behaviour without respect to the variation of cutting conditions. On the basis of these practical experimental results, the relationships between the average dynamic shear stress in the shear plane, the

frictional shear stress in the tool-chip interface, and the sliding frictional stress in the tool flank and workpiece surface interface, it can be established that the shear stresses generated in the three plastic deformation zones are equal to the average dynamic shear stress of a metal [24, 137-139, 144, 145].

3.2.2.3 Non-Uniform Stress Distribution at the Tool-Chip Interface

It is both complicated and difficult to determine the forces and stresses between the chip and the tool rake face. There are two significant difficulties in predicting the relationships between the stress distributions. With variations of basic cutting process parameters such as feed rate, rake angle and cutting speed, the accurate analysis of the tool-chip contact length distributed on the rake face of the cutting tool, is one of the most important factors [49]. Another is to indicate the actual stress distribution on the tool rake face.

With the help of the actual experiment evidences which are related to the variety of experimental techniques (photoelastic techniques), and observations by several researchers such as Zorev (1963) [19], Kato (1972) [146], De Chiffre (1977) [26], Shaw (1980) [147] and Usui (1984) [80], it has been found that the stress distributions on the rake face of the tool are not uniform. However, many different assumptions need to be made to accommodate the theoretical relationships. As a result of the practical experiments and theoretical assumptions of the above researchers, which seems to originate from the empirical theory of Zorev [19], the chip flow has been separated into two major regions of sticking and sliding on the tool rake face. This empirical theory was based on the distribution of shear stress (τ_f) and normal stress (σ_f) along the cutting tool face

The concepts of the sticking and sliding zones in the tool-chip interface are quite different from the influences that depend largely on the dependent output variables

such as the cutting forces, the high interface temperature, the high cutting pressure, the shear angle, the sliding friction and wear of the cutting tool. For instance, the high interface temperatures and pressures generated at the cutting tool edge (point **A** in Figure 3.3) cause sticking and generate maximum normal stress. Therefore, special conditions of cutting process parameters, tool and workpiece materials are required to maintain a good machining condition. Whereas, the distribution of normal stress in the sliding region σ_f, is zero at point **I** in Figure 3.3 where the chip leaves the rake face of the tool. The normal stress is defined as a power function of the distance from the cutting tool edge to the last contact point of the chip on tool rake face. Finally, it can be stated that the normal stress is non-uniformly distributed on the rake face of the cutting tool.

The frictional shear stresses in the tool-chip interface (τ_f), are more uniformly distributed than the normal stress (σ_f). However, it is more complicated to evaluate because of the chip behaviour. With the change of cutting process parameters, the behaviour of chip flow between the workpiece material and the cutting tool edge is entirely dependent on the properties of the workpiece material. According to the behaviour of the deformed chip, frictional shear stress can be evaluated differently in the sticking and sliding regions.

As can be seen in the derived equation (3.15), the ratio of contact length (seize ratio) which is moved along the tool rake face by the deformed chip in the sticking and sliding zones, has an effect on the magnitude of cutting forces generated in those zones. As described later in the theoretical section 4.2.3 and the experimental section 4.5.2 of chapter 4, the seize ratio formula of the sticking and sliding zones which include the parabolic (power) constant (n), will be significantly dependent on the variations of cutting process parameters, such as feed rate, rake angle and cutting speed.

The frictional stress in the sticking zone is the same as the average dynamic shear stress τ_{st}. As evident from the results of experiments on the seize ratio in the tool-chip interface, the frictional stress in the sliding zone τ_{sl} depends significantly on the variation of the value of parabolic (power) constant (n) whether it is uniformly distributed or not. In other words, the frictional shear stress in the sliding zone can be uniformly altered by the variation of the parabolic constant (n), as shown in the hidden lines from point **H** to point **I** in Figure 3.3.

A large number of different assumptions from previous work done by several researchers needs to be made to accommodate the realistic deformation of the workpiece at the tool-chip interface, as shown in Figure 3.3. Furthermore, the theoretical equations in the tool-chip interface were derived from the empirical relationship for the average dynamic shear stress of a metal which is readily useable to determine the relationship of stresses generated in various cutting zones by the irreversible deformation of the workpiece.

(1) the apparent chip contact length (l_{cn}), is equal to the total length of contact (l) between the chip and the rake face, (ie, $\frac{l_{cn}}{l} = 1$) [49].

(2) the maximum value of the normal stress (σ_f) on the rake face, $\sigma_{\max}$, exists at the cutting edge, and the minimum value is at the point at which the deformed chip leaves the rake face of the cutting tool [19, 148].

$$\sigma_f = \sigma_{\max}(\frac{x}{l})^n \qquad (0 \le x \le l) \qquad (3.11)$$

(3) The frictional stress (τ_{sl}) in the sliding zone decreases exponentially [19, 148]. However, its variation depends on the value of the parabolic (power) constant (n) which itself is dependent on the variation of the cutting process parameters [49].

$$\tau_{sl} = \mu\sigma_f$$

$$\tau_{sl} = \mu\sigma_{\max}(\frac{x}{l})^n \qquad (0 \le x \le l_{sl}) \qquad (3.12)$$

(4) the frictional stress (τ_{sl}) in the sliding zone is equal to the average dynamic shear stress (τ_a) of the work material,when the bulk deformation of the material begins at the boundary between the sticking and the sliding zone [24].

$$\tau_{sl} = \tau_a \qquad (0 \le x \le l_{sl}) \qquad (3.13)$$

(5) the frictional stress (τ_{st}) in the sticking zone remains constant and equals the average dynamic shear stress (τ_a) of the work material [19, 148].

$$\tau_{st} = \tau_a \qquad (l_{sl} \le x \le l) \qquad (3.14)$$

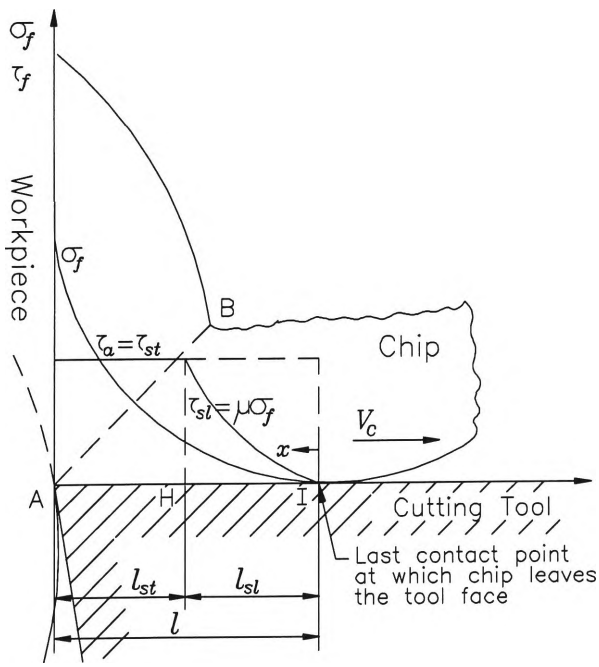

Figure 3.3 Stress distribution on the rake face of the cutting tool.

Based on the logically presented assumptions and the empirical theories on the distribution of normal stress and frictional stress, the total frictional force on the tool-chip interface can be combined by the integration of two forces.

$$F_{tf} = F_{sl} + F_{st}$$

$$F_{tf} = \int_0^{l_{sl}} \mu\sigma_{\max}(\frac{x}{l})^n b dx + \int_{l_{sl}}^{l} \tau_a b dx$$

$$F_{tf} = \tau_a b(l_{st} + \frac{l_{sl}}{n+1}) \qquad \text{(from eq. 3.13 and 3.14)} \qquad (3.15)$$

and the normal force on the tool-chip interface can be presented as :

$$N_{tf} = \int_0^{l} \sigma_f b dx$$

$$N_{tf} = \int_0^{l} \sigma_{\max}(\frac{x}{l})^n b dx = \frac{\sigma_f b l}{n+1} \qquad \text{(from eq. 3.11)} \qquad (3.16)$$

3.2.2.4 Stress Distribution in the Tool Flank and Workpiece Surface Interface

As evident from the experimental results in [109, 149], the relationship of machining forces and flank wear lands increases linearly. When the wear land of tool flank increases, the applied cutting force ($F_{c_{fw}}$), and tangential force ($F_{t_{fw}}$), between the tool-flank and the newly machined surface of the workpiece will have to be considered. In the theoretical analysis in Figure 3.4, the component force generated on the clearance (tool flank) face in the two-dimensional cutting operation is composed of the two types of cutting forces [9, 52].

$$R_{fw} = F_{c_{fw}} + F_{t_{fw}} \qquad (3.17)$$

The total resultant force generated in the tool flank and workpiece interface, called tertiary deformation zone R_t, can be obtained from the component of the resultant force generated in the tool-chip interface zone and the tool flank and workpiece.

$$R_t = R_{tc} + R_{fw} \qquad (R_s = R_{tc}) \tag{3.18}$$

On the basis of the experimental results and physical theories, it can be seen that the increase of the forces created in the shear zone, the tool-chip interface zone, and the tool-flank and workpiece zone, is accelerated due to the influences of each of the plastic deformation zones. The stress distribution between the tool flank and workpiece surface can be presented in terms of the cutting force and the actual contact area

$$\tau_{fw} = \frac{F_{c_{fw}}}{A_{r_{fw}}} \tag{3.19}$$

However, measurement of the cutting force in the tertiary plastic deformation zone ($F_{c_{fw}}$) is impossible because a major cutting force (F_c), measured by using a tool dynamometer, can not be separated into the cutting force of each plastic deformation zone. Accordingly, empirical assumptions and many different experimental techniques have been used for the purpose of comparison with the experimental tests, using fresh tools and worn tools. The chip formation [7] and chip thickness [150], which play an important role in the shear plane angle, are not affected by the cutting forces and wear lands, as identified by the experimental result of this research. Because of this, the frictional stress (τ_{fw}) and sliding speed (V_{fw}), resulting from rubbing action between the tool-flank and the new surface of the workpiece, are assumed as equal to the average dynamic shear stress and the cutting velocity, viz $\tau_{fw} = \tau_a$ and $V_{fw} = V$ [139]. The real area of sliding contact interface $A_{r_{fw}}$, can be described from the analysis of the sliding friction contact in the two metal faces as :

$$A_{r_{fw}} = \eta A_a \tag{3.20}$$

Where, A_a is the apparent area of sliding contact, and η is the proportionality constant of the condition of the two contact faces (ie the roughness of the machined surface) which depends on the properties of the tool and workpiece material. All the possible contact conditions in which the ratios (η) of the real and apparent contact area, are less than or equal to one. The value of η has been taken into account by using the theory of the slipline field combined with the sliding friction of the tool-workpiece interface and the bulk deformation of the workpiece material [151, 152]. Modelling the joint of tool-workpiece interface sliding friction and workpiece material bulk deformation in the metalworking process has been defined in one of three slipline fields as follows :

Table 3.1 Modelling of workpiece bulk deformation in the metal cutting process.

Types of slip line field	Single-fan field	Double-fan field	Full-contact field
Ratio of real contact area	$0 < \eta \leq 0.5$	$0.5 < \eta < 1.0$	$\eta = 1.0$

From the theories described in this section, it can be seen that the realistic applied sliding friction force between the tool-flank and the new surface $F_{c_{fw}}$, is dependent on the average dynamic shear stress (τ_a), width of cut (b), the average wear length of the tool-flank (l_{fw}) and the ratio of contact area (η) and can be expressed by :

$$F_{c_{fw}} = \int_0^{l_{fw}} \eta \tau_{fw} b dx$$

$$F_{c_{fw}} = \eta \tau_a b l_{fw} \tag{3.21}$$

The applied normal force in the tertiary deformation zone is also derived from the relationship between the cutting force and tangential force generated by rubbing action.

$$N_{fw} = \int_0^{l_{fw}} \eta \sigma_{fw} b dx$$

$$N_{fw} = \eta \sigma_{fw} b l_{fw} \tag{3.22}$$

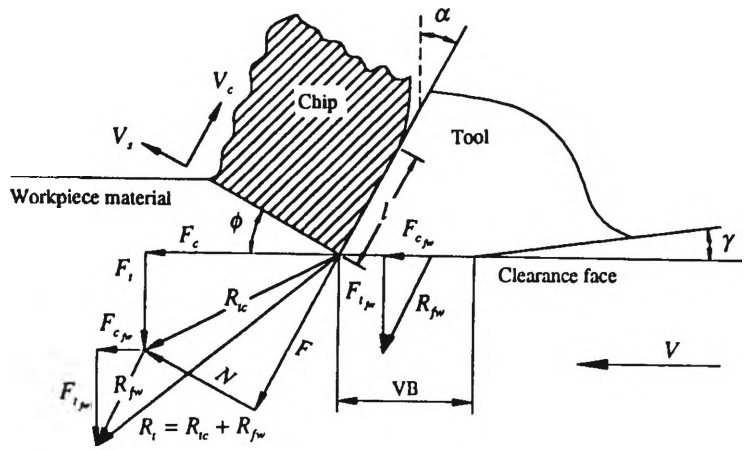

Figure 3.4 Forces acting between the tool-flank and the new surface.

In Figure 3.4, the direction vectors of the forces and velocities were considered relative to the cutting tool face only, but the forces and velocities exerted on the workpiece will be exactly opposite to those shown in Figure 3.4.

3.2.3 Energy Expenditure in Plastic Deformation Zones

Consumption of the total energy in the metal cutting process can be altered through the input variables such as cutting process parameters, workpiece and tool parameters, and conditions of the cutting environment. It is also differently determined in the three plastic deformation zones in accordance with the cutting forces and velocities generated per the unit area. The total energy power (E_t), consumed per unit time during machining, is based on the fundamental power theory and the theoretical

equation which was expressed first by Merchant [6], as described in chapter 2, section 2.4.3.

$$E_t = F_c \cdot V \tag{3.23}$$

The cutting velocity is calculated using the diameter of the workpiece material (d) and the revolutions per minute (N).

$$V = \frac{\pi dN}{1000} (m / \min) \tag{3.24}$$

However, the energy content consumed in the metal removing process can be separated into the three main deformation zones, such as :

(1) the energy rate of shear deformation per unit time E_s, on the shear plane, $E_s = F_s V_s$.

(2) the energy rate of the sticking and sliding deformation per unit time E_{tc}, in the chip-tool interface, $E_{tc} = (F_{st} + F_{sl}) V_c$.

(3) the energy rate of the tertiary zone per unit time E_{tw}, between the tool-flank and workpiece surface, $E_{fw} = F_{c_{fw}} V_{fw}$.

The total energy power consumption rate generated per unit time during the orthogonal machining process can be defined as :

$$E_t = E_s + E_{tc} + E_{fw} \tag{3.25}$$

3.3 MONITORING TECHNIQUES OF THE MACHINING PROCESS

Despite cutting methods of materials having been devised from the earliest of times, in some respects the science of metal cutting processes has not progressed significantly.

The relationships of basic mechanics that are closely related to the generation of cutting forces and the tool wear, have not definitely been identified in relation to the changes of cutting process parameters in the primary, secondary, and tertiary deformation zones.

Acoustic emissions which originate from the elastic stress or pressure waves during dynamic processes in materials, make it possible to analyse AE signals generated in each cutting zone. With use of the acoustic emission (AE) technique which has come out of recent research and development, the metal cutting process methods have advanced more rapidly.

The measurement of acoustic emissions (AE) and cutting forces using a monitoring system such as an AE monitor, a tool dynamometer, A/D converter, IBM personal computer and peripheral devices, is one of the most promising non-destructive testing techniques for the detection of tool failure and progressive tool wear [84, 92-96, 109, 153-158]. In this research work, these two analysis techniques were also utilised simultaneously to observe the cutting forces and acoustic emission signals from the variation of cutting process parameters, and a close relationship was evident in the experimental investigation, as later described in the chapter 4 of an experimental procedure.

3.3.1 Analysis of Acoustic Emissions

Acoustic emission is a transient elastic vibrational energy which is obviously emitted and readily detected from the surfaces of a specimen, as the workpiece material or cutting tool undergoes irrecoverable deformation. The transient elastic stress waves are redistributed to an analogue signal in the form of the strongly fluctuating speed of sound. As presented in the later section 3.4.3, acoustic emission signals in the metal

cutting process are propagated by the two types of irreversible deformation in the internal structure of workpiece material and the cutting tool :

(1) micro-damage such as increase of micro-gaps, movement of dislocation groups, and so on.

(2) macro-damage such as fracture, suddenly crack propagation and progressive wear of the cutting tool.

The AE signals detected in metal cutting operations are usually of low amplitude, are non-periodic, and of a high frequency range from 100 KHz to 1 MHz [140, 155-157]. However, a most useful experiment has been done in the filtered frequency range of 50 to 500 KHz [114] or 100 to 300 KHz [109, 157], which gives confidence in the use of AE sensor dynamics, without any concern that the AE signals are excessively contaminated by lower frequency machine harmonics. The AE signal detected is amplified and fed through a high-pass filter to eliminate any low frequency noise components resulting from vibrations. In addition, the low-pass filter range of 0 to 2 KHz, is usually used to get rid of the high frequency noise components resulting from electric sparks [109, 157-158]. The raw signal must be filtered before it is converted to a digital signal, and the filtered AE signal (the digitised RMS voltage of the AE signal) is fed into a IBM personal computer, as depicted in Figure 4.5 "Experimental Set-up" in chapter 4, section 4.4.2.

3.3.2 Advantages and Troubleshooting Using the AE technique

Among the indirect measurement methods used to observe the variation of dependent output parameters, the analysis of the AE signal detected in metal cutting has several advantages as follows :

- the AE technique allows prediction of the extent of tool wear by means of on-line monitoring without any interruption of the consecutive cutting operation.

- the AE sensor can be completely separated from peripheral obstacles like the interference of the chip formation.
- in order to avoid damage to the workpiece or the machine, the worn cutting tool can be immediately replaced when the range of AE signals is suddenly increased.
- the AE signal monitoring can save machine time because it performs consistently.
- the AE technique reduces economic losses for the following reasons :
  - tool life can be optimised,
  - machine down time is lessened,
  - operator involvement is limited.
- use of the AE technique can be accomplished as a feedback control system in untended machining operations.

However, the AE signal analysis technique which has been proposed for the detection of the tool wear, suffers from the variations of cutting conditions such as cutting process parameters, the geometry of the cutting tool, the workpiece and tool materials.

3.3.3 AE Sources in Turning Operations

Acoustic emission referred to as elastic stress waves, is generated by a sudden release of energy in materials undergoing deformation, fracture or both. In turning operations, AE is generated from several sources, as listed below and illustrated in Figure 3.5.

(1) the primary deformation zone (shear zone)

(2) the secondary deformation zone (tool-chip interface)

(3) the tertiary zone (rubbing and friction between the tool-flank and newly machined surface)

(4) the chip breaking and entanglement of continuous chips on the tool face or workpiece.

(5) tool chipping or fracture.

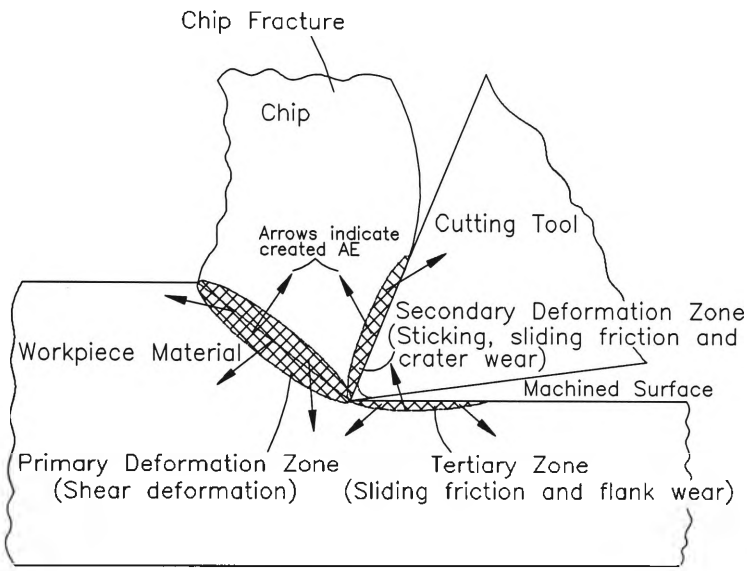

Figure 3.5 Acoustic emissions generation in plastic deformation zones.

3.3.4 Acoustic Emission Signal Measurement

The AE signal generated by the above mentioned five sources [23-24, 138-139, 145, 159] propagates through the cutting tool and can be collected by a piezoelectric transducer mounted at an appropriate place on the tool. The raw AE signals can be confirmed from the screen of an oscilloscope connected to the output signal port in the AE monitor, through the input signal port of the AE sensor. The collected AE signal is non periodic and contains many frequencies, due to the effects of different mechanisms at the sources.

The primary deformation zone, called the shear zone, is the largest source of acoustic signal emission and produces in excess of 75 percent of the total energy content rate when the AE signal attenuattion is not considered , as presented by Cohen [148]. This means that the AE signal is closely related to plastic deformations, in terms of the inherent or physical imperfections of a workpiece material : such as vacancy coalescence, incohesion of inclusions and phase transformation, and abrupt fracture of the workpiece or cutting tool [23-24]. As shown in Figure 3.6, these factors are due to the movement of vacancies and the dislocation motions caused by slips on the grain

boundaries in micro-areas with high stress around the plasticity limit of the work material.

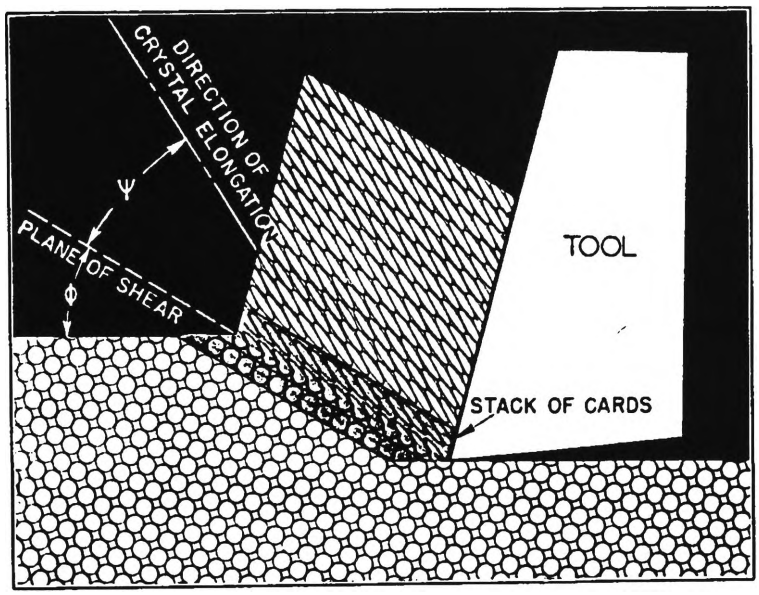

Figure 3.6 Dislocation motion in a metal structure [5].

The acoustic emission signal generated in the secondary deformation zone is closely related to the tool-chip contact length. The AE energy level reflects the existence of the deformed chip sticking and sliding on the rake face of the cutting tool. The gradient of AE_{RMS} generated in the sticking region, increases rapidly due to the contribution of AE from the primary deformation zone (shear zone). The reduction of AE_{RMS} at the higher tool-chip contact length, is based on the lack of bulk deformation by sliding friction [24].

For the successful management of machining processes, an important aspect during cutting operations is the condition of the cutting tool. The cutting action and friction at the two contact surfaces increase the cutting tool temperature and accelerate the physical and chemical wear. As the cutting time elapses, the combined effects of both the crater and flank wear have been observed in the experimental tests, as discussed later in the chapter 4, section 4.5.2 (Figure 4.17). Also in this research, in studying the progressive wear of the cutting tool, it has been found that the growth of both the

crater and flank wear has a much more significant influence on the average AE_{RMS} voltage, with any variation of the cutting process parameters.

In general, as can be seen in Figure 3.7, typical AE signals can be classified into two categories : **continuous signal** or **burst AE signal**. The continuous type of AE signals are associated with plastic deformation due to gradual wear, and the burst type AE signals are based on sudden fractures, the crack growth of the workpiece and cutting tool material. These two types of AE signals are affected by the input variables of cutting process parameters, especially tool geometry, and depend entirely on two types of chip formation : **continuous chip**, which causes to make an entanglement of the chip, and **discontinuous chip**, which results from the breaking of the deformed chip.

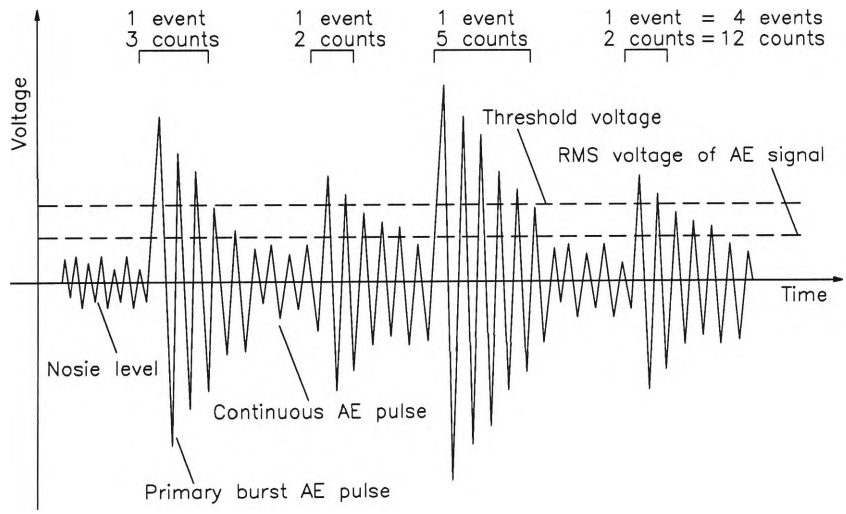

Figure 3.7 The typical AE signals during cutting process.

Acoustic emission signals show dominantly on the screen when the cutting tool is engaging the workpiece material and undergoes irrecoverable deformations. AE signals are conspicuously marked at the partially fractured point of discontinuous chip and at the tangled point of continuous chip [159]. As well, the cutting environment has a significant effect when the lathe or cutting conditions such as chatter, vibration and incomplete set-up are not stable [160].

As presented in the previous chapter, section 2.4.2, one of the most important output variables in estimating the sources of AE signals, is the root mean square (RMS) voltage that converts the AE analogue signals into AE digital signals through the A/D converter. An analysis technique of the RMS voltage of AE signals will be discussed in the next chapter.

3.3.5 Composition of Acoustic Emission Signals

The digitised raw AE signal is expressed as the sound emitted during the machining process, and this is made up from the major factors affecting the AE signal generated through sensing and transmission [122].

$$AE_{RS} = (AE_C \times D_R) + AE_N \tag{3.26}$$

Where AE_{RS}, is the digitised raw AE signal. AE_C is the AE signal generated from the cutting operation. D_R is the transmission response of sensor location. AE_N is the background noise generated during cutting. The actual AE signal obtained via the AE transducer is considered to be the true AE signal only, as :

$$AE_{ts} = (AE_C \times D_R) - AE_N \tag{3.27}$$

The unwanted noise from the detected AE signal is negligible because, (1) the amount of the background noise is a very small value as compared with the realistic raw AE signal and, (2) the background noise can be eliminated using the appropriate filtering device such as high-pass filtering, low-pass filtering or band-pass filtering [24, 109, 122, 145, 154-158]. The true AE signal AE_{ts}, is generally represented as follows :

$$AE_{ts} = AE_C \times D_R \tag{3.28}$$

3.3.6 *Acoustic Emission Signal Function*

The general signal function in alternating current circuits is represented by an ideal amplitude such as a sinusoidal. However, as shown in Figure 3.8, the typical raw AE signal is composed of the component of the exponential curve and the sinusoidal curve which is more damped, observed as a raw AE signal triggered in the oscilloscope, rather than the ideal sinusoidal function.

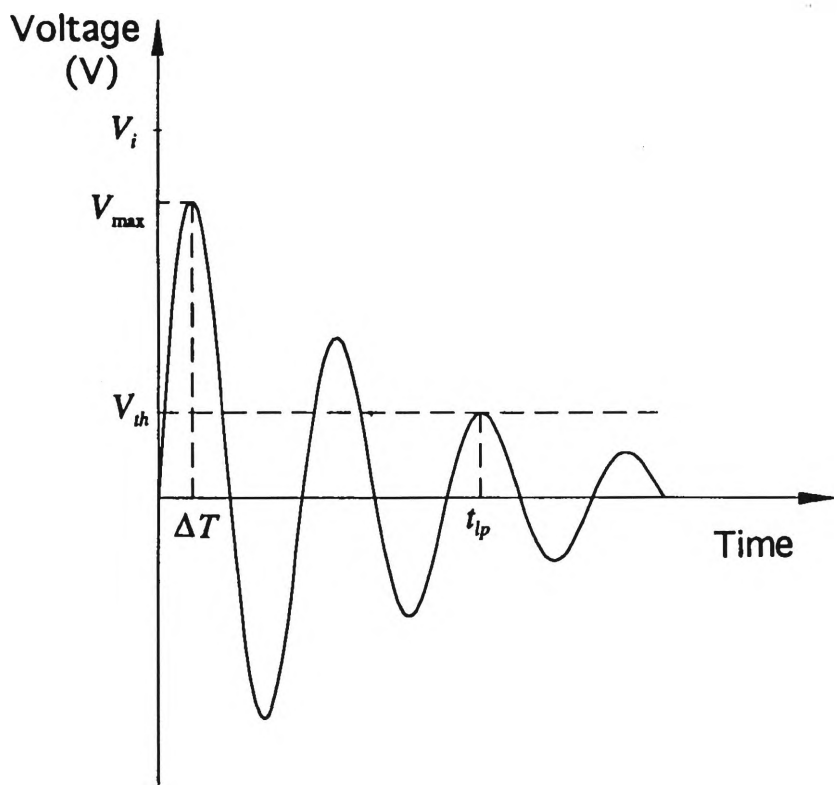

Figure 3.8 Definition of the typical AE signal function over the threshold voltage.

The AE signal function can be applied by using the theory loop of alternating current circuits, as has been described by Teti and Dornfeld [107] and Tetelman and Evans [161].

$$V(t) = V_i e^{-kt} \sin \varpi t \tag{3.29}$$

Where V_i is the initial voltage of AE signals. k is the damping constant. ϖ is the angular frequency ($\varpi = 2\pi f_a$). f_a is the measured linear frequency per unit time($f_a = \frac{1}{\Delta T}$).

In the AE signal function, formed on the basis of the typical amplitude of AE signals, determination of the initial voltage, the damping constant and threshold voltage plays an major role in the analysis of the AE signal function. Through the development of these three basic models, it is possible to predict the voltage of the raw AE signal displayed on the screen of an oscilloscope during the practical cutting test, and to better understand the relationship between the digitised AE_{RMS} value and the generated AE signal. As schematically depicted in Figure 3.8, the triggered raw AE signal function theoretically assumed that the sine function is equal to be 1 (viz, $\sin \varpi t = 1$). The maximum and initial voltage of the signal created for the constant period of time can be expressed as :

$$V_{\max} = V_i e^{-k\Delta T} \tag{3.30}$$

$$V_i = V_{\max} e^{k\Delta T} \tag{3.31}$$

The damping constant formula k, can be derived from the differential of the basic AE signal function of the equation (3.29) and the following predictions :

$$\frac{dV}{dt} = V_i[e^{-kt}(\varpi \cos \varpi t) + ke^{-kt}(\sin \varpi t)] \quad (V_i \neq 0 \text{ and } e^{-kt} \neq 0) \tag{3.32}$$

From the equation (3.32), the component function of sine and cosine must be equal to zero, namely : $(\varpi \cos \varpi t - k \sin \varpi t) = 0$. Accordingly, the damping constant can be expressed by the substituted the linear frequency (f_a) and the angular frequency (ϖ) :

$$k = \frac{\varpi \cos \varpi t}{\sin \varpi t} = \frac{2\pi f_a \cos 2\pi f_a t}{\sin 2\pi f_a t} = \frac{\frac{2\pi}{\Delta T}\cos(\frac{2\pi t}{\Delta T})}{\sin(\frac{2\pi t}{\Delta T})} \tag{3.33}$$

The equation of the threshold voltage can be derived from the assumption that $\sin \varpi t = 1$ [107], and expressed by the instant time when the last peak reaches the preset threshold value (t_{lp}).

$$V_{th} = V_i e^{-kt_{lp}} \text{ or } t_{lp} = \frac{1}{k} \ln \frac{V_i}{V_{th}} \tag{3.34}$$

The number of counts measured for a single event which is over the threshold value can be described as :

$$N = f_a t_{lp} = \frac{\varpi t_{lp}}{2\pi} = \frac{\varpi^2 \cos \varpi t}{2\pi \sin \varpi t} \ln \frac{V_i}{V_t} \tag{3.35}$$

Deciding the threshold voltage (V_{th}) is also one of the most important factors in an experimental stage, because it exerts a strong influence on the number of counts per a signal event of amplitudes, when the peaks are over the preset threshold voltage. However, as can be seen in equation (3.34), V_{th} can not be predicted without the values of the initial (V_i) and maximum (V_{max}) voltages and damping constant (k).

CHAPTER FOUR

DEVELOPMENT OF THEORETICAL MODELS FOR PREDICTION OF ACOUSTIC EMISSIONS

4.1 INTRODUCTION

Cutting processes, such as turning on a lathe, drilling, milling, or thread cutting which remove material from the surface of the workpiece, are among the most important of manufacturing operations. Because of the number of variables involved and the variety of tool and workpiece materials and conditions available, the analysis of the cutting process is very difficult. The most important task in the cutting process is to understand how cutting process parameters affect acoustic emissions, cutting forces, power consumption, temperature rise, the desired surface finish and dimensional accuracy of the workpiece, and how they significantly influence the development of mathematical models for prediction of the cutting tool condition. The objectives were to fully characterise cutting process parameters for the development of theoretical mathematical models which study the influences of cutting process parameters on the level of the RMS voltage of acoustic emission signals.

This chapter presents theoretical mathematical models for prediction of AE signals which are capable of monitoring the condition of the cutting process based on the variation of AE_{RMS} voltage. The analytical AE models, based on the basic mechanics

of the cutting process, were derived from the energy rate consumed in each deformation zone, related to the dependent output variables such as the influences of stresses, strain rate, the deformed volume of the workpiece material, cutting forces and velocities. The deviation of a realistic seize ratio and the parabolic constant for the optimal cutting process in the tool-chip interface play an important role in the development of theoretical models. The aims of this chapter are to set out the characteristics of the developed mathematical models and to identify the various problems that result from the previously developed models and establishing guidelines for the most effective cutting operations.

4.2 ANALYSIS OF AE SIGNALS USING THE RMS VOLTAGE

The RMS voltage of AE signals is to be measured from the AE analog signals which are being transmitted from the AE sensor, and it is convenient to investigate the relationship of the main problems for unmanned control process. The AE_{RMS} value of the AC signal can be directly expressed relative to the AE_{RMS} value of the DC signal through the AE monitor, A/D converter and peripheral devices, without converting between AC signals and DC signals. As discussed in chapter 2, section 2.4.2, among the several analysis methods of AE signals, the most common and reliable analysis technique for monitoring the cutting condition is to estimate the level of AE_{RMS} voltage. Generally, the RMS voltage of emission signals can be derived from two types of signal function : an ideal signal function and a typical AE signal function. The AE_{RMS} voltage is widely used to establish a comprehensive analytical relationship between acoustic emissions and the cutting process parameters.

4.2.1 Ideal Signal Function

An AC voltage that flows from a power socket is equivalent to the DC voltage that is fed into the signal generator (oscilloscope), when employing the same electrical circuit

for the same period time. The equivalent voltage can be readily identified through a simple test and calculation using the multi-meter tester to compare the same energy dispersion between the AC and DC voltage. As shown in Figure 4.1, the RMS voltage value of any quantity that varies the sinusoidal function, equals to the maximum voltage value of that quantity divided by $\sqrt{2}$ [162]. In other words, the RMS voltage that comes from the outport of the oscilloscope, is the same as the maximum output voltage indicated on the screen of the oscilloscope divided by $\sqrt{2}$. Generally speaking, the RMS voltage based on the sinusoidal function which is an ideal electrical signal wave, is represented as :

$$V_{RMS} = \frac{V_{\max}}{\sqrt{2}} \tag{4.1}$$

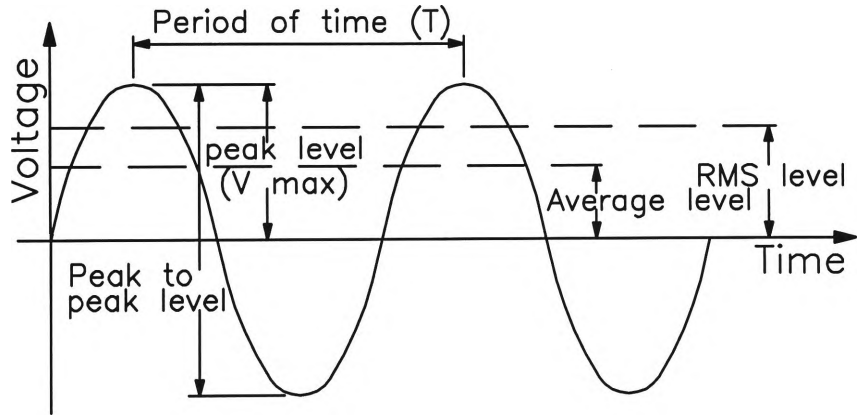

Figure 4.1 An ideal sinusoidal function of electrical signal waves.

4.2.2 *Quantitative Relationship Between the AE_{RMS} Voltage of AE Signals and the Consumed Energy Rate*

Acoustic emission signals can be monitored in several ways. The RMS voltage, an indicator of the energy of AE signals, has been observed to have many advantages over count and count rate monitoring techniques [163]. A proper technique for analysing and interpreting the raw AE signal created in the metal cutting process, is to estimate the measurement of the energy content corresponding to the value of the

digitised AE signal (AE_{RMS} voltage). A complete analysis of the cutting process requires the establishment of quantitative relationships between all the independent input parameters and the dependent output parameters. The digitised AE_{RMS} voltage is to be converted from the analogue signal to the numeric value, and is quantitatively evaluated by the AE signal emitted for the period of time. The energy expenditure ΔE, during an interval time ΔT, can be related to the RMS voltage of the AE signal as.

$$(V_{RMS})^2 \propto \frac{\Delta E}{\Delta T} \tag{4.2}$$

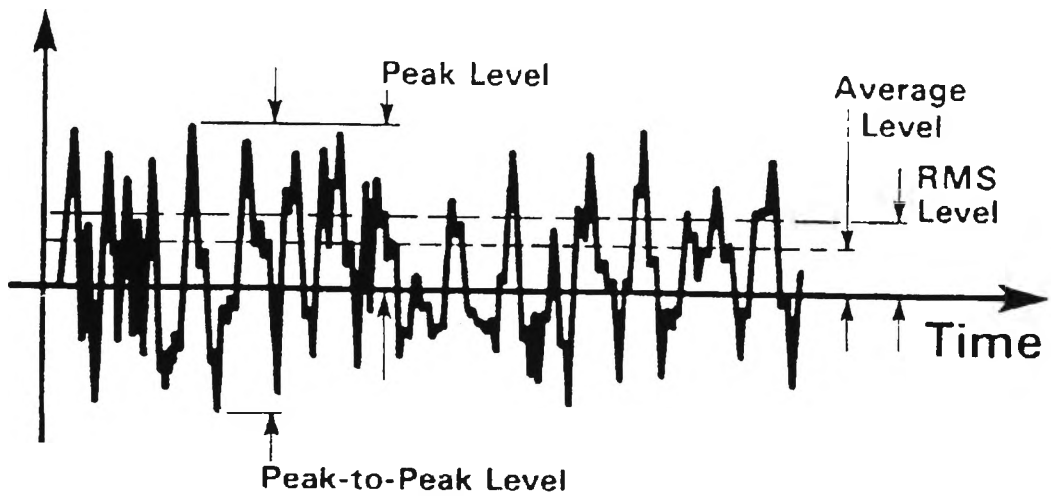

Figure 4.2 The schematic figure of typical AE signals [164].

Definition of the AE signal dissipated in the period of time interval can be derived from the quantitative relationship with the AE_{RMS} voltage and the consumed energy rate using the steps following :

(1) $V(t)$: AE signal function in the unit time

(2) $V^2(t)$: square of the AE signal function

(3) $\frac{1}{\Delta T}\int_0^{\Delta t} V^2(t)dt$: the mean energy value of the dissipated signal in an interval time

(4) $\sqrt{\frac{1}{\Delta T}\int_0^{\Delta T} V^2(t)dt}$: RMS value or energy rate in a machining process

$$V_{RMS} = \sqrt{\frac{1}{\Delta T}\int_0^{\Delta T} V^2(t)dt} \tag{4.3}$$

4.2.3 Energy Rate in the Primary Deformation Zone

The energy rate in the shear zone (E_s), based on the dislocation motion, can be simply determined by the shear force, shear velocity, strain rate, shear plane thickness and the deformed volume of the workpiece.

$$dE_s = dF_s \cdot V_s = \tau_s \cdot dA_s \cdot (\dot{\gamma} \cdot \Delta Y)$$

$$E_s = \int_U \tau_s \dot{\gamma} dU_s = \tau_s \dot{\gamma} U_s \tag{4.4}$$

Where $\dot{\gamma}$ is the shear strain rate ($\dot{\gamma} = \frac{V_s}{\Delta Y}$), ΔY is the thickness of a slip plane produced by the dislocation motion in the shear zone, and U_s is the deformed volume of the workpiece material on the shear plane ($U_s = A_s \cdot \Delta Y$). So as to determine the energy rate in the shear plane, it is assumed that the average dynamic shear stress and shear strain rate are constant under the uniformed stress distributions [137, 144]. The relationship between the average dynamic shear stress (τ_a), called shear strength of workpiece, and the shear stress, can be expressed using the identified experimental result as $\tau_a = \tau_s$.

The energy rate consumed in the shear zone can be described under the uniformed stress distributions by using the basic models of Ernst and Merchant [5, 6].

$$E_s = \tau_a bt \frac{\cos\alpha}{\sin\phi\cos(\phi - \alpha)} V \tag{4.5}$$

4.2.4 Energy Rate in the Secondary Deformation Zone

As described in the previous section of 4.2.3, the total friction force (F_{tc}) of the two regions distributed on the tool face is derived from the relationship between the average dynamic shear stress and the normal stress as follows :

$$F_{tf} = \tau_a b(l_{st} + \frac{l_{sl}}{n+1}) \tag{4.6}$$

The energy rate (E_{tc}) consumed in the sticking and sliding zones can be estimated by using the total friction force F_{tf} and chip velocity V_c, as below :

$$E_{tc} = \tau_a b(l_{st} + \frac{l_{sl}}{n+1}) \cdot \frac{\sin\phi}{\cos(\phi - \alpha)} V \tag{4.7}$$

As can be seen from the above mentioned equation (4.7), the energy generation in the tool-chip interface zone can be predicted more accurately by using the seize ratio (l_{st}/l and l_{sl}/l) distributed in the sticking and sliding regions and the value of parabolic constant (n).

4.2.5 Seize Ratio and Parabolic Constant for Stress Distribution in the Secondary Deformation Zone

The seize ratio, which indicates the distribution of sticking zone and sliding zone contact lengths at the tool-chip interface, plays an important role in the prediction of the consumed energy rate (equation 4.7). In the present research, it was possible to estimate realistic values of this seize ratio by determining the value of the parabolic constant. Considering the non-uniformly distributed normal stress in Figure 4.3, the seize ratio can be determined by using the Spandrel formula of a n-th degree parabola which applies to the generating point of an inertia moment on the centroid [165].

$$l_{sl} = \frac{(n+1)}{n+2} l \tag{4.8}$$

$$l_{st} = l - l_{sl} = \frac{l}{n+2} \tag{4.9}$$

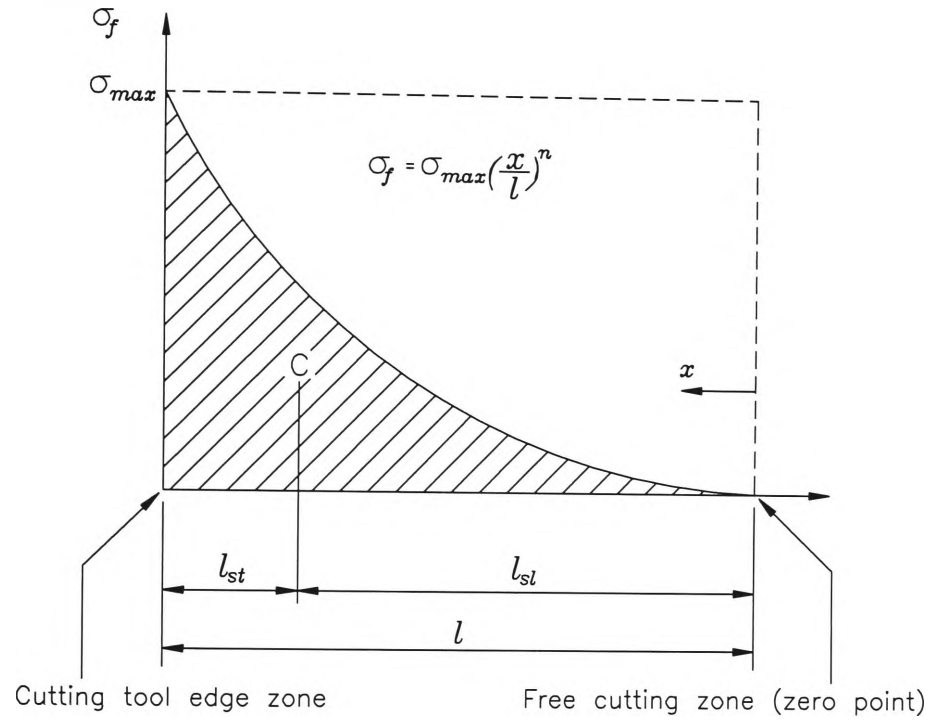

Figure 4.3 Application of the Spandrel formula of the normal stress generated on the tool rake face.

The seize ratio of the contact length in the sticking and sliding zone which depends particularly on the variation of the cutting process parameters, has an critical influence on the wear of the tool. Increasing the normal stress with the decreased distance rate of x (sliding contact length) will generate high temperature and pressure due to the increasing cutting force [148]. Therefore, to reduce the chip contact length of the sticking zone on the rake face will result in longer tool life, good surface finish and lower power consumption. These can be improved by the selection of the best fit cutting parameters, tool and work materials, and by using artificially controlled geometry of cutting tools.

The contact lengths of the two regions (l_{st} and l_{sl}), however, can not be computed without the value of the parabolic constant (n). Distribution of normal stress, can be determined, based on the variation of n value [19, 49, 148]. The formula for estimation of the parabolic constant can be derived from the frictional force relationships on the tool-chip interface. The friction force F, based on the Coulomb's laws of friction [5, 6], can be assumed as equal to the total amount of friction force F_{tf}, estimated by Zorev's relationships [19]. The force F can be computed by using the cutting and tangential force components measured by a 3D dynamometer in the experiments. Hence,

$$F = F_{tf}$$

$$F_c \sin\alpha + F_t \cos\alpha = \tau_a b(l_{st} + \frac{l_{sl}}{n+1}) \tag{4.10}$$

By substituting the equations (4.8) and (4.9) to equation (4.10), the parabolic constant can be given by :

$$n = \frac{2\tau_a bl}{F_c \sin\alpha + F_t \cos\alpha} - 2 \tag{4.11}$$

Likewise in the derived equation (4.11), the parabolic constant (n) can be obtained by the relationship between the average dynamic shear stress of a metal, tool-chip contact length and the mechanics of the friction force at the tool-chip interface zone. The parabolic constant will be determined based on the experimental measurements, and these realistic values will then be employed in the model for prediction of AE_{RMS}.

4.2.6 Energy Rate in the Tertiary Zone

As experimental results by previous researchers [139-140, 153-155] which the worn cutting edges produce higher energy of acoustic emission signals than the sharp cutting tool edge, the wear land of tool flank (VB) plays a major role in the energy consumption between the tool flank and the newly machined workpiece surface. Based on the theoretical analysis in the section 3.2.2.4 of chapter 3, the energy rate consumed in the tertiary zone E_{fw}, can be represented as given by :

$$\dot{E}_{fw} = dF_{c_{fw}} \cdot V_{fw}$$

$$\dot{E}_{fw} = \tau_{fw} dA_{r_{fw}} \cdot V$$

$$E_{fw} = \eta \tau_a b l_{fw} V \qquad (4.12)$$

4.3 DEVELOPMENT OF AE MODELS FOR PREDICTION OF THE AE_{RMS} VOLTAGE

For the application of AE techniques between the cutting mechanics and the consumed energy rate, the fundamental nature of metal deformation and the geometry of metal cutting, which is extremely dependent on variations of the cutting process parameters, need to be illustrated so as to improve the knowledge base of machining operations. The major sources of the acoustic emission signals are the dislocation of the internal metal structure of the workpiece material and the progressive wear of the cutting tool. Therefore, the development of AE models has been applied in the three deformation zones

As summarised in the literature survey, in chapter 2, section 2.4.3, "developed models for prediction of AE_{RMS}", a few models which relate the RMS voltage of AE signals

with machining parameters and work material properties have been developed [23-24, 138-139, 145]. These AE models have been derived from the consumed energy rate in each deformation zone, and rely upon the work of plastic deformation caused by the influences of cutting forces and velocities. The model for AE developed in the present research, also relies on the consumed energy and the plastic deformation work in various zones of the turning operation. However, this model was devised using a more precise seize ratio on the tool-chip contact length (ie, distribution ratio of sticking and sliding region of chip in the secondary deformation zone) and realistic values of signal attenuation constants in various deformation zones.

4.3.1 AE_{RMS} and Energy Rate in Plastic Deformation Zones

The theoretical AE_{RMS} voltage during the orthogonal cutting operation can be computed by using the combined total energy content consumed in various plastic deformation zones, as derived from the three major irrecoverable deformation zones described in chapter 3, sections 3.2.2.1 to 3.2.2.4. The observed AE_{RMS} voltage is however, entirely different when compared with the theoretically calculated AE_{RMS} voltage. The variance between the two values is assumed to be caused by AE signal losses during propagation from the various zones.

4.3.1.1 A New Model for Prediction of Acoustic Emissions

The condition of the tool is an important aspect of machining operations. When a new tool is employed for the orthogonal turning operation, the tool has no crater wear or flank wear land at the initial cutting stage. In the present research, fresh (sharp) tools have been used for conducting tests and the wear land of the tool flank has been measured. After that, measured worn (blunt) tools were employed in an attempt to better understand the generation of AE signals in turning operations However, the cutting conducted for each set of observations employing fresh tools was very brief,

and did not allow any development of crater or flank wear land on the tool. Hence, in the absence of any rubbing in the tertiary zone, the AE generated in this area will be considered negligible. The relation for prediction of AE_{RMS} voltage (V_{RMS}) during the orthogonal cutting can be expressed as :

$$V_{RMS} = C\sqrt{\{\tau_a bV[C_1 \frac{f\cos\alpha}{\sin\phi\cos(\phi-\alpha)} + C_2(\frac{2l}{n+2})\frac{\sin\phi}{\cos(\phi-\alpha)}]\}} \quad (4.13)$$

AE_{RMS} measured in the experiments is detected by a sensor placed at a suitable location on the tool holder. As the signal propagates from the three deformation zones to the tool and then to the transducer, transmission losses occur [23-24, 138-139, 145]. Hence C is the constant of proportionality, C_1 and C_2 are the signal attenuation constants to compensate for the transmission losses from primary and secondary deformation zones respectively.

Association of tool-chip contact length with forces, temperature and wear makes it an important factor in the analysis of orthogonal cutting operations. A realistic chip contact length is very vital because it exerts a significant influence on the energy rate in the secondary deformation zone. Precise estimation of tool-chip contact length is therefore necessary for accurate prediction of acoustic emissions in turning operations. An in situ contact length monitoring technique was employed by Venkatesh and Chandrasekaran [166] for measurement of contact length in turning operations. Models for prediction of tool-chip contact length have also been developed by some researchers. Rubenstein's model [166] for estimation of contact length ($l = m\frac{\sin(\phi+\beta-\alpha)}{\sin\phi\cos\beta}$) has been found to be reasonably accurate. When the chip contact length as estimated by Rubenstein [46] is substituted in equation (4.13). The V_{RMS} can be expressed as :

$$V_{RMS} = C\sqrt{\{\tau_a bV[C_1 \frac{f\cos\alpha}{\sin\phi\cos(\phi-\alpha)} + C_2\frac{2mf\sin(\phi+\beta-\alpha)}{(n+2)\cos\beta\cos(\phi-\alpha)}]\}} \quad (4.14)$$

For a better contribution of AE model developed in this research work, computational statistical analysis techniques were employed to obtain the mean values of coefficient C_1 and C_2. The values of the coefficients obtained by the computational work are C_1=0.00098 and C_2=0.00157 and C=1.007. These values are for fresh tools with no wear-land on the tool-flank, and the source of these values will be explained in the next section, 4.3.2.

4.3.1.2 A New Model for On-Line Monitoring of Tool Wear in the Cutting Process

As shown in Figure 4.4, there are two types of wears on the cutting tool : regular and irregular [21]. The regular tool wear belongs to the crater wear on the rake face of the tool and the flank wear on the primary cutting edge. The flank wear often accompanies notch wear and groove wear occuring at the end of the flank wear land, and . Irregular wear includes the chipping, cracking and breaking of the cutting edge, which can usually be avoided according to the determination of proper cutting process parameters, tool and workpiece material.

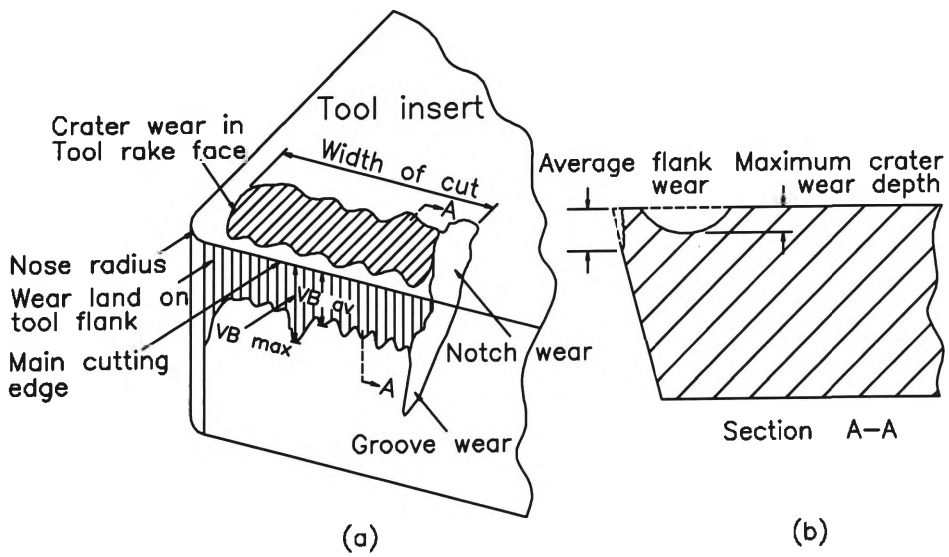

Figure 4.4 Geometry of tool wear. (a) Wear zones on cutting tools. (b) Tool wear parameters.

During the machining process, most tool failure exists either by fracture or by progressive wear. The actual deterioration of cutting tool is due to the gradual wear rather than a sudden tool fracture. Moreover, the progressive deterioration of the tool flank exerts a strong influence on the newly machined surface quality and the dimensional integrity. The flank wear is caused by abrasive mechanisms [80], when the tool flank rubs on the newly formed strain-hardened surface of workpiece.

The formation of crater wear is based on the high pressure and temperature generated by the action of the chip flowing along the tool rake face [149]. The crater wear on the rake face can also result in early catastrophic tool failure from the round and edge breakage of the minor cutting edge, due to the weakness of the cutting edge by the sticking and sliding of chip and the rubbing on the tool flank.

As time elapses, both the crater wear and the flank wear are developed simultaneously, crater wear in the secondary deformation zone and flank wear in the tertiary zone. The flank wear has been observed to increase the AE_{RMS} voltage, whereas the growth of crater wear decreases AE_{RMS} voltage, due to increase in the effective tool rake (+) angle [139]. Hence the combined influence of the growth of both the crater and flank wear on the AE_{RMS} is very complex. A more generalised formula considering the wear land of tool flank and the constant of signal attenuation in the plastic deformation zones, can be presented as follows :

$$V_{RMS} = C\sqrt{\{\tau_a bV[C_1 \frac{f\cos\alpha}{\sin\phi\cos(\phi-\alpha)} + C_2 \frac{2mf\sin(\phi+\beta-\alpha)}{(n+2)\cos\beta\cos(\phi-\alpha)} + C_3\eta l_{fw}]\}} \quad (4.15)$$

Lan and Dornfeld [139] employed lead break calibration tests to estimate the value of C_1 ($0.2 \le C_1 \le 0.25$), and made assumptions for the values of C_2 and C_3 ($C_2 = C_3 = 1$). The values of the coefficients obtained by the computational work, including the value

of the AE signal attenuation constant in the tertiary zone, are C_1=0.00091, C_2=0.00142, C_3=0.00066 and C=1.002. These values are for the initial cutting with the measured flank wear land (VB), and show a big difference from the values assumed by Lan and Dornfeld.

The predicted AE_{RMS} values were computed on assumptions that : (1) the mean value of the C is equal to 1 due to the result of the computational work, (2) the ratio (η) of the real and apparent contact areas between the sliding friction of the tool-workpiece interface and the bulk deformation of the workpiece material is also equal to 1.

Based on the full-contact SLF theory of Kopalinsky et al [151] and Li [152], as described in the previous chapter 3, section 3.2.2.4, the value of η can be derived from the relationship between the apprent contact pressure (p_a) and the frictional shear stress in the tool-workpiece interface. The experimental results of Kopalinsky have shown that the real contact area is the same as the apparent contact area, in accordance with the increasing apprent contact pressure. This situation can be applied to the flank wear land-workpiece contact in tertiary zone in orthogonal cutting operations.

In the developed equation (4.15), the energy consumption (the AE_{RMS} voltage) of the tertiary zone is significantly dependent on the cutting force ($F_{c_{fw}}$) generated in that zone. The cutting force in the tertiary zone depends on the apparent contact pressure and the friction coefficient, viz $F_{c_{fw}} = \mu_{fw} p_a$. The cutting force increases linearly with the increasing the flank wear land (l_{fw}), as evident from the experimental result in this chapter, section 4.5.2 (Figure 4.15). From this result, it can be seen that an increase in the flank wear land causes an increase in the apparent contact pressure in the tertiary zone. An increase of the apparent contact pressure with the increasing flank wear places the tool flank in full-contact field with the workpiece surface. Therefore, it is reasonable to assume that the ratio of the real and apparent contact area in the tool-

workpiece interface (η) is equal to 1 when applied to the full-contact field theory of Kopalinsky and Li.

4.3.2 Determination of AE Signal Attenuation Constants

The theoretical equation (4.15) derived from the relationships between the consumed energy rate and experimental AE_{RMS} voltage observed in the variations of the basic cutting process parameters, can be defined in the form of the basic regression model for linear analysis. The objective of the multiple regression analysis is to establish the ideal model with the statistically fitted AE signal attenuation constants. The mean value of AE signal attenuation constants was determined by computation, when the experinental AE_{RMS} values were compared with the theoretical AE_{RMS} values. The correlation matrix related to the input and output variables, should be arranged to produce the best unbiased evaluating in the least squares estimation, and this substantially affects the result of the regression analysis. Steps for a regression analysis using the SAS are as follows :

(1) Prediction of a regression model,

(2) Construction of the correlated matrix,

(3) Writing the simplified program,

(4) Running the program,

(5) Analysis of the statistically fitted data.

The simplified fundamental structure of the linear regression analysis model can be defined as :

$$(V_{RMS})^2 = X_0(C_1X_1 + C_2X_2 + C_3X_3) \tag{4.16}$$

$$Y = C_1X_1 + C_2X_2 + C_3X_3 \tag{4.17}$$

$$(V_{RMS})_{Expt} = C\,(V_{RMS})_{Theo} \tag{4.18}$$

From the correlation matrix of the equation (4.17) applied in the three plastic deformation zones, it can be seen that the model is in the type of a simple order equation in not having an intercept. The equation (4.17) was substituted from the equation (4.15) as below :

$$Y = \frac{(V_{RMS})^2}{X_0} \tag{4.19}$$

$$X_0 = \tau_a bV \tag{4.20}$$

$$X_1 = \frac{f\cos\alpha}{\sin\phi\cos(\phi-\alpha)} \tag{4.21}$$

$$X_2 = [\frac{2mf\sin(\phi+\beta-\alpha)}{(n+2)\cos\beta\cos(\phi-\alpha)}] \tag{4.22}$$

$$X_3 = \eta l_{fw} \tag{4.23}$$

As mentioned in the previous section, estimation of coefficients C, C_1, C_2, C_3, was separated into two stages to decide the range of the value of coefficients when using both fresh tools and worn tools. The numeric results of the parameters (C, C_1, C_2, C_3) were produced to estimate the theoretical models, which it is possible to compare the computed AE_{RMS} value with the measured AE_{RMS} value. The results were based on the introduction of modern statistical techniques (SAS) using the correlation matrix (sample data) obtained from the relationship of independent input and dependent output parameters [167].

4.4 EXPERIMENTAL PROCEDURE

The experiments were separated into two stages. The first stage was independent of the flank wear, and the second stage took into consideration the flank wear. The experimental work was carried out to investigate the relationship between acoustic emission, tool condition and the cutting process parameters under general cutting conditions. The collected and stored AE signal data were observed to verify any trends between the cutting process parameters and the AE_{RMS}.

The tests of the first stage using fresh tools, were plotted to analyse the behaviour of the dependent output variables, such as the AE_{RMS} voltage, cutting force, seize ratio in the sticking zone and shear angle, with the variations of the basic cutting process parameters.

The wear tests were carried out to measure the wear land of tool flank at the second stage of the experimental work. After that, the experiments using the measured worn tools were observed in order to isolate the effects of the tool wear on the AE_{RMS} voltage and the variation of cutting process parameters. The purpose of this experimental stage was to study the influences between the altering basic cutting process parameters and increasing tool flank wear lands (initial, gradual and final wear). The experiments were based on the conditions of identical tests as in the first stage of experiments.

4.4.1 Experimental Design

Experiments were performed to verify the developed theoretical models under realistic cutting conditions. The experimental design for orthogonal cutting operations was constructed using a wide range of cutting conditions to obtain the actual RMS voltage of the sensed AE signal.

As summarised the experimental design and results in Appendix B, **the cutting test ranges of the first experimental stage** were based on the simple design (7x5x3x1) of experiments for the correlation matrix, $\psi(f,V,\alpha,b)$ of the basic cutting parameters. The feed rates and cutting speeds employed, varied from 0.15 to 0.45 mm/rev and 150 to 250 m/min. The rake angles ranged from -5° to 5°.

Previous researchers [23-24, 138-139] verified their models through cutting tests which mainly employed positive rake angle tools. The negative rake angles more commonly used in modern industry were employed in the present research. The bottom of the tool shank and the tool holder bracket, was ground to make a wide range of tool rake angles (-5°, 0° and 5°).

Hot rolled seamless pipe made of ASTM A106-51T steel, with an outside diameter of 114.3 mm and thickness of 6 mm, was used as workpiece material. However, the pipe was turned to reduce its thickness from 6 mm to 2.5 mm and to avoid the tool fracture at the high speed during orthogonal cutting operations. The specifications of the workpiece material are given in tables 4.1 and 4.2.

Table 4.1 The chemical composition of an A106-51T

Carbon (C)	Manganese (Mn)	Phosphorous (P)	Sulfur (S)	Silicon (Si)
0.27 %	0.35-1.0 %	0.04 %	0.05 %	0.12 %

Table 4.2 Mechanical properties of an A106-51T

Tensile Strength		Yield Strength		Hardness (BHN)	
Mpa	Kpsi	Mpa	Kpsi	Hot Rolled	Cold Drawn
414	60	241	35	121	149

The indexable, CVD Tri-phase coated carbide inserts of Kennametal TPG-432 (KC-810) grade, corresponding to the ISO grade known as P10-P30, with no chip breaker, were employed at 11° clearance angle. The specifications of the workpiece material, tool material, the geometry of tool insert and tool holder are listed in tables 4.3 to 4.5.

Table 4.4 The Geometry of a tool insert, TPGN 220408T

Insert Shape	Nose Angle	Relief Angle	Tool thickness	Nose Radius
Triangular	60^0	11^0	4.76 mm	0.8 mm

Table 4.3 Tool grade and composition

Tool Insert		Tool Grade		Composition
ISO	ANSI	ISO	ANSI	CVD Tri-phase
TPGN 220408T	TPG - 432T	P 10 - P 30	C 6 - C 7	TiC/TiC-N/TiN

Table 4.5 Identification of tool holder, CTGPR -2525 M22 (Right hand)

Type of angle	Side cutting edge angle	Insert clearance angle	Cutting edge length
Positive	5°	11^0	22 mm

The second stage experiments were also carried out to identify the validity of the theoretical model developed with considering the wear land of tool-flank under particular cutting conditions. The cutting conditions were determined to simulate the experimental conditions as closely as possible to practical machining operations.

The cutting tests range of the basic cutting process parameters was based on the simple factorial design (3^3x2) of experiments for the correlation matrix, $\psi(f,V,\alpha,l_{fw},b)$. As listed in table 4.6, the feed rates and cutting speeds varied in the range of low, intermediate and high. The rake angles employed in the experiment were at the positive and negative rake angle (5^0 and -5^0).

Table 4.6 Cutting process parameters and limits

Items		Ranges			Remarks
Input Variables	Units	Low	Intermediate	High	Coated tool
Feed rate	mm/rev	0.15	0.3	0.45	-
Cutting speed	m/min	150	200	250	-
Rake angle	deg	-5	-	+5	Ground toolholder
Wear land	mm	0.289	0.493	0.687	-
Width of cut	mm	2.5	2.5	2.5	-

4.4.2 Experimental Set-up

An Hitachi Seiki Hitec CNC Lathe (Hi 20 SII) was employed in conducting the cutting tests for verification of the model. Figure 4.5 shows a schematic arrangement of the experimental set-up. The modified tool holder along with the insert is mounted on a 3D Kistler 9272 dynamometer which is rigidly bolted on the CNC lathe turret through a specially designed bracket.

A piezo-electric AE transducer, PAC I15I (150KHz, Resonant frequency) with an inbuilt preamplifier was mounted on the ground and finished end of the tool holder for collection of acoustic emissions generated during the turning operations.

The amplified force signals and the collected AE signal (40 dB Gain) are all synchronously digitised through a 4 channel A/D converter and stored on the hard disk of an IBM 386 computer for analysis at a later stage.

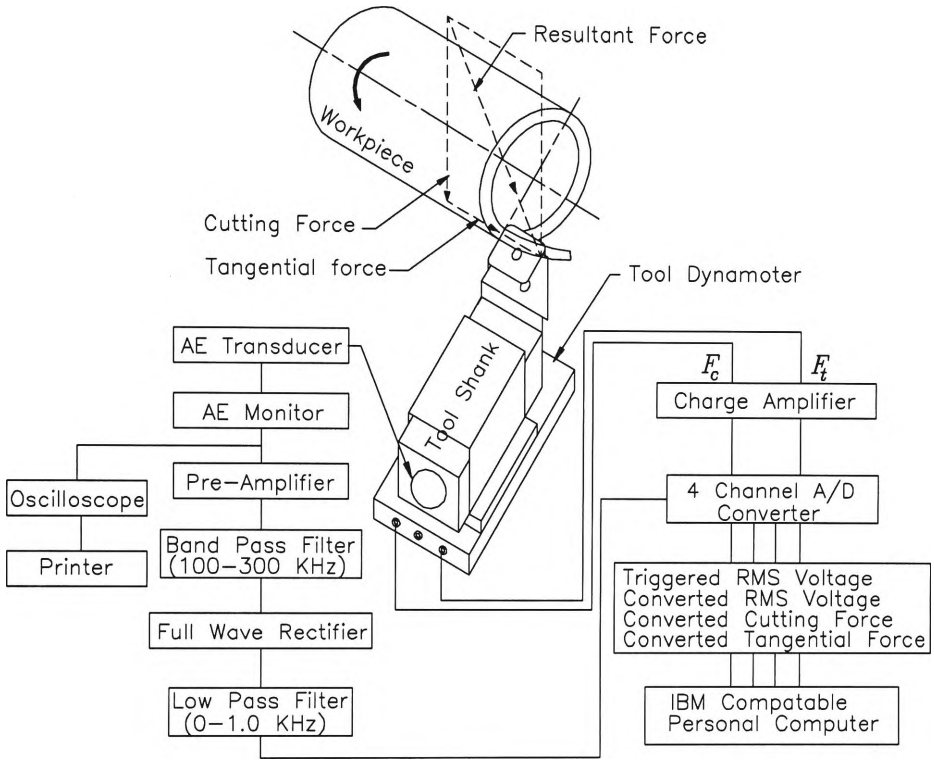

Figure 4.5 Experimental set-up.

In the experimental stage one, the triggering voltage of 1.25 V was employed only for triggering the A/D converter, so as to record the RMS voltage of AE signals from the time the cutting tool engaged the workpiece and commenced orthogonal cutting action. However, in the experimental stage two, the stored and converted mean values of AE_{RMS} voltages, were obtained by normal tests without triggering AE_{RMS} voltages in the A/D converter. This was in order to avoid the low RMS voltage of AE signals triggered as soon as the cutting tool approached the workpiece material.

4.5 RESULTS AND DISCUSSION

4.5.1 Experimental stage one

The cutting tests were performed in such a way that when one input parameter was varied, all other input parameters were maintained as constant. The averages of all measured values of AE_{RMS}, cutting force F_c and the tangential force F_t were estimated and employed for computation of the predicted AE_{RMS} values and the plotting of graphs. The width of cut was observed to have no influence on AE_{RMS} magnitude [139], and hence was maintained constantly at 2.5 mm in the present tests.

Figure 4.6 shows the influence of cutting speed on the Experimental AE_{RMS} voltage. A similar trend is also observed when predicted AE_{RMS} is plotted against the cutting speed (Figure 4.7). Increased cutting speed appears to increase both the measured and predicted AE_{RMS} voltage. The cutting tool rake angle also appears to have a distinct effect on both the measured and predicted AE_{RMS}, as evident from Figures 4.6 and 4.7, and confirmed in Figures 4.8 and 4.9.

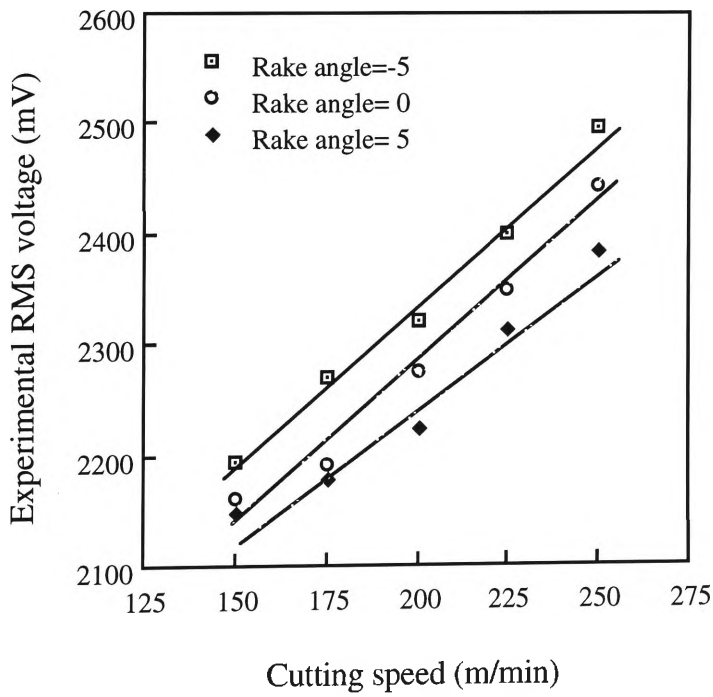

Figure 4.6 Variation of measured RMS values in cutting zones with cutting speeds.

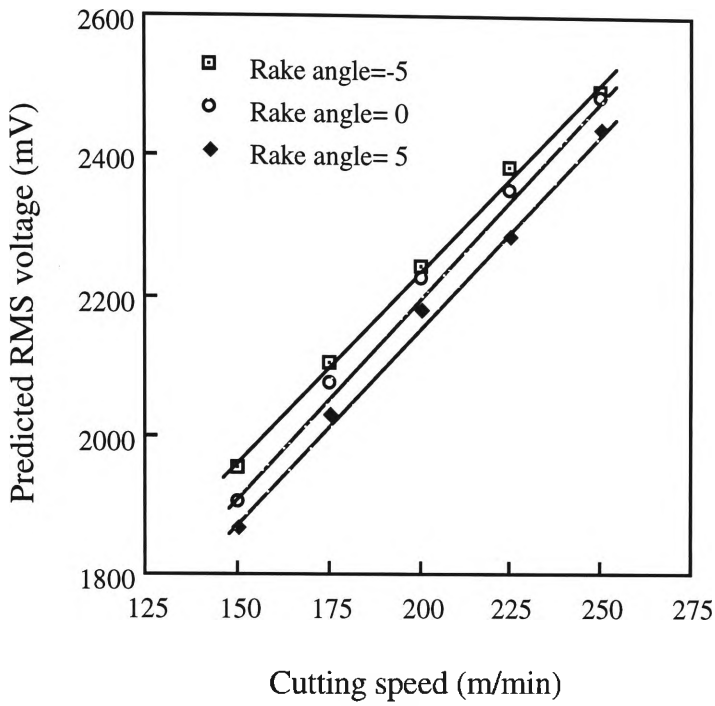

Figure 4.7 Variation of predicted RMS values in cutting zones with cutting speeds.

The cutting forces produced when cutting with 5° rake angle tools have been observed to be much smaller when compared with 0° or –5° rake angles, and hence the resultant decreased AE_{RMS}. The decrease in AE_{RMS} with an increase in positive rake angle, contrasts the results of orthogonal cutting tests observed by Kannatey-Asibu and Dornfeld [24], when turning AA6061-T6 aluminium and SAE 1018 steel, and those of Lan and Dornfeld [139], when cutting SAE 4310 steel.

The AE_{RMS} was found to increase with increasing positive rake angle. The model developed by Dornfeld and K-Asibu [23] employed a proportionality factor C. This proportionality factor was grouped with the sine function of rake angle (ie $\sin\alpha$) in their another model [24] for prediction of AE_{RMS}. However this modified model has still a very important limitation of not being able to predict AE_{RMS} when a zero rake angle tool is employed.

The predicted AE_{RMS} based on the consumed energy rate of the cutting operation, is influenced by dependent and independent cutting parameters, including shear angle, cutting forces, stresses, the tool-chip contact length, cutting speed, rake angle and feed rate.

The AE_{RMS} decreases with the increasing rake angle as predicted by the present model and confirmed by the experimental results (Figures 4.8 and 4.9). It is also worth noting that the AE_{RMS} appears to be in good agreement with that experimentally measured.

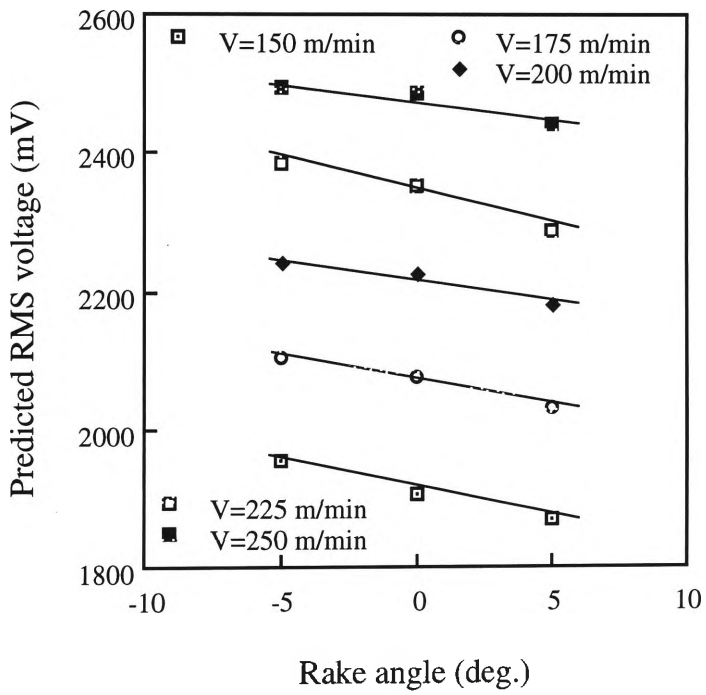

Figure 4.8 Variation of predicted RMS values in cutting zones with rake angles.

The present model (Equation 4.13) eliminates such a limitation, and is able to predict the AE_{RMS} values for tools with negative, zero and positive rake angles employed for orthogonal turning (Figure 4.8).

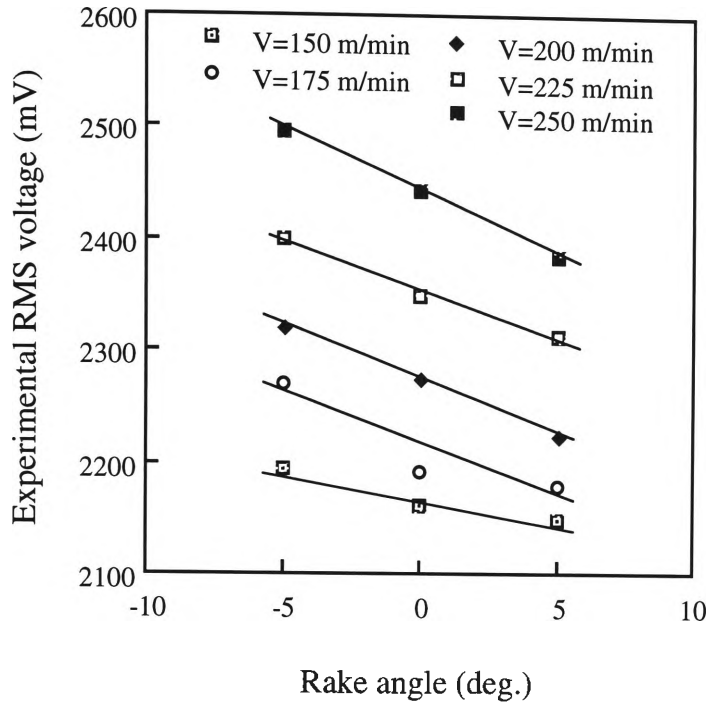

Figure 4.9 Variation of measured RMS voltage in cutting zones with rake angles.

The parabolic constant is a very important factor in estimation of AE_{RMS} values when using the present model. An examination of equations (4.8), (4.9) and (4.11), derived on the basis of relationships established by Zorev [19], indicates that the length ratio of the sticking to sliding zone will vary with the variation of cutting parameters. The present findings (Figures 4.10 and 4.11), however, appear to contradict the assumptions made by K-Asibu and Dornfeld [24], that the length of the sticking zone is equal to half of the total chip contact length.

The seize ratio as indicated in Figures 4.10 and 4.11 increases with increases in the cutting speed and rake angle. It is significantly lower than the value of 0.5 assumed by K-Asibu and Dornfeld. The present results concerning seize ratio tend to agree with the assumption made by Schmenk [138], that the length of the sliding zone is greater than that of sticking zone on the tool-chip interface.

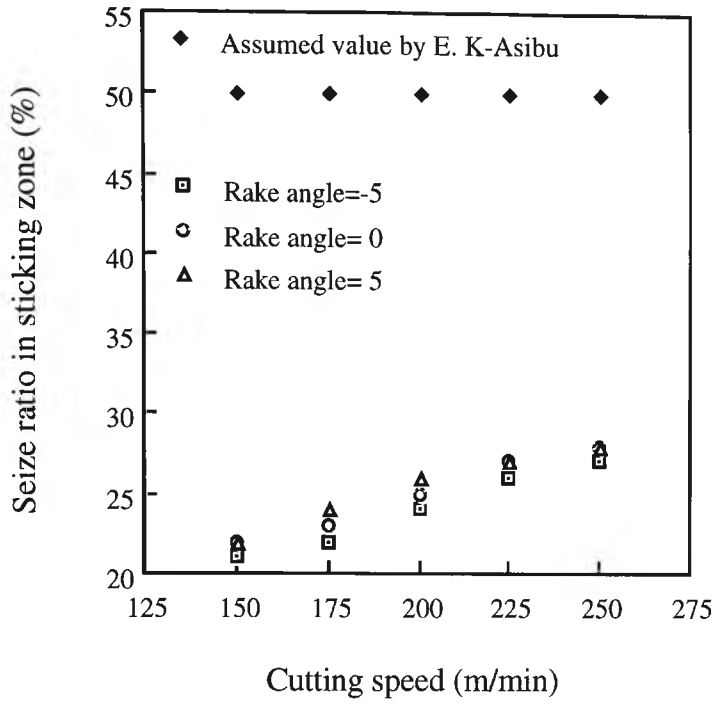

Figure 4.10 Seize ratio of the sticking zone in the tool-chip contact interface versus cutting speeds.

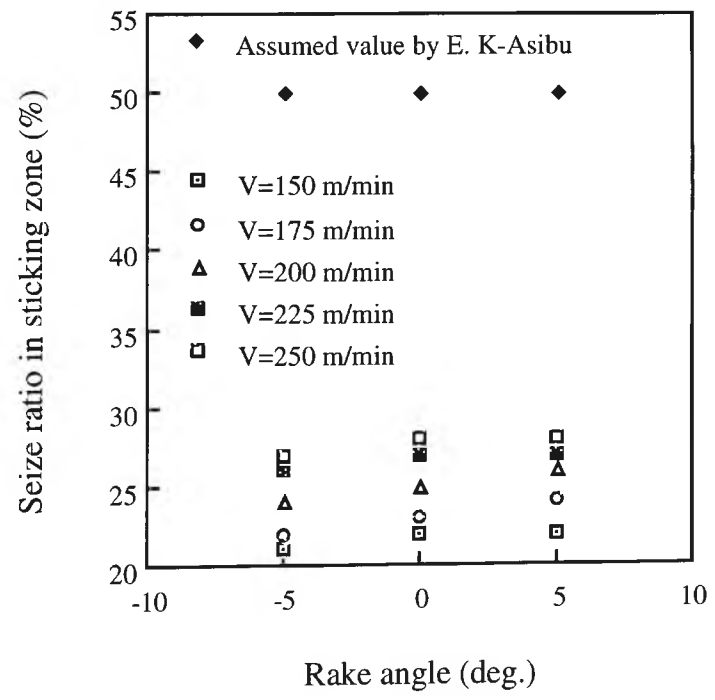

Figure 4.11 Seize ratio of the sticking zone in the tool-chip contact interface versus rake angles.

Figure 4.12 shows a plot between average experimental AE_{RMS} and average theoretical AE_{RMS} obtained by ignoring the influence of both the cutting speed and feed rate on the values. The straight line relationship indicates a fairly close agreement between the predicted and experimental AE_{RMS} values.

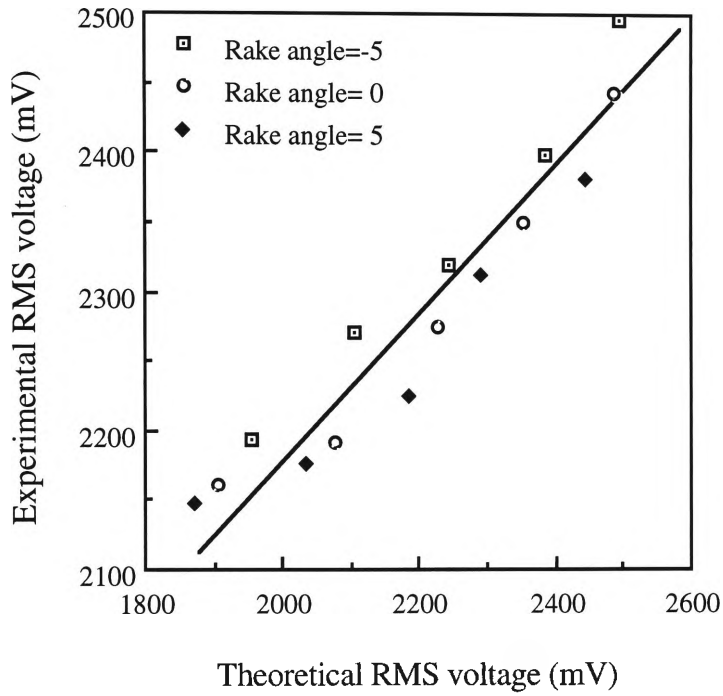

Figure 4.12 The theoretical RMS values versus the actual RMS values.

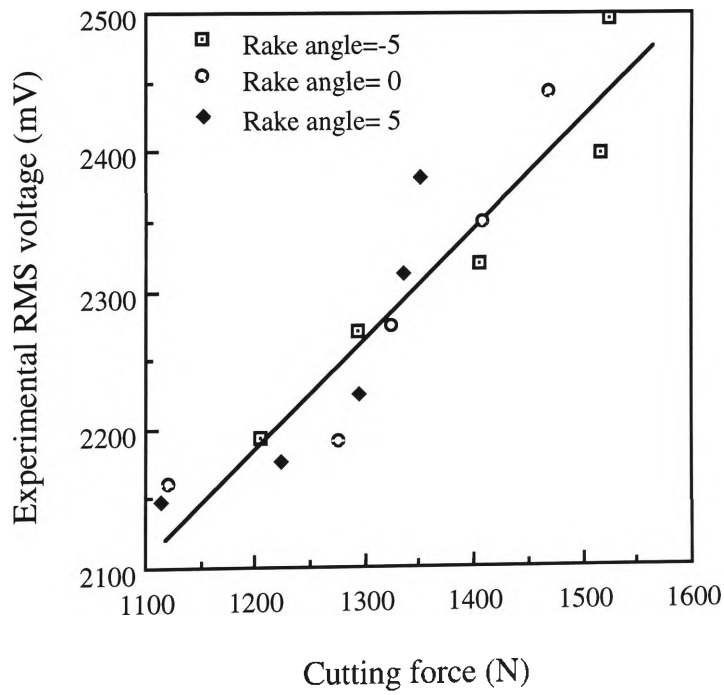

Figure 4.13 The actual RMS values versus cutting forces.

The experimental AE_{RMS} in Figure 4.13 represents the average of the measured values by ignoring the influence of cutting speed and feed rate. The cutting force appears to have a significant influence on the AE_{RMS} as evident from the experimental observations (Figure 4.13) and the model.

The experimental observations of chip thickness were employed to estimate the shear plane angles in the shear deformation zones. The shear plane angle appears to influence the predicted AE_{RMS} in orthogonal turning operations (Figure 4.14). This trend is also confirmed by the AE_{RMS} observations from orthogonal cutting tests (Figure 4.15). The increased rake angle of the tools results in larger shear plane angles and greater dislocation speeds, thus causing higher acoustic emission for the negative rake angle tools.

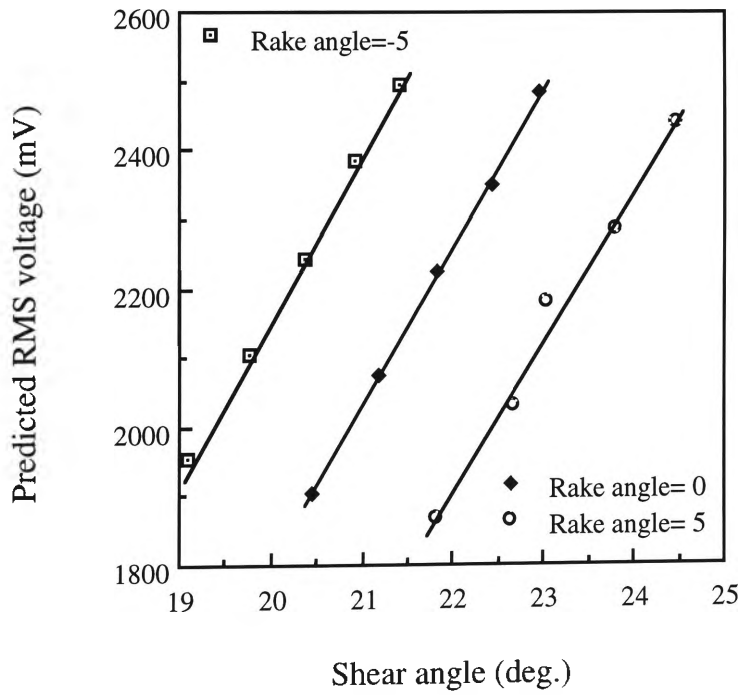

Figure 4.14 Variation of predicted RMS values in cutting zones with shear angles.

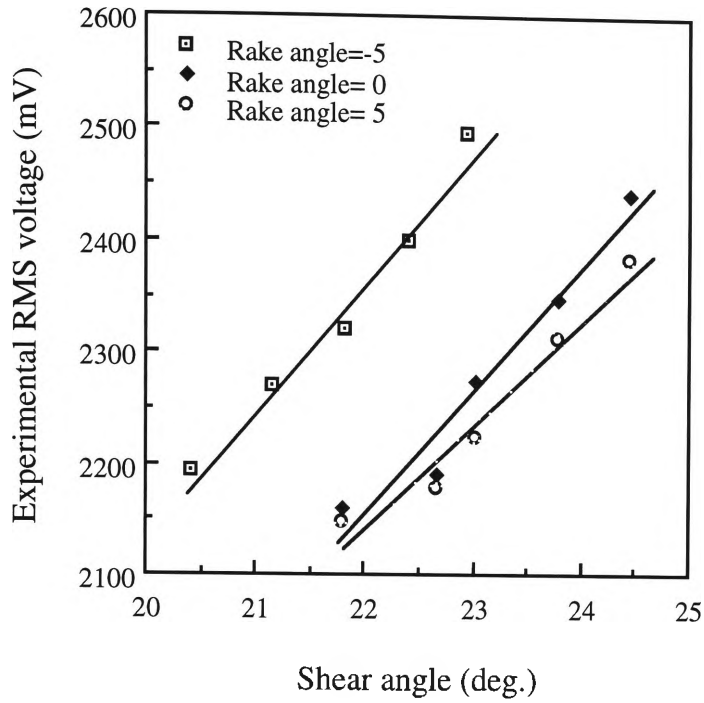

Figure 4.15 Variation of measured RMS values in cutting zones with shear angles.

4.5.2 Experimental Stage Two

Experiments were carried out to study systematically the influences of the dependent output variables on the variations of the tool flank wear, during two-dimensional cutting operations. As can be seen in equation 4.15, the investigation of the quantitative relationships between the AE_{RMS} voltage and the energy content increasing with an increase in the flank wear land, would be essential so as to verify the validity of the theoretical model developed for prediction of the AE_{RMS}. The growth of tool-flank wears (VB) were observed, as shown in Figure 4.16. The range of wear lands in the wear tests was from 0 mm (initial cutting stage with the fresh tool) to 0.687 mm.

The wear tests on four similar inserts (TPGN 220408T P10-P20) were conducted by employing four combinations of cutting speed and feed rate as shown in Figure 4.16. With the first insert when it was fresh tests were performed to study the effects of cutting speed, feed rate and rake angle on the AE_{RMS} voltage. For variation of rake

angle the insert was mounted on a different tool holder and then the tests were carried. After these short tests, long wear test on this insert was continued till maximum 40 minutes cutting. The observations of the AE_{RMS} voltages, cutting forces and chip-thickness were taken at several intermediate stages of this long wear test, as can be seen in Figures 4.17 to 4.20. The cutting operation was temporarily stopped for measurement of wear.

The long wear test with the first insert was interrupted after 20 minutes of cutting (0.289 mm wear) to perform tests to study the effect of cutting speeds, feed rates and rake angles. As in previous test, for the variation of rake angle the insert was mounted on a different tool holder and then tests were conducted. The insert wear was measured before and after this intermediate set of tests. The growth of wear due to this intermediate set of tests was observed to be very small and negligible. After these tests, the long wear test was continued with this insert till 40 minutes of cutting. Again at several intermediate stages of this long wear test, observations of the AE_{RMS} voltages and cutting forces were taken. The cutting operation was temporarily stopped for the measurement of respective tool flank wear.

The long wear test with the second insert was interrupted after 30 minutes of cutting (0.493 mm wear) to conduct tests to study the effects of cutting speeds, feed rates and rake angles. The tool holder of the insert was changed to allow variation in rake angle. The insert wear was also measured before and after this intermediate set of tests. The growth of wear due to this intermediate set of tests was observed to be very small and therefore neglected. After these tests, the long wear test was continued with this insert till 35 minutes of cutting. Again at several intermediate stages of this long wear test, observations of the AE_{RMS} voltages and cutting forces were taken. The cutting operation was temporarily stopped for the measurement of respective tool flank wear.

The long wear test with the third insert was continued till 25 minutes of cutting. However, this insert was not utilised to conduct tests to study the effects of cutting speeds, feed rates and rake angles due to the cutting edge chipping.

The long wear test with the fourth insert was interrupted after 25 minutes of cutting (0.687 mm wear) to perform tests to study the effect of cutting speeds, feed rates and rake angles. As in previous test, for the variation of rake angle the insert was mounted on a different tool holder and then test were conducted. The insert wear was measured before and after this intermediate set of tests. The growth of wear due to this intermediate set of tests was observed to be very small and negligible. Again at several intermediate stages of this long wear test, observations of the AE_{RMS} voltages and cutting forces were taken. The cutting operation was temporarily stopped for the measurement of respective tool flank wear.

Except for the initial stage of cut (2.5 minutes), machining operations were periodically interrupted for measurement of wear lands on the tool-flank at 5 minutes intervals. The stop time of the machining was based on the points computed from the relationship between the cutting length and the cutting time. Machining was also stopped to remove the tangled continuous chip after every 20 mm cut, in order to prevent small chipping on the cutting tool edge from the tangled continuous chip. As a result, the measured wear lands have not taken into consideration the influences of the high temperatures generated in continuous cutting. When the machining was restarted after interruption to measure the total amount of the flank wear, the small piece of cutting edge chipping, which sometimes occurred in the middle or final of wear test, was not avoidable. Measuring the average wear length on the tool flank with sufficient accuracy was very difficult on occasions because of the large scatter.

Figure 4.16 shows the growth of flank wear land on a 5^0 rake angle tool in relation to the elapsed cutting time. The wear lands rapidly increase between 20 and 35 minutes.

The result shows a trend similar to the trend of the minor flank wear created in the oblique cutting processes using the ceramic coated tool [155] and the carbide tool [168]. The critical points at which the flank wear land begins to accelerate, vary between 0.412 mm and 0.506 mm. However, the measurement of a particular tool wear through the experiments suggests that using relatively softer tools will save both time and costly tool wear experiments.

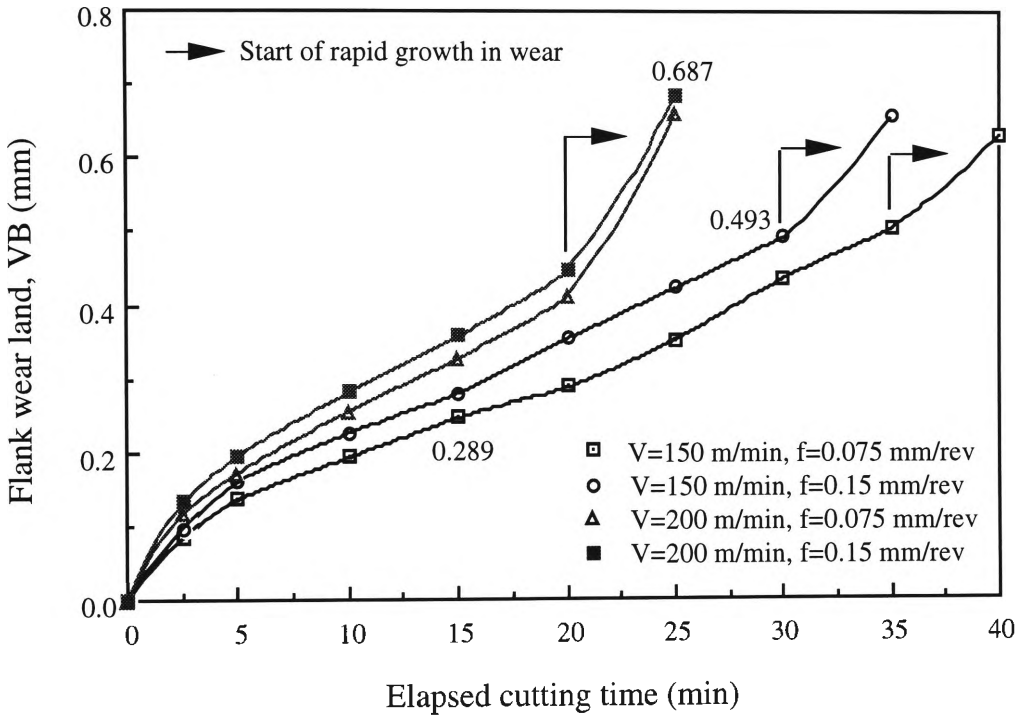

Figure 4.16 Variation of flank wear (VB) in elapsed cutting time.

When the flank wear increases, the RMS voltage of AE signals tends to increase, as shown in Figure 4.17. The measured AE_{RMS} voltage abruptly increases when the level of the flank wear land arrives at between 0.128 mm and 0.161 mm, which corresponds to the tear off the coating on the tool rake face. This result shows a close agreement with the results observed by the previous researchers, in which the level of the AE_{RMS} voltage on the flank wear land is similarly increased and saturated at 0.13 mm to 0.15 mm [153-155] and 0.16 mm to 0.18 mm [156]. On the other hand, as can be seen in Figure 4.17, the level of the AE_{RMS} decreased at some intermediate levels of the wear land (0.227-0.319 mm), when the coating had worn through to the

bare face of the tool [155]. This phenomenon can be attributed to the influence of the development of crater wear [154, 156], which causes increase in effective rake angle. Therefore, it is noted that the level of the AE_{RMS} voltage is dependent on the tool flank wear land, development of the crater wear, the cutting fluids [169], and the material of the tool and workpiece [169].

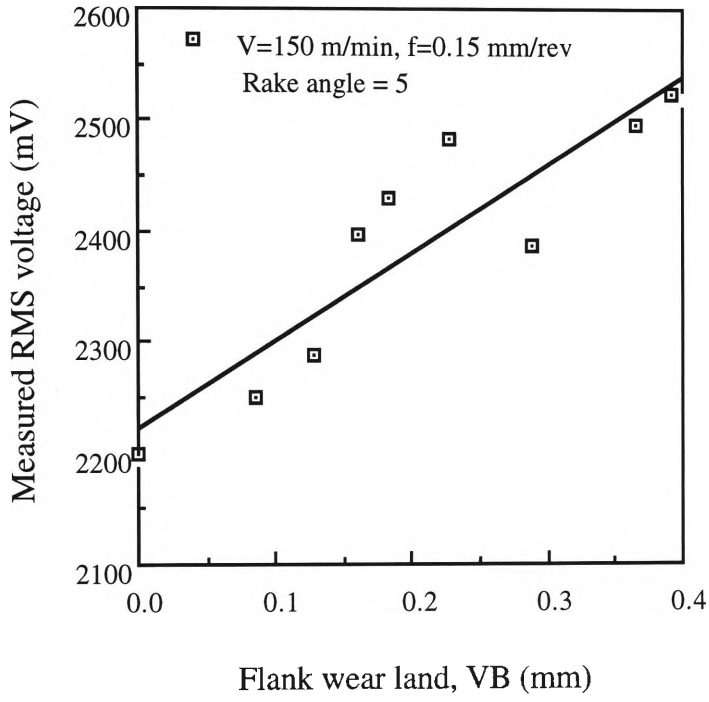

Figure 4.17 Variation of the experimental RMS value with flank wear.

There are minor limitations in the accurate measurement of cutting forces, because of the difficulty in measuring the forces (cutting, tangential and radial forces) triggered simultaneously in the A/D converter, but in these experiments the cutting force appears to have a significant effect on the variation of cutting process parameters.

As evident from the experimental observation shown in Figure 4.18, the cutting forces varied linearly with the development of the wear land and decreased at some intermediate levels of wear lands. The cause of the decrease of cutting forces in some intermediate flank wear levels is the increase of effective rake angle at the point at which the crater wear increases on the tool rake face [9].

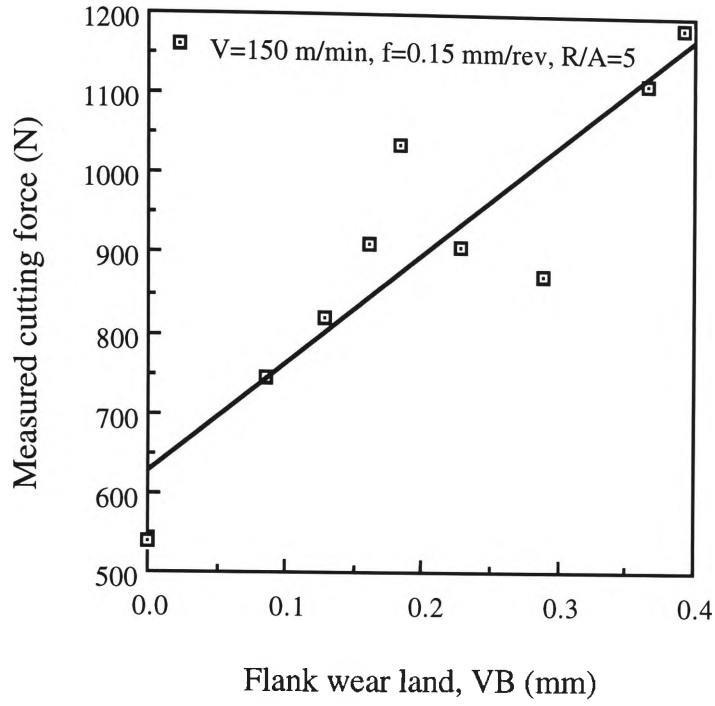

Figure 4.18 Variation of cutting forces with flank wear (VB).

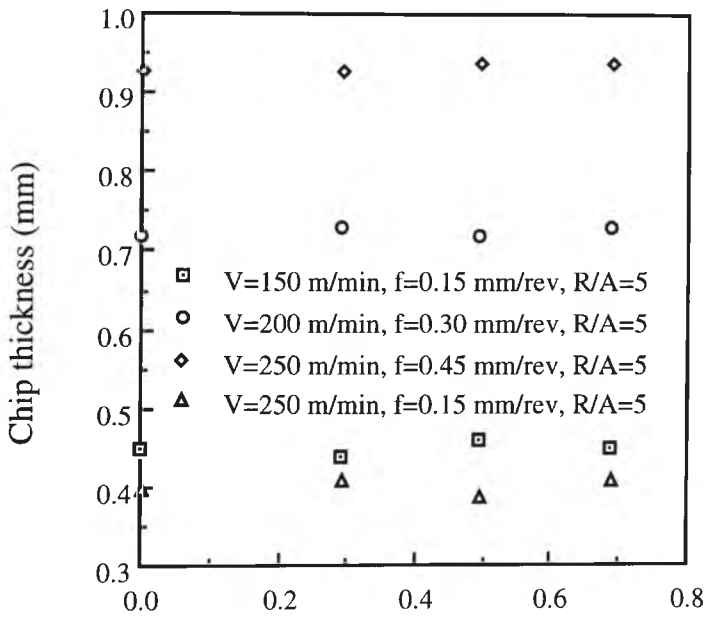

Figure 4.19 Variation of the measured chip-thickness with flank wear (VB).

Chip thickness generally increases with the increasing feed rates and rake angles, and decreasing cutting speeds. An increase of chip thickness makes a decrease in a shear plane angle, and the shear plane angle gives an influence of the cutting force and the tool wear such as crater wear on the tool rake face. However, as shown in Figures

4.19 and 4.20, the measured chip thickness does not have a strong effect on the variations of the cutting forces and flank wear lands.

From the results in Figures 4.19 and 4.20, it can be predicted that the cutting mechanism of the tertiary deformation zone does not affect the shear plane angle which plays an important role in the primary and secondary deformation zones. The results in Figures 4.19 and 4.20 obtained by using the measured flank wear land, show a similar trend to the results of experiments using artificial (ground) wear lands [7, 150].

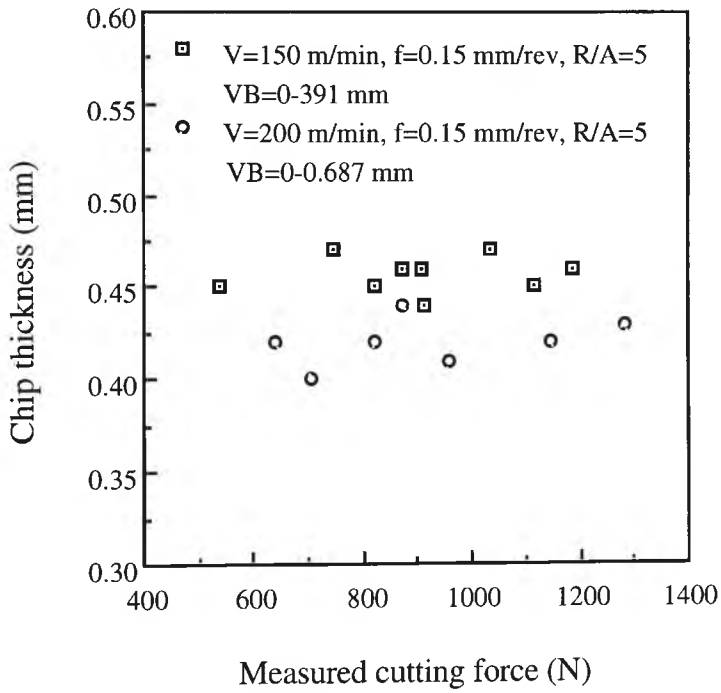

Figure 4.20 Variation of the measured chip-thickness with cutting force.

Figures 4.21 and 4.22 show the effect of tool-flank wear on the measured and predicted AE_{RMS} voltage for different cutting speeds. It can be seen that both the mean AE_{RMS} values increase in portion to the amount of the flank wear land. In all, the measured and predicted AE_{RMS} increase linearly at a constant cutting speed, with an increase in the flank wear land. The plotted AE_{RMS} values were calculated by taking the average values, without considering the effects of feed rates and rake angles.

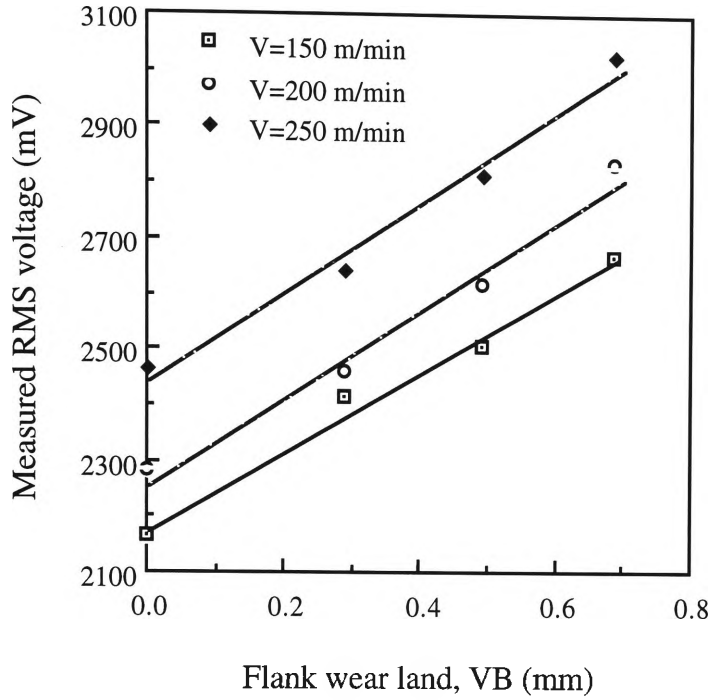

Figure 4.21 Variation of experimental RMS values in various cutting zones with flank wear (VB) for different cutting speeds.

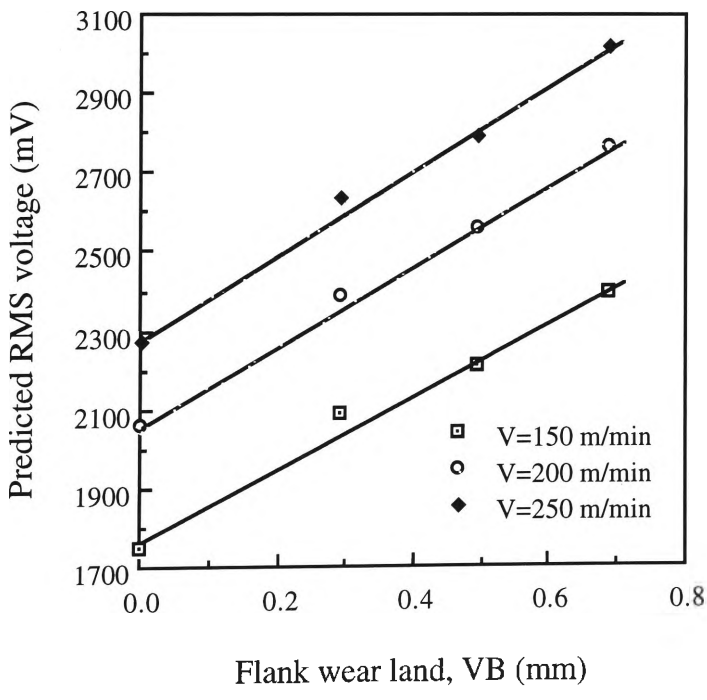

Figure 4.22 Variation of theoretical RMS values in various cutting zones with flank wear (VB) for different cutting speeds.

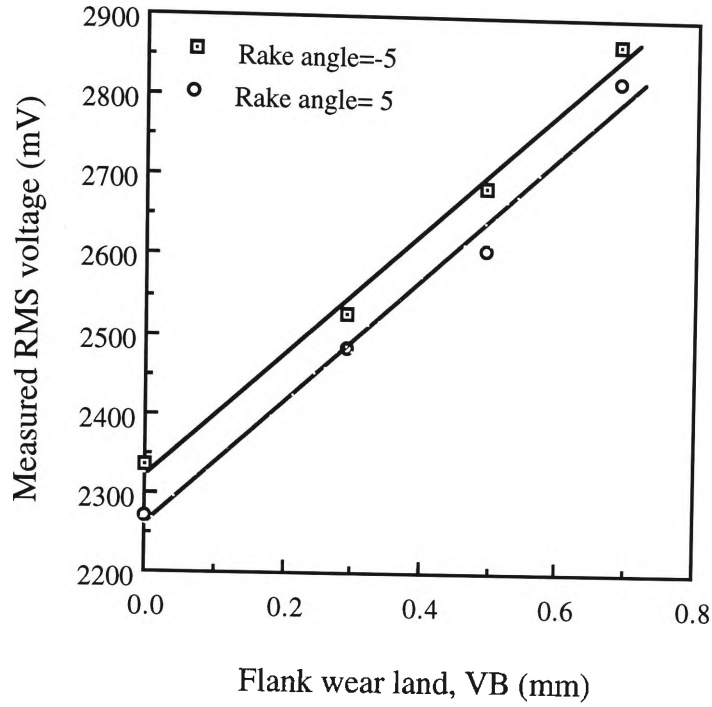

Figure 4.23 Variation of experimental RMS values in various cutting zones with flank wear (VB) for different rake angles.

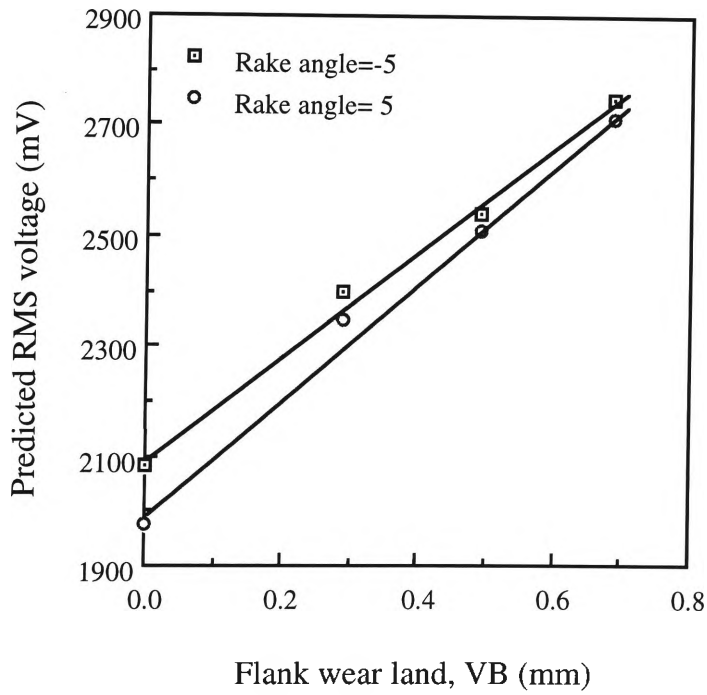

Figure 4.24 Variation of theoretical RMS values in various cutting zone with flank wear (VB) for different rake angles.

As shown in Figures 4.23 and 4.24, both the measured and predicted AE_{RMS} voltages increase as the wear land of the tool-flank increase. However, values in the two

straight lines plotted using different rake angles (-5^0 and 5^0) indicate that the AE_{RMS} voltages **decrease** with the increasing rake angles in the increasing flank wear lands.

These results shown in Figures 4.21 to 4.24, indicate a similar trend to the experimental results of the first stage, demonstrated in the initial cutting, when sharp tools which ignore tool flank wear were used. This results were published by the present author [145]. Through the contrast of these two results, it is clear that the AE_{RMS} value conspicuously increases with the increasing flank wear [109], as the cutting speed increases and the rake angle decreases.

The magnitude of the cutting force in Figure 4.25 changes significantly as the cutting edge on the rake face is progressively worn, and the cutting force decreases when the rake angle increases. Hence the average cutting force is directly related to the amount of tool wear. Cutting forces shown in Figure 4.25 are the average of the experimental values computed by ignoring the influences of feed rates and cutting speeds.

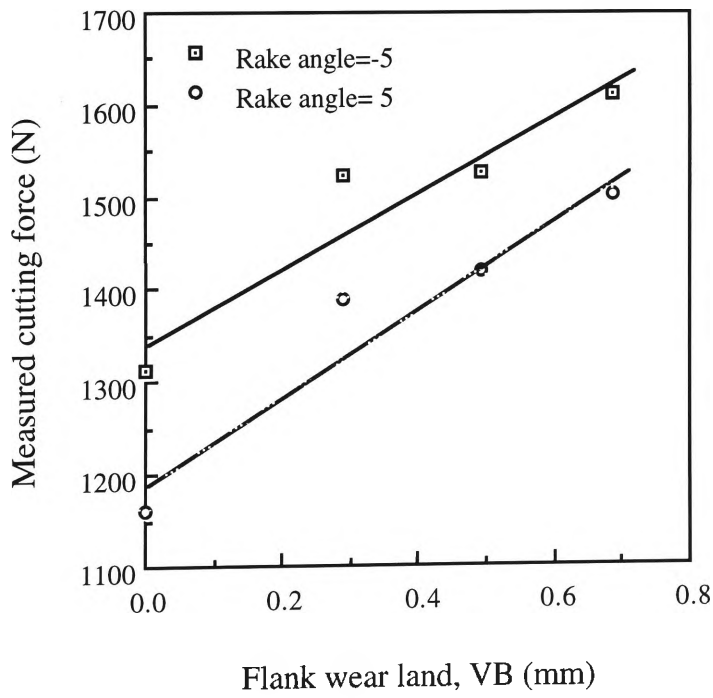

Figure 4.25 Variation of the average cutting force with flank wear (VB) for different rake angles.

On the basis of the experimental results in Figures 4.21 to 4.25, the average AE_{RMS} can be predicted by the simple equation as given by :

$$(V_{RMS})_{ave} = \varepsilon VB + (V_{RMS})_i \tag{4.24}$$

$$(F_c)_{ave} = \varepsilon VB + (F_c)_i \tag{4.25}$$

Where, ε is the gradient of the plotted function. $(V_{RMS})_i$ and $(F_c)_i$ represent the initial AE_{RMS} voltage and cutting force obtained at the initial cutting stage using sharp cutting edge tools.

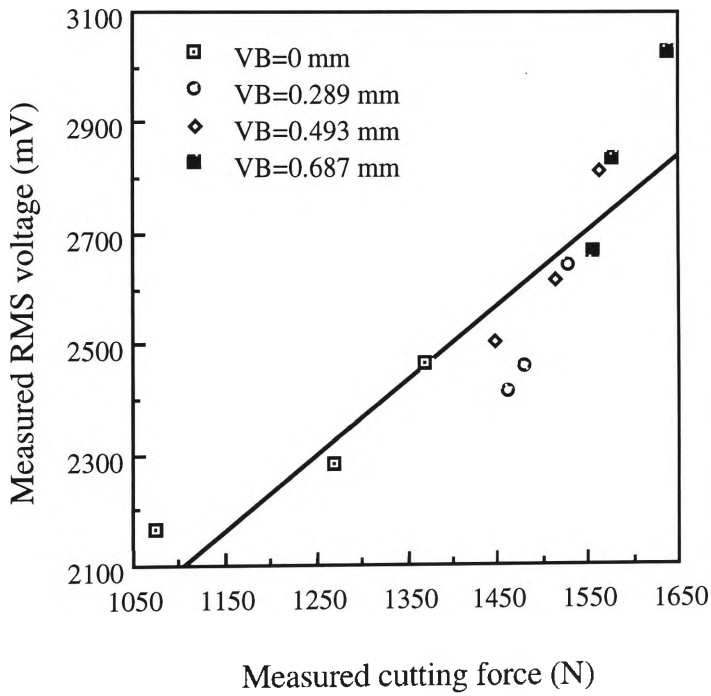

Figure 4.26 Relationship between the experimental RMS value and cutting force for the variation of flank wear lands.

Figures 4.26 and 4.27 show the plots between the average experimental AE_{RMS}, the average experimental cutting force, and the average theoretical AE_{RMS} obtained without taking into account the effects of either the feed rate or the rake angle on the measured

value. Generally, the AE techniques analysed in cutting tests have indicated a higher sensitivity than the cutting force measurement technique [155]. However, Figure 4.26 shows a good relationship between the cutting forces and the AE_{RMS} values. The AE_{RMS} voltages in Figures 4.26 and 4.27 were calculated by taking the average value of each of the cutting speeds (150, 200 and 250 m/min) for different flank wear lands (VB), without considering the effects of the feed rate and rake angle. The linear relationship between the predicted and measured AE_{RMS} values indicated in Figure 4.27, is satisfactory.

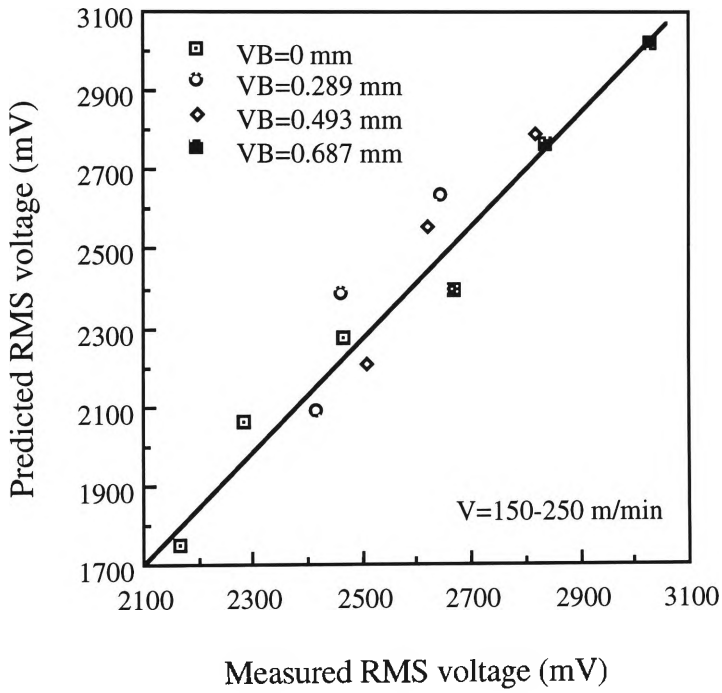

Figure 4.27 Relationship between the computed RMS value and the experimental RMS value for the variation of flank wear lands.

4.6 CONCLUSIONS

1. The interaction of many factors in a turning operation makes AE generation very complex. The development of an analytical model for prediction of AE_{RMS} in turning operations is therefore difficult. Some realistic assumptions concerning

the tool and deformation process were made. They were necessary to develop new models for prediction of AE_{RMS} in orthogonal cutting operations .

2. The models have been verified by experimental observations of AE_{RMS} voltage and found to be accurate under a wide range of cutting conditions. Computational statistical analytical techniques were employed in this research to eliminate the problems faced by previous researchers [23-24, 138-139], in estimation of proportionality and signal attenuation constants generated in the plastic deformation zones.
3. Seize ratio values have been determined based on realistic assumptions of the frictional stresses in the sticking and sliding zones on the tool-chip interface. These values are significantly different from those previously employed by Kannatey-Asibu and Dornfeld [24].
4. The influence of some input and output parameters of the turning operation on acoustic emission has been examined in the experimental stages one and two. The results of the experiments indicate that the variations of cutting process parameters have major effects on acoustic emission signal generation. The variations of cutting process parameters have shown a significant potential for prediction of the energy rate consumed in orthogonal cutting operations with both fresh and worn tools.
5. In the experimental stages one and two, both the measured and predicted AE_{RMS} have been observed to increase with the greater cutting speed, cutting force and shear plane angle. However with an increase in positive rake angle of the tools, the AE_{RMS} was found to decrease. A linear relationship showed between the measured AE_{RMS} and cutting forces.
6. The correlation between the flank wear and the crater wear in the orthogonal cutting operations, was investigated in the second stage of the experimental work. The level of the AE_{RMS} and cutting force have been measured to increase with the flank wear. However, both the measured AE_{RMS} and cutting force were

observed to decrease with the flank wear at certain intermediate wear levels by the bare face of the coating on the tool flank and rake face.

CHAPTER FIVE

EMPIRICAL MODELS FOR PREDICTION OF ACOUSTIC EMISSIONS

5.1 INTRODUCTION

Estimation of the state of the cutting tool is one of the major obstacles to on-line process control and optimisation of the metal cutting process. Monitoring and diagnosis of the tool condition in cutting operations are essential for reliability and the implementation of adaptive control which is vital for productivity and manufacturing efficiency. One possible solution for assessment of the tool condition in-process cutting operations is to establish the empirical mathematical models based on the experimental tests.

This chapter will discuss first the results obtained in the two stages of the detailed experimental studies. Based on the effects of cutting process parameters on the AE_{RMS} voltage generated during orthogonal cutting operations, this chapter proposes the development of empirical models. The three types of empirical equations (curvilinear, polynomial and linear equations) have been developed by multiple regression analysis techniques using standard statistical package (SAS). Also, the accuracy of the mathematical equations developed will be verified by the SAS program. In addition, the effective interactions of cutting process parameters were investigated and evaluated

by the regression analysis. Accordingly, the focus of this chapter is (1) to develop all mathematical equations and (2) to find the best mathematical model in conjunction with the basic cutting process parameters and AE_{RMS} output. With the help of statistically computed equations using regression analysis techniques, the best condition of the cutting tool and the cutting process parameters can be determined based on the variation of AE_{RMS} values. Once this has been done, guidelines for selection of the most important and effective cutting process parameters can be established.

5.2 EXPERIMENTAL WORK

5.2.1 Selection of Basic Cutting Process Parameters

In general, a major difficulty for cutting process optimisation is the number of cutting parameters involved. The usual single variable experiment which changes one variable at a time relative to the other fixed parameters, is unsuitable in testing a complex system such as the metal cutting process. However, the statistical design of experiments which are based on a simple factorial technique and involve simultaneous variations of all the variables, greatly reduces the number of trials and enables mathematically reliable predictions to be made of the optimum conditions [170, 171]. Therefore, it was decided to use a well established statistical tool at the level of a simple factorial technique in designing the experiments which reduce the experimental runs to the fewest possible.

The cutting process parameters which affect the RMS voltage of AE signals and overall workpiece quality in metal cutting operations are :

- feed rate (f : mm/rev)
- cutting speed (V : m/min)
- rake angle (α : deg)
- width of cut (b : mm)

- depth of cut (d : mm)
- flank wear land (l_{fw} : mm)
- tool-chip contact length (l : mm)
- tool material and its condition
- tool shape, surface finish, and sharpness
- workpiece material, condition, and temperature
- cutting fluid

In studying the effects of these parameters which significantly affect the dependent output variables, it is essential to control these cutting process parameters. The dependent output variables include : surface finish, dimensional accuracy, wear and failure of the cutting tool, force and energy dissipated in the cutting process, the type of chip produced and temperature rise in the workpiece, the chip, and the cutting tool. The basic cutting process parameters which have been employed for investigation of the effects of cutting process parameters on the AE_{RMS} voltage are feed rate, cutting speed, rake angle and flank wear land (VB).

5.2.2 Experimental Procedure

As described in the article on experimental procedure in chapter 4, sections 4.5 and 4.6, the experimental conditions (ie the experimental design and set-up), the cutting conditions (ie the workpiece and tool material, the geometry of tool and tool holder, and the range of cutting process parameters) and the experimental results were based on the previous experiments which were separated into two stages. The first experimental stage provides a study of the effects of cutting process parameters on the AE_{RMS} voltage. The second experimental stage takes into consideration the effects of tool flank wear. Experimental results of these two stages were employed for the development and verification of empirical models.

5.2.3 Design of Correlation Matrix

Simple factorial experiments [170] (3^2x5 and 3^3x2), which would provide sufficient data for determining the relationship and interaction between the cutting process parameters and the AE_{RMS} voltage, were designed keeping in mind the limitations described in chapter 4, section 4.5. The cutting test ranges of the first experimental stage for sharp tools used the three cutting process parameters which ignored the effect of the flank wear. The three levels of low, intermediate and high ranges were used in feed rate (0.15, 0.30 and 0.45 mm/rev) and rake angle (-5°, 0° and 5°). Five cutting speeds were employed : 150, 175, 200, 225 and 250 m/min. Width of cut remained constant at 2.5 mm for all experiments.

Four factors were employed in the second experimental stage to isolate the main effects of the tool wear. As listed in table 4.6 of chapter 4, the feed rates and cutting speeds varied in the ranges of low, intermediate and high. The rake angles employed in the experiment were at the positive and negative rake angle (5° and -5°).

The levels were selected, partly in anticipation of known consequences of change and partly in respect of quality control. The cutting process parameters determined in factorial design are important and have a significant effect on the variations of the dependent output parameters.

5.3. EXPERIMENTAL RESULTS

Forty-five tests were carried out using fresh tools and 54 tests were performed by using tools with measured wear. The results of these tests were employed to examine the relationships between cutting process parameters, tool conditions and the AE_{RMS} voltage under realistic cutting conditions. A summary of experimental tests in terms of

cutting process parameters and the AE_{RMS} voltage is given in Appendix C. Experimental results were also used for development of empirical mathematical models, when using sharp and worn tools. The experimental results were arranged to link the mean values of the AE_{RMS} voltage measured with changes in cutting process parameters.

Figures 5.1 and 5.2 show the effects of each cutting process parameter on the AE_{RMS} voltage without consideration of the flank wear land (VB), and Figures 5.3 to 5.5 give the results considering the wear land of tool flank.

Figure 5.1 shows the influences of the cutting speed and rake angle on the measured average AE_{RMS} voltage. The average AE_{RMS} were calculated by taking the average of all measured values without considering the effect of the feed rate. As can be seen in Figure 5.1, it is noted that the voltage of the AE_{RMS} decreases with an increasing rake angle and increases with an increasing cutting speed.

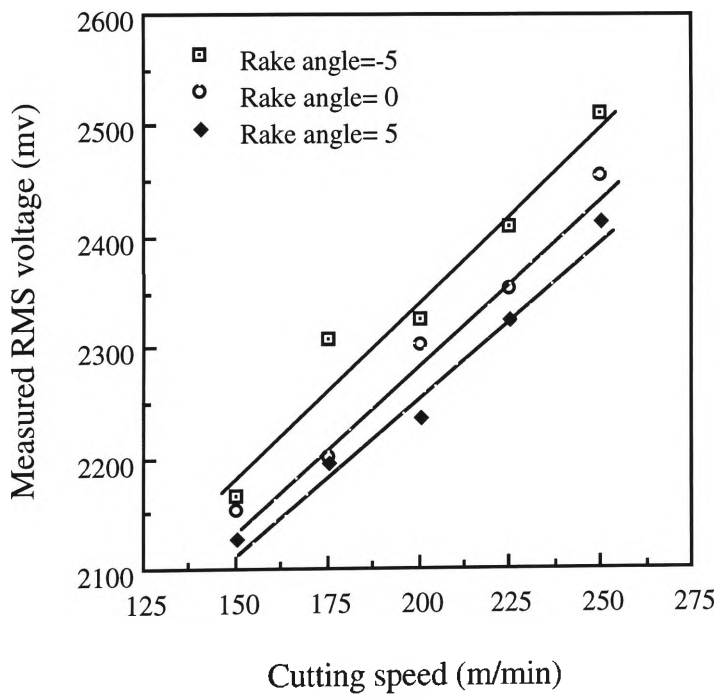

Figure 5.1 Relationship between measured RMS values and cutting speeds.

The effect of the rake angle and feed rate on the measured AE_{RMS} shown in Figure 5.2, indicates that the AE_{RMS} value decreases as the rake angle increases, but it increases as the feed rate increases. The results show a similar experimental trend as compared with the results of previous researchers [107]. The average AE_{RMS} values were produced by taking the average of all values without taking into account the effects of the cutting speed.

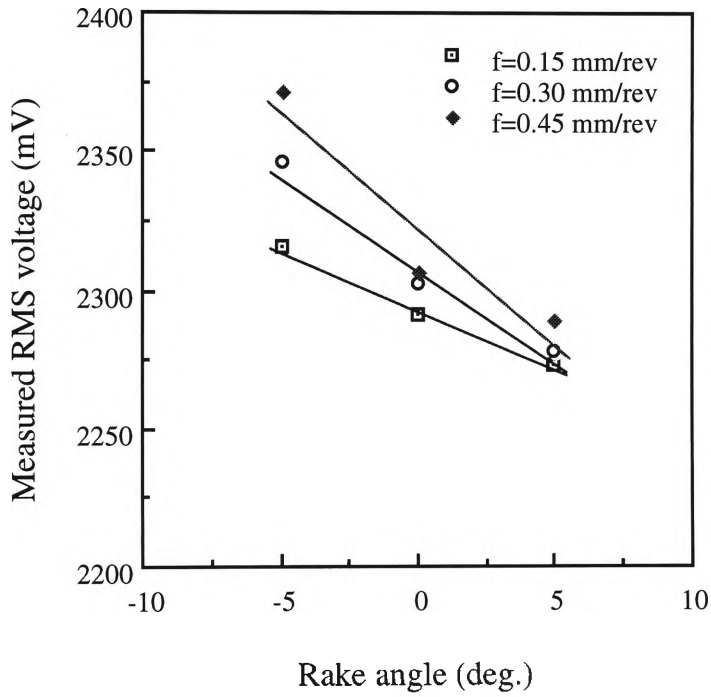

Figure 5.2 Relationship between measured RMS values and rake angles.

Figure 5.3 indicates a distinct effect of the cutting speed and flank wear land (VB) on the measured AE_{RMS} voltage. As evident from the experimental observations (Figure 5.3), the AE_{RMS} values increase when the cutting speed increases, and it significantly increases when the flank wear land increases. The result was observed a similar trend as the experimental work done by previous researchers [109]. The average AE_{RMS} values were calculated by taking the average of all values without considering the effects of the feed rate and rake angle.

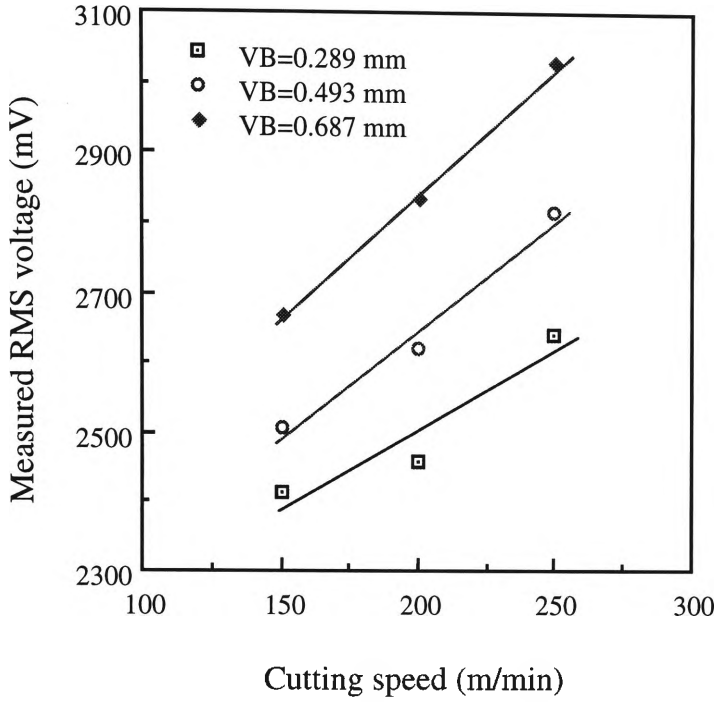

Figure 5.3 Variation of measured RMS values with cutting speeds for different flank wear lands (VB).

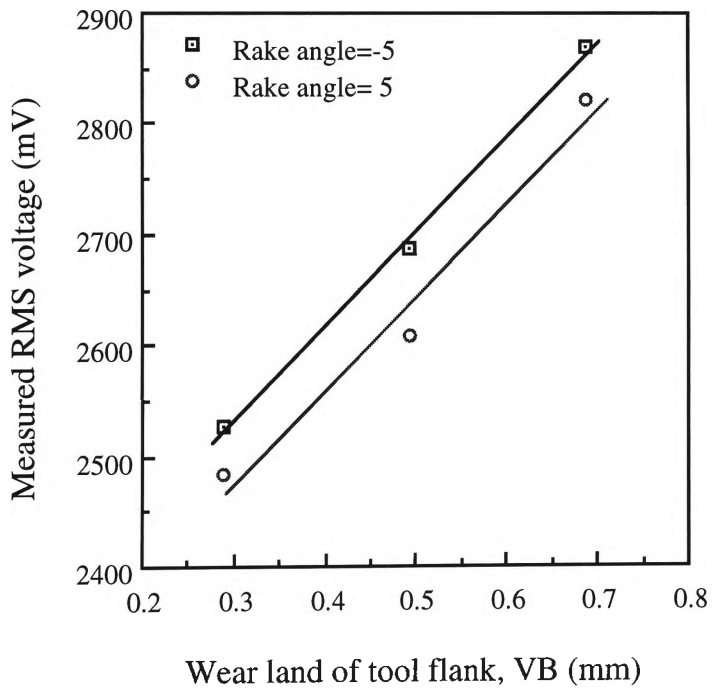

Figure 5.4 Variation of measured RMS values with flank wear lands (VB) for different rake angles.

Figure 5.4 displays the effect of flank wear land (VB) and rake angle on the experimental AE_{RMS} voltage. The result indicates that the AE_{RMS} voltage increases with the increasing flank wear land, but it decreases with the increasing rake angle (from -5° to 5°). The values of the average AE_{RMS} were plotted by taking the average of all values, ignoring the effects of the cutting speed and feed rate.

Figure 5.5 shows the influence of the flank wear land and feed rate on the experimental AE_{RMS} voltage. The increasing wear land causes an increase in the AE_{RMS} value, and the AE_{RMS} value also increases when the feed rate increases. The average AE_{RMS} values were calculated by taking the average of all observed values, without considering the effects of the cutting speed and rake angle.

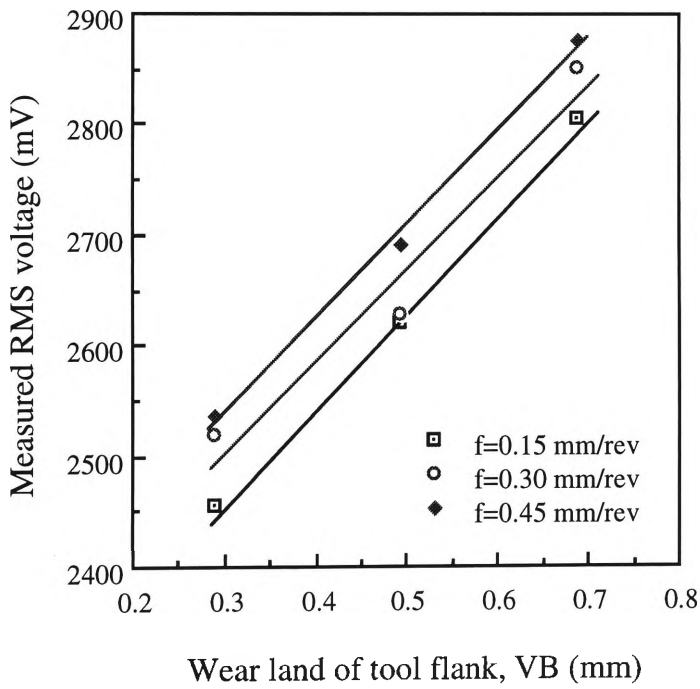

Figure 5.5 Variation of measured RMS values with flank wear lands (VB) for different feed rates.

When comparing the variation of the measured AE_{RMS} in Figures 5.1 to 5.5, similar trends in the changes of AE_{RMS} values were observed in experimental tests. Figures 5.1 and 5.2 ignored flank wear lands (VB). But Figures 5.3 to 5.5 considered the

different stages of flank wear lands (VB). The AE_{RMS} voltage increases with the decreasing rake angle when using sharp tools (Figure 5.2), and increases with the increasing flank wear land (Figure 5.5). An increase of AE_{RMS} voltages with the increasing flank wear in orthogonal cutting operations can be attributed to the influence of the decrease of end clearance angle at the tool flank caused by abrasive mechanism [80].

5.4 DEVELOPMENT OF MATHEMATICAL MODELS

5.4.1 Derivation of Empirical Mathematical Models

The experimental results have shown that the AE_{RMS} voltage is influenced by cutting speed, rake angle, feed rate and flank wear land. The mathematical model can be effectively employed for prediction of the optimal cutting conditions in the cutting process. Therefore, a formalised model for process optimisation could successfully establish combinations of cutting process parameters. The models formed by statistically fitted constants can be separated into two types of empirical mathematical models according to whether they neglect or consider the wear land of the tool flank. The dependent output variable (Y), called the response parameter, is an AE_{RMS} voltage in relation to the basic cutting process parameters :

$$Y = \psi(f, V, \alpha) \tag{5.1}$$

$$Y = \psi(f, V, \alpha, l_{fw}) \tag{5.2}$$

Where f is feed rate, α is rake angle, V is cutting speed and l_{fw} is flank wear land.

Likewise, the empirical mathematical models can also be categorically divided into three parts :

(1) Curvilinear equation

(2) Polynomial equation

(3) Linear equation

Investigation of the effects of cutting process parameters on the AE_{RMS} voltage and the relationships between input and output parameters, would provide a clear knowledge of methods suitable for prediction of output parameters and estimation of the cutting tool wear.

Teti and Dornfeld [107] introduced curvilinear formulae for oblique cutting operations which assumed a linear relationship between the V_{RMS} and the cutting conditions, such as the cutting process parameters $0.05 \le f \le 0.10$, $400 \le V \le 1200$ and $0.1 \le d \le 0.2$, and the cutting tools TPG 321 and TPG 322, and aluminium and brass as workpiece materials. The fundamental concept of the formula was as follows :

$$V_{RMS} = K(f)^a (V)^b (d)^c + D \tag{5.3}$$

where, K, a, b and c are statistically fitted constants. d is depth of cut. D is offset value for the equation.

However, the above model did not take into consideration the influence of the effective rake angle (α_e) [1], which is one of the significant important cutting process parameters for oblique cutting operations. Teti and Dornfeld only developed the curvilinear equation. Other models such as a polynomial and linear models were not considered for finding the best equation for the empirical models. Also, the models did not incorporate the effect of the flank wear land (VB).

Ravindra, Srinivasa and Krishnamurthy [72] proposed the curvilinear equation, called the log-linear model, in order to estimate force components for sharp cutting

edge tools in the oblique cutting. Using the statistical package SPSS, force models for prediction of the three component forces (cutting force, tangential force and radial forces) were developed, incorporating cutting speed, feed rate and depth of cut.

$$F_{x,y,z} = K(f)^a(V)^b(d)^c \tag{5.4}$$

Among the equations proposed by [72], linear equations were also presented to describe the effect of flank wear on the cutting force components when considering the machining time in seconds, as follows :

$$V_b = a_1 + a_2F_x + a_3F_y + a_4F_z + a_5T \tag{5.5}$$

Where V_b is the wear land of tool flank. a_1, a_2, a_3, a_4 and a_5 are statistically fitted constants. F_x, F_y and F_z are cutting force, tangential force and radial force, respectively. T is machining time in seconds.

5.4.2 New Empirical Mathematical Models

Best fit equations for investigating the interrelationship of cutting process parameters and the AE_{RMS} voltage, were computed by using the standard statistical techniques such as multiple regression analysis. These analyses were performed with the help of a standard statistical package program, SAS, using an IBM compatible personal computer [167].

5.4.2.1 Development of empirical mathematical models for prediction of the AE_{RMS} voltage using fresh tools

The following curvilinear, polynomial and linear equations for predicting the AE_{RMS} voltage and correlating cutting process parameters were derived from the experimental

data. The response parameter Y, could be expressed by three major cutting process parameters of the orthogonal cutting operation using the sharp cutting edge of fresh tools.

$$Y_{(Log)} = K(f)^a(90+\alpha)^b(V)^c \tag{5.6}$$

The polynomial model which includes the main effects of cutting process parameters and first order interactions, can be expressed as :

$$Y_{(Pol)} = a_1 + a_2 f + a_3(90+\alpha) + a_4 V + a_5 f(90+\alpha) + a_6 fV + a_7(90+\alpha)V \tag{5.7}$$

The experimental results were used for studying linear and first order interactive effects between the cutting process parameters and the AE_{RMS} voltage. The technique of arriving at the polynomial equation involves an analysis of the variance (ANOVA) test which quantified the effects of cutting process parameters on the variation of the AE_{RMS} voltage. This has been done in order to verify the significance of each cutting process parameter on the optimisation variable, and detect whether there were any interaction effects among the cutting process parameters themselves. Next the multiple correlation coefficient and the Fisher's F-ratio were employed to gauge appropriateness of fit and indicate the significance of each of the cutting process parameters. As a result, a function based on the analysis of variance was developed for describing the experimental results.

The linear equation for orthogonal cutting operations can be expressed as :

$$Y_{(Lin)} = b_1 + b_2 f + b_3(90+\alpha) + b_4 V \tag{5.8}$$

Where K,a,b,c, a_1,a_2,a_3,a_4,a_5,a_6 and b_1,b_2,b_3,b_4 are statistically fitted constants, and estimation of these values is required to be determined from the sampled data. f is feed rate. α is rake angle. V is cutting speed.

The basic models for curvilinear (log-linear), polynomial and linear equations in orthogonal cutting operations are obtained from the experimental outputs, as shown below :

The curvilinear equation for a sharp cutting edge tool is :

$$V_{RMS(Log)} = 2.4691(f)^{0.0091}(90+\alpha)^{-0.3017}(V)^{0.2457} \tag{5.9}$$

The polynomial equation for a sharp cutting edge tool is :

$$\begin{aligned} V_{RMS(Pol)} &= 1.1458 + 0.6318f + 0.0082(90+\alpha) + 0.0073V \\ &\quad +0.0033fV - 0.0133f(90+\alpha) - 0.00001(90+\alpha)V \end{aligned} \tag{5.10}$$

The linear equation for a sharp cutting edge tool is :

$$V_{RMS(Lin)} = 2.3912 + 0.0964f - 0.0078(90+\alpha) + 0.0029V \tag{5.11}$$

Where V_{RMS} = the RMS voltage of acoustic emission signals, subscript (Log) = curvilinear regression analysis, subscript (Pol) = polynomial regression analysis, and subscript (Lin) = linear regression analysis.

The standard error of estimates SEE, coefficients of multiple correlations R, coefficients of determinations R^2 for three equations (5.9) to (5.11) are listed in table 5.3. These results of the computational work indicate the accuracy of the developed

empirical mathematical models and the significance of the computed coefficients. It is noted that the coefficient of multiple correlation for equation (5.10) is higher than those for equations (5.9) and (5.11), but all the models are adequate.

Table 5.1 Analysis of variance tests for empirical models using sharp tools.

Models	SEE	R	$100R^2$
Log-linear (Eq 5.9)	0.2443	0.9108	82.96
Polynomial (Eq 5.10)	0.1480	0.9309	86.66
Linear (Eq 5.11)	0.1672	0.9184	84.34

5.4.2.2 Development of empirical mathematical models for prediction of the AE_{RMS} voltage using worn tools

Based on the functional form of three empirical models described in previous section 5.4.2.1, the mathematical models which can indicate the condition of the cutting tool, can be proposed from the quantitative relationship between cutting process parameters including the levels of flank wear lands and the AE_{RMS} voltage. The statistical models determined from the experiments are as follows :

The curvilinear equation for a worn cutting edge tool is :

$$V_{RMS(Log)} = 2.3088(f)^{0.0083}(90+\alpha)^{-0.1939}(V)^{0.2150}(l_{fw})^{0.1424} \tag{5.12}$$

The polynomial equation for a worn cutting edge tool is :

$$\begin{aligned} V_{RMS(Pol)} = {} & 2.0237 - 0.3681f - 0.0015(90+\alpha) + 0.0043V + 0.2926l_{fw} \\ & -0.0009fV + 0.0071f(90+\alpha) + 0.0521fl_{fw} \\ & -0.00003(90+\alpha)V + 0.0033(90+\alpha)l_{fw} - 0.0012Vl_{fw} \end{aligned} \tag{5.13}$$

The linear equation for a worn cutting edge tool is :

$$V_{RMS(Lin)} = 2.1337 + 0.1163f - 0.0058(90 + \alpha) + 0.0030V + 0.8529l_{fw} \qquad (5.14)$$

Table 5.2 Analysis of variance tests for empirical models using worn tools.

Models	SEE	R	$100R^2$
Log-linear (Eq 5.12)	0.1814	0.9399	88.35
Polynomial (Eq 5.13)	0.1293	0.9620	92.55
Linear (Eq 5.14)	0.1596	0.9547	91.14

The standard error of estimates (SEE), coefficients of multiple correlations (R) and coefficients of determinations (R^2) for the equations (5.12) to (5.14) given in table 5.4, indicate that the coefficient of multiple correlation of equation (5.13) is higher than those of equations (5.12) and (5.14), but all equations are equally useful for prediction of the AE_{RMS} voltage due to the insignificant differences in accuracy of the equations.

5.4.3 Correlation Coefficients of Mathematical Models

Some significant statistical outputs employed in the present research work for comparison of different equations are : the standard error of estimates (SEE), the coefficient of multiple correlation (R), the coefficient of determination (R^2) and F values [167].

The standard error of estimates denotes the deviation of a dependent output variable by the differences between the measured values of each experimental data and the values calculated by using the empirical equation. The standard error of estimates can be

used to estimate the extent to which future results can be expected to differ from the prediction made by using the equation.

The coefficient of multiple correlation gives an idea of the appropriateness of fit or the amount of variance in the dependent output variable computed by the regression equation.

The coefficient of determination represents the percentage of the total variability observed in the dependent output variable. The dependent output variable is capable of being described by the cutting process parameters included in the equations.

5.5 DISCUSSION

Empirical mathematical models can determine the level of the RMS voltage of acoustic emission signals, and provide useful guidelines for estimation and control of tool wear and failure. The effects of each cutting process parameter on the AE_{RMS} voltage were measured and plotted in Figures 5.1 to 5.5, as discussed in the section 5.3 of this chapter. On the basis of the experimental results in Figures 5.1 to 5.5, the three types of empirical models were developed for fresh tools and worn tools respectively. Among the statistically fitted three types of empirical equations, only the polynomial equations which showed the highest coefficient of multiple correlation in tables 5.3 and 5.4, were employed to plot the predicted AE_{RMS} values in Figures 5.6 to 5.10. The predicted AE_{RMS} values in Figures 5.6 to 5.10 were arranged to calculate the average values of the AE_{RMS} voltage on the variations of cutting process parameters. Figures 5.6 to 5.10 show a similar trend between the predicted AE_{RMS} values and the measured AE_{RMS} values, as has been explained the trends of the measured AE_{RMS} values in this chapter, section 5.3.

5.5.1 *Discussion of the Regression Models for Fresh Tools*

The predicted AE_{RMS} values in Figures 5.6 and 5.7 were calculated by using a polynomial equation (5.10) which neglected the flank wear land (VB).

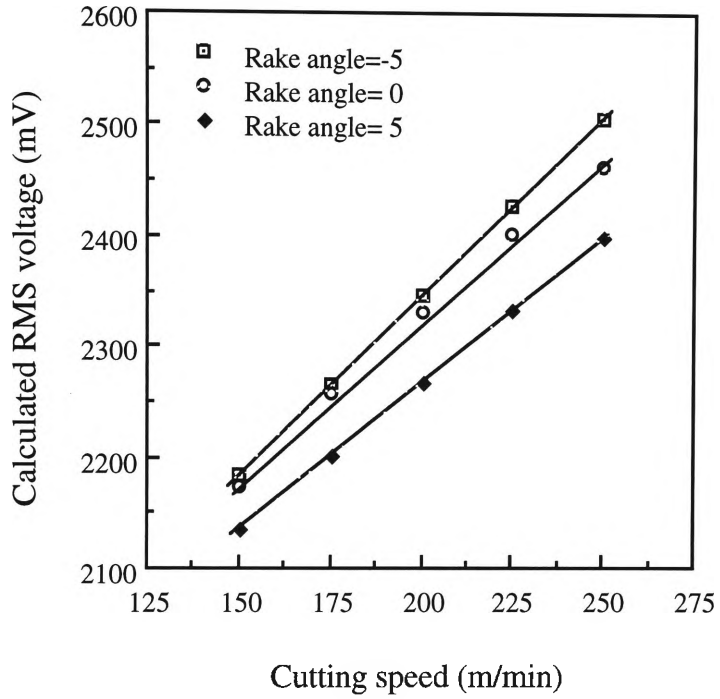

Figure 5.6 Relationship between RMS values predicted by using a polynomial equation and cutting speeds.

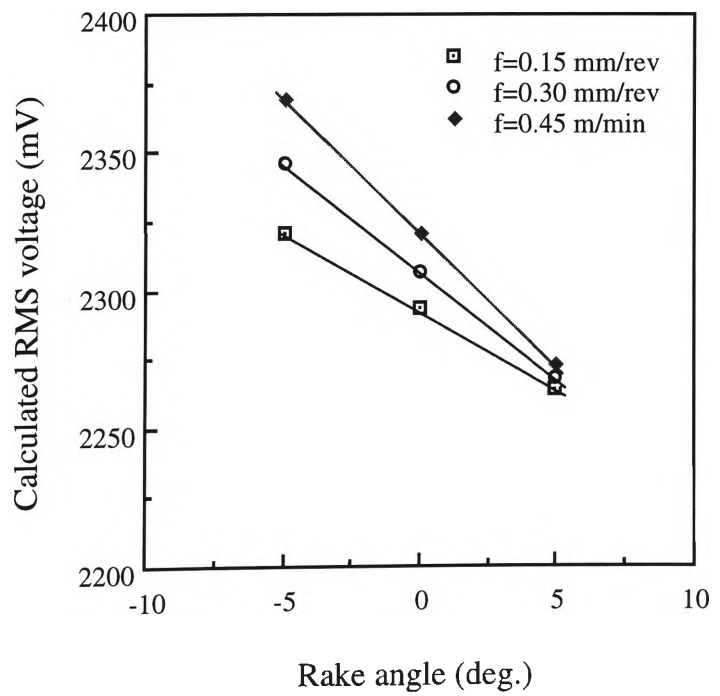

Figure 5.7 Relationship between RMS values predicted by using a polynomial equation and rake angles.

The calculated AE_{RMS} values showed similar trends for the variations of each cutting process parameter (cutting speed, rake angle and feed rate), as plotted in Figures 5.1 and 5.2 and Figures 5.6 and 5.7.

The scatter graphs in Figures 5.8 to 5.10 were plotted to show the agreement between experimental and calculated AE_{RMS} values. The lines of the best fit for the plotted points were drawn by using the empirical mathematical models of the curvilinear, polynomial and linear regression computations, respectively. It is evident from these results (tables 5.3) that all empirical equations for using the sharp cutting edge tools are suitable and applicable because they are highly accurate. Table 5.3 which shows that the total variability explained by the regression analysis is more than 0.91.

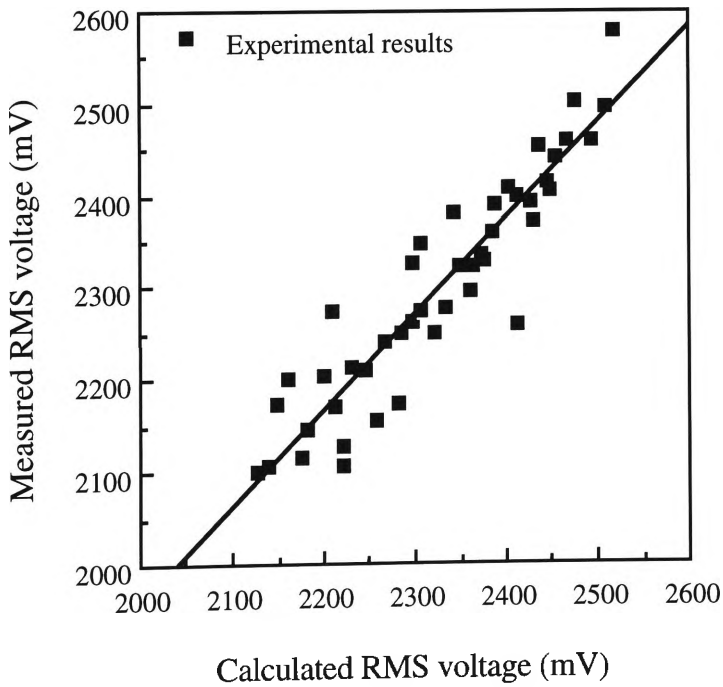

Figure 5.8 Comparison of the measured RMS values with the predicted RMS values by using a curvilinear equation for fresh tools.

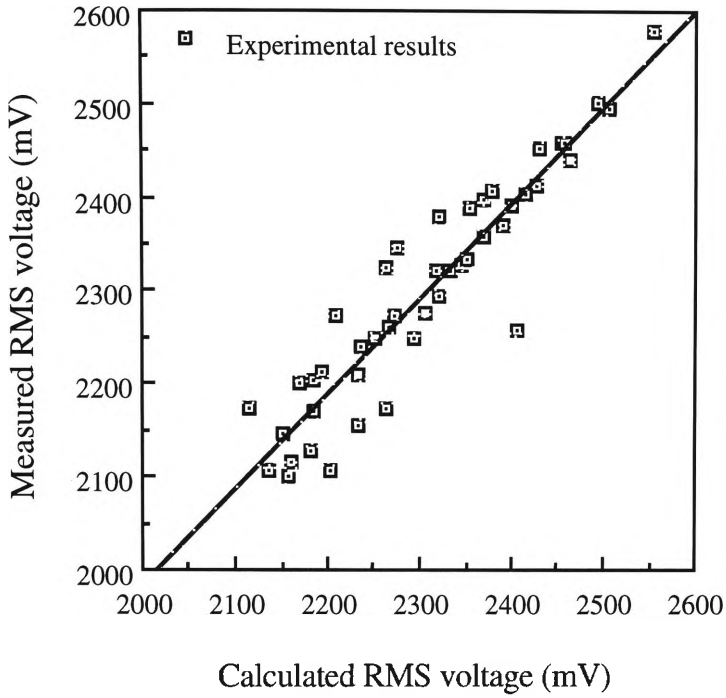

Figure 5.9 Comparison of the measured RMS values with the predicted RMS values by using a polynomial equation for fresh tools.

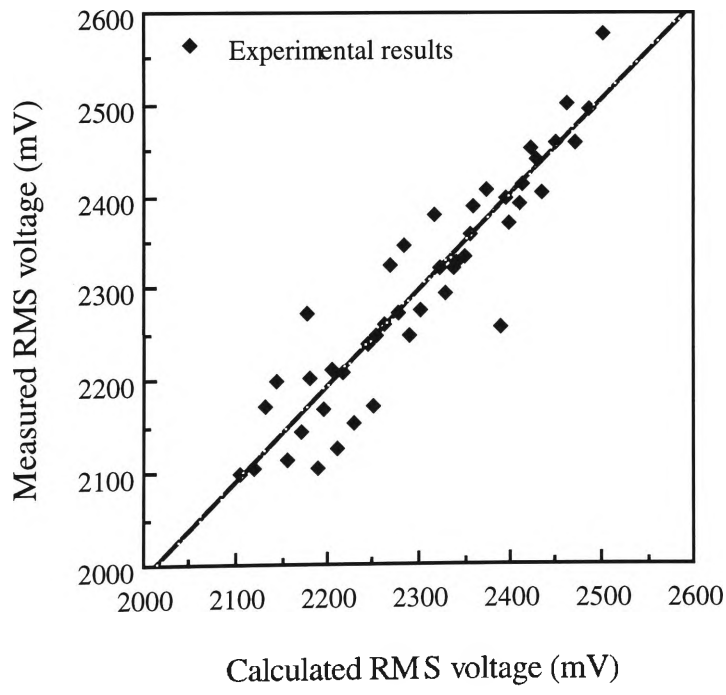

Figure 5.10 Comparison of the measured RMS values with the predicted RMS values by using a linear equation for fresh tools.

5.5.2 *Discussion of the Regression Models for the Worn Tools*

Figures 5.11 to 5.13 were drawn by using a polynomial equation (5.13) which took into account the wear land of tool flank (VB).

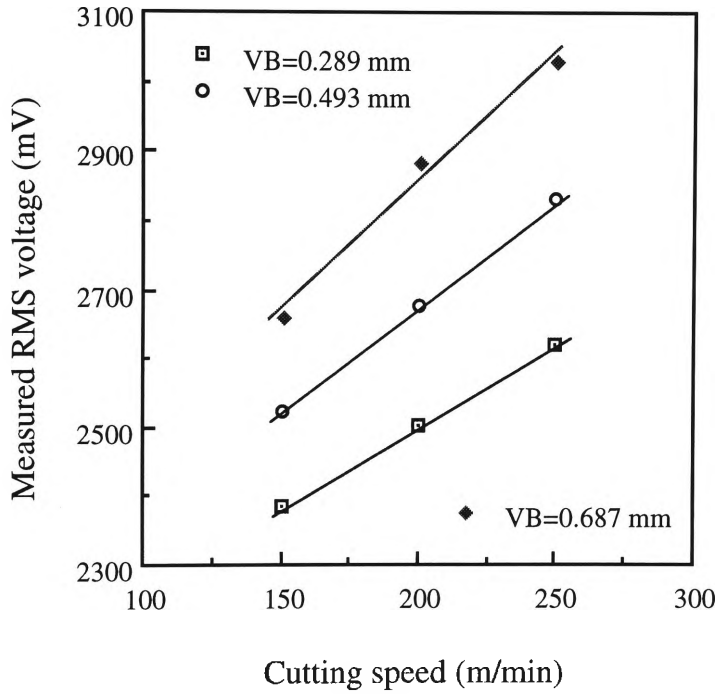

Figure 5.11 Variation of RMS values predicted by using a polynomial equation with cutting speeds for different flank wear lands (VB).

Figures 5.11 to 5.13 present the influences of each cutting process parameter on the AE_{RMS} voltage, considering the tool flank wear land (VB). Similar trends of the predicted AE_{RMS} value for the variations of each cutting process parameter in different flank wear were plotted in Figures 5.11 to 5.13, as shown in Figures 5.3 to 5.5.

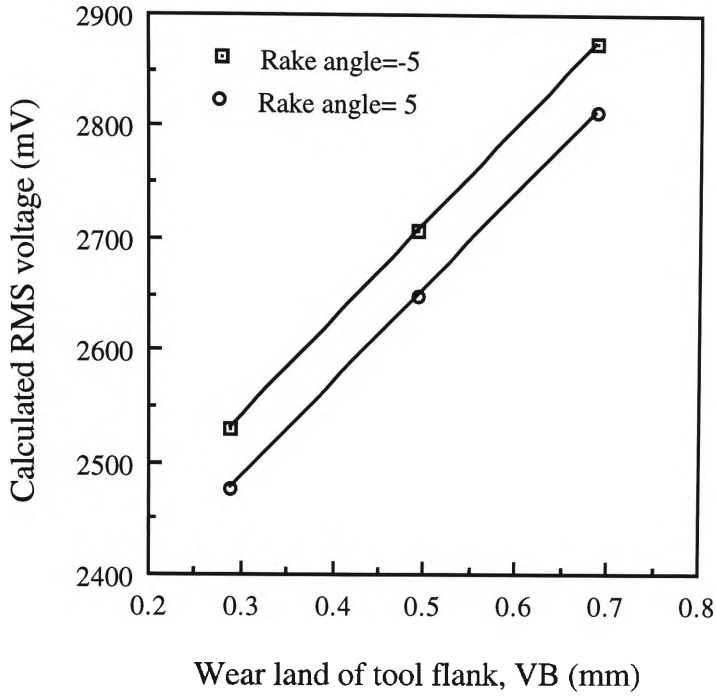

Figure 5.12 Variation of RMS values predicted by using polynomial equation with flank wear lands (VB) for different rake angles.

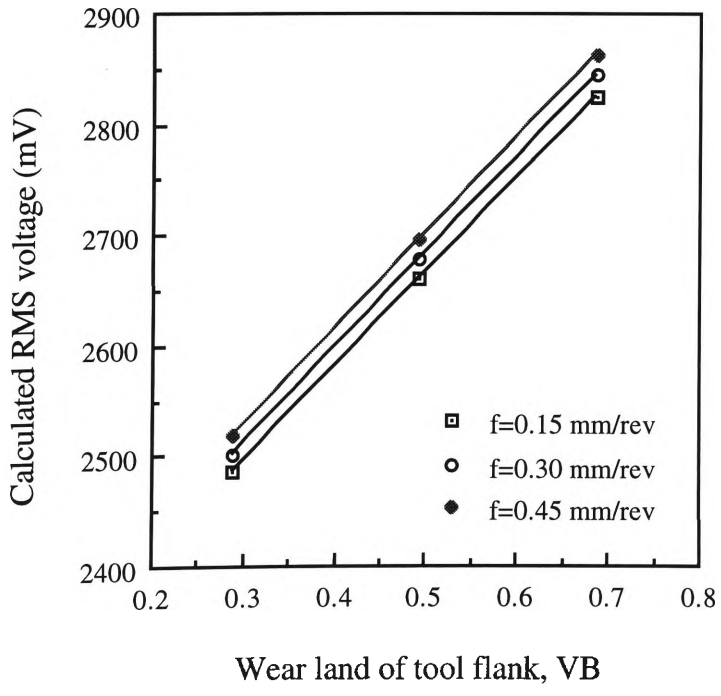

Figure 5.13 Variation of RMS values predicted by using a polynomial equation with flank wear lands (VB) for different feed rates.

The verification of the validity of the empirical equations for worn tools (5.12), (5.13) and (5.14), can be determined from the coefficient of multiple correlation (more than 0.93) given in table 5.4 and the results of the AE_{RMS} values plotted in Figures 5.14 to 5.16.

Figure 5.14 shows the measured AE_{RMS} values against the calculated AE_{RMS} values obtained by using a curvilinear equation. For estimation of the accuracy of the equations, a straight line has been added to indicate ideal values between the measured and predicted AE_{RMS} voltages. The coefficient of multiple correlation value (more than 0.96) and Figure 5.15 which shows a plot between the measured AE_{RMS} values and the predicted AE_{RMS} values obtained by using a polynomial equation, describe the variability of equation (5.13). Finally, the validity of equation (5.14) is indicated by the coefficient of multiple correlation (more than 0.95) and Figure 5.16 which was drawn by using the experimental AE_{RMS} values and the AE_{RMS} values predicted by using a linear equation.

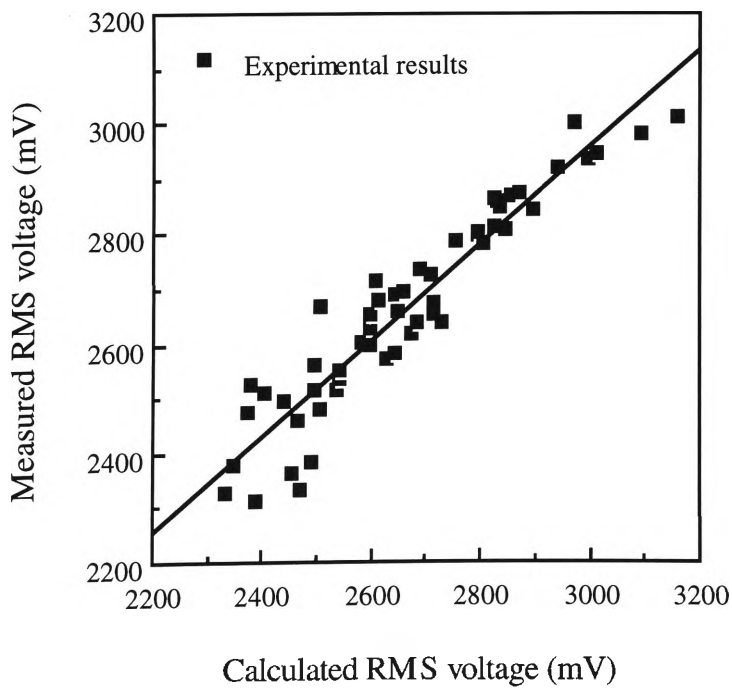

Figure 5.14 Comparison of the measured RMS values with the predicted RMS value by using a curvilinear equation for worn tools.

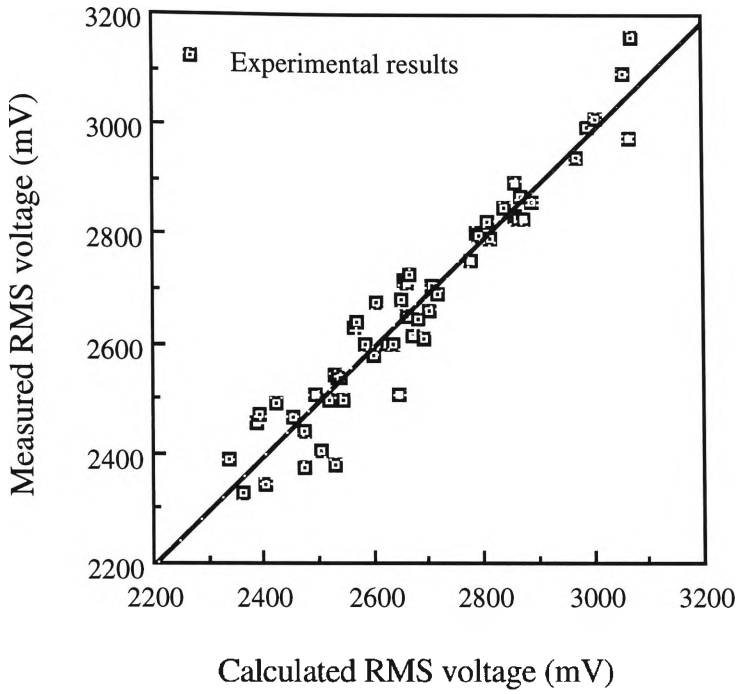

Figure 5.15 Comparison of the measured RMS values with the predicted RMS values by using a polynomial equation for worn tools.

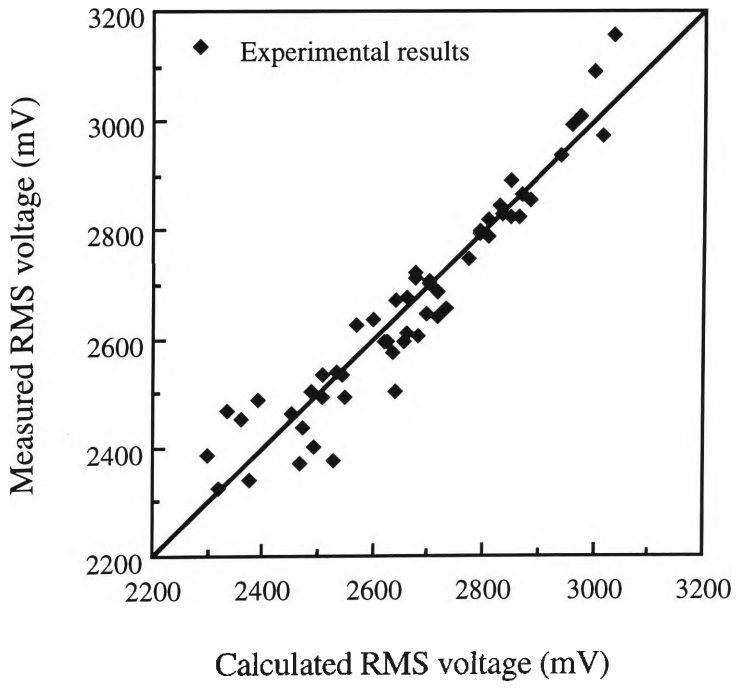

Figure 5.16 Comparison of the measured RMS values with the predicted RMS values by using a linear equation for worn tools.

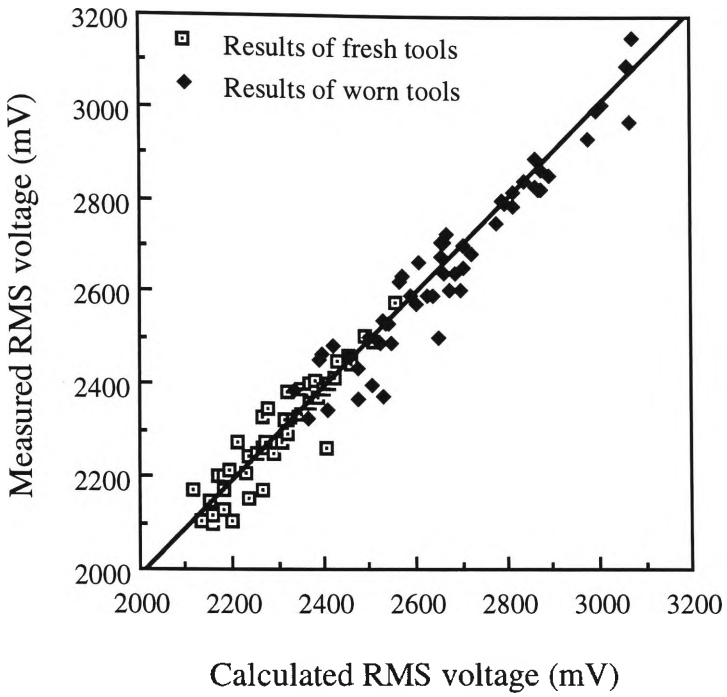

Figure 5.17 Comparison of the measured RMS values with the RMS values predicted by using a polynomial equations for fresh and worn tools.

The values shown in Figure 5.17, include all the measured AE_{RMS} voltages for both fresh and worn tools, and all the predicted AE_{RMS} voltages for each of these by using the polynomial equations (5.10) and (5.13). Figure 5.17 shows that the measured and predicted AE_{RMS} voltages increase when worn tools are used, compared to when fresh tools are used. The results are indicated from the respective starting points of the AE_{RMS} voltage for the condition of the cutting tool. Therefore, the results in Figure 5.17 show that the tool condition plays a major part in the increase of the AE_{RMS} voltage.

The appropriateness of all empirical mathematical models (5.9) to (5.14) has been shown from a reasonable correlation between the cutting process parameters, the experimental and theoretical investigations. The polynomial equations (5.10), which ignores the tool flank wear, and (5.13) which takes into consideration the flank wear, provide better correlation results, as shown in tables 5.3 and 5.4 and in Figures 5.8 to

5.10 and 5.14 to 5.16. However, all mathematical equations are satisfactory and applicable to the automated machining control process, because the differences in accuracy of the developed equations are insignificant.

5.6 CONCLUSIONS

The conclusions based on the experimental results and development of empirical mathematical models can be summarised as follows:

1. Experimental work in this research was designed to predict the effect of the cutting process parameters on the AE_{RMS} voltage and to find the best condition of the cutting tool. The AE_{RMS} voltages observed have been found to correlate well with the variation of cutting process parameters and tool wear.
2. Statistically designed experiments that are based on factorial techniques, proved a powerful means for investigating the relationship between cutting process parameters and the AE_{RMS} voltage.
3. The experimental results indicate that the cutting process parameters have significant influence on the variation of the AE_{RMS} level. Both the observed and predicted AE_{RMS} voltage have been shown to increase with the increasing cutting speed and feed rate, and decreasing rake angle. Moreover, the greater flank wear land (VB) has been shown to increase the level of the AE_{RMS} voltage significantly.
4. The experimental results obtained by using fresh and worn tools were used to develop three empirical equations : curvilinear, polynomial; and linear equations. These results were also employed to find the best mathematical model for prediction of the AE_{RMS} voltage.
5. Comparison of coefficients of multiple correlations for curvilinear, polynomial and linear regression equations correlating cutting process parameters to the AE_{RMS} voltage, indicated that all these equations can be used with the reasonable

of accuracy. Among the developed three pairs of empirical equations using both the sharp and worn cutting edge tools respectively, the polynomial equations were found to be the best.

6. Based on the prediction accuracy of the AE_{RMS} level, empirical mathematical models developed from experimental results can be used to control the cutting process parameters and to find the best condition of the cutting tool for improving the quality of metal products.

CHAPTER SIX

SUMMARY AND RECOMMENDATIONS

6.1 SUMMARY OF THIS THESIS

The complete mathematical models for prediction of acoustic emissions in turning operations, have been developed to investigate the influences of the cutting process variables on the RMS voltage of AE signals and the condition of cutting tools. Development of the mathematical models has been achieved in this research by separate theoretical and empirical analysis. The conclusions of this research work are as follows :

1. Some theoretical equations, such as the equations which determine the initial voltage (V_i), maximum voltage (V_{max}) and damping constant (k), were constructed to enable prediction of the AE signal function in metal cutting operations. These equations play an important role in the determination of the threshold voltage in the experiment work. (Chapter 3)

2. The mathematical models including both theoretical and empirical equations, are necessary to investigate the interactive effects between the independent input parameters and dependent output parameters. These models were developed to

correlate the cutting process parameters, the condition of the cutting tool, and the AE_{RMS} voltage. The models can be used to assist in the process optimisation for automated cutting operations to achieve the desired cutting quality of products.

3. An analytical model has been develpoed from the quantitative relationship between the consumed energy rate and the AE_{RMS} voltage. However, the development of analytical models was very difficult, because of the complexity and somewhat unpredictable nature of the machining process. The major problems, such as the interrelationships of the dependent output variables (force and stress distributions, shear angle, seize ratio of the tool-chip contact length, etc) and the AE signal losses in various cutting zones, have been solved using empirical theory and computational work. The AE_{RMS} values computed by using the analytical model have been found to correlate well with the variations of cutting process parameters and tool conditions.

4. Seize ratio based on the definition of the parabolic constant in the tool-chip interface was determined. It plays an important role in the development of theoretical models for prediction of the AE_{RMS} value. The experimental results show that the seize ratio increases with the increasing cutting speed and rake angle. The seize ratio in the sticking zone is lower than the value of 0.5 assumed by K-Asibu and Dornfeld.

5. The variation of cutting process parameters has a significant influence on the variation of AE_{RMS} voltages. Both the observed and predicted AE_{RMS} voltages have been shown to increase with the greater cutting speed, cutting force, shear plane angle and feed rate. However, the AE_{RMS} voltages were found to decrease with the increasing rake angle.

6. The AE_{RMS} voltages have been observed to increase significantly with the greater flank wear land (VB).

7. Experimental results have shown that empirical equations (curvilinear, polynomial and linear) can establish interactive effects between the basic cutting process parameters (feed rate, cutting speed, rake angle and flank wear land) and the AE_{RMS} voltage. The polynomial equations obtained by using both the sharp and worn cutting edge tools respectively, were found to be the best among the three pairs of empirical equations developed. However, the comparison of the coefficients of multiple correlation for the three pairs of empirical equations indicated that the coefficients of the three pairs of the equations are almost equal. Consequently, all of the equations are reasonably applicable.

8. The modelling process for development of mathematical models provided an efficient method for analysis of the automated metal cutting performance. Adaptive control using the developed models can be achieved by employing an appropriate computer interface for the control and monitoring of the automated cutting process.

6.2 RECOMMENDATIONS FOR FUTURE RESEARCH WORK

Recommendations for further study and experiments in associated fields are suggested and briefly summarised as follows :

1. The analytical models developed in chapter 4 are suitable models for prediction of the AE_{RMS} voltage in the orthogonal cutting operation relative to the condition of cutting tools. However, using the variations of cutting process parameters, the models could be extended to investigate the effects of the tool and chip fractures

on the variation of the AE_{RMS} voltage. In all, the temperature distribution in the cutting tool which increases the progressive tool wear can also be taken into account in the models. The infrared thermography and the machine vision sensing (image analysis) could be used for measurement of the cutting tool and chip temperature.

2. The empirical models developed for establishing the influence of cutting process parameters on the AE_{RMS} value, were closely related to the realistic experimental results. It is suggested that these equations could be developed using the influences of the other dependent output variables instead of the AE_{RMS} voltage. Possibilities in development of other empirical models are the use of variations in spindle power, surface roughness, noise level and many other variables which are not included in this research. Examination of interactive effects between the dependent output variables mentioned above could be very useful for the control and analysis of the cutting process problems.

3. The modelling technique considered in this research employed the multiple regression analysis only. For estimating the accuracy of the developed mathematical models, different modelling techniques such as the group method of data handling (GMDH), neural network, and fuzzy logic, could be used to evaluate the theoretical data computed by mathematical models and experimental data. Combining the different modelling techniques could be more useful in the selection of a range of cutting process parameters for use in machining control.

4. Process modelling with the combined techniques as in 3, could more effectively determine a range of process parameters with which cutting operations could be optimised. In this way, **(1)** a closed-loop feedback control system could be established, and **(2)** possible errors from the variations uncontrolled in the

machining process can be minimised . Figure 6.1 depicts the appropriate layout for adaptive control techniques on machine tools.

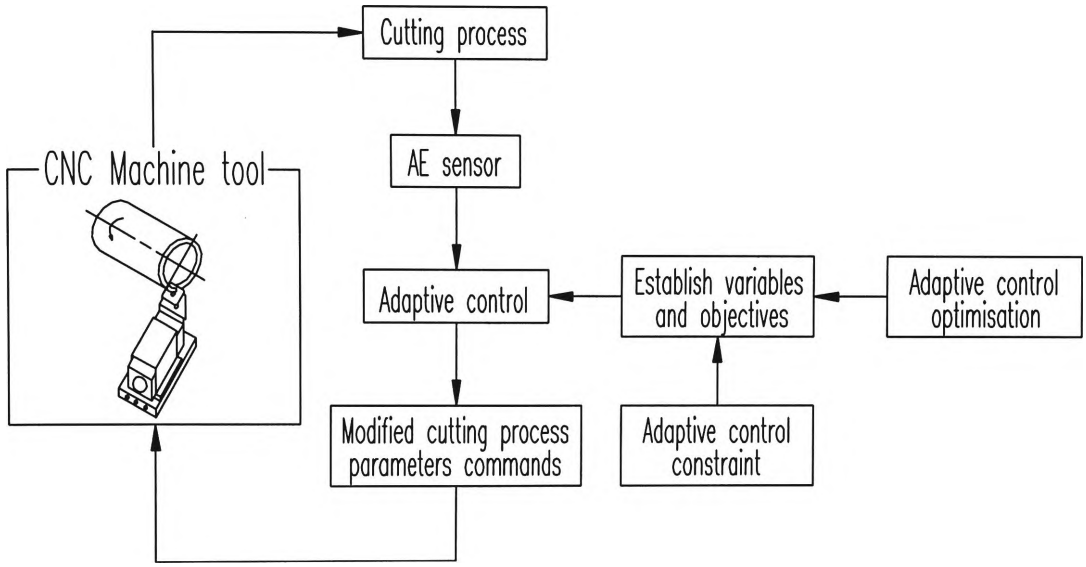

Figure 6.1 Feedback control system for adaptive control techniques on the CNC machine tool.

REFERENCES

1. M. C . Shaw, "*Metal Cutting Principles*", Oxford University Press, 2nd Edition, New York, 1991.
2. K. A. Zvorykin, *"Rabota ; Usilie Neobkhodimyya dlya Oteleniya Metallischeskikh Struzhek"*, Moscow, Russia, 1893.
3. I. Finnie, *"Review of Metal -Cutting Analyses of the Past One Hundred Years"*, Mechanical Engineering, Vol. 78, No. 8, 1956, pp. 715-721.
4. V. Piispanen, *"Lastunmoudostumisen Teoriaa"*, Teknillinen Aika Kauslehti, Vol. 27, 1937, pp. 315.
5. H. Ernst and M. Eugene Merchant, *"Chip Formation, Friction, and High Quality Machined Surfaces"*, Surface Treatment of Metals, Transaction of the ASME, Vol. 29, 1941, pp 299-379.
6. M. Eugene Merchant, *"Mechanics of the Metal Cutting Process"*, Journal of Applied Physics, Vol. 16, No. 5, 1945, pp. 267-275, and No. 6, pp. 318-324.
7. N. N. Zorev, *"Metal Cutting Mechanics"*, Pergmon Press, Oxford, 1966.
8. M. C. Shaw, *"In Metal Tansformations"*, Gordon and Breach, New York, 1968, pp. 211-260.
9. R.M.D. Mesquita, Marques and M.J.M. Barata, *"Experimental Determination of the Dynamic Shear Stress in Metal Cutting"*, Journal of Materials Processing Technology, Vol. 33, No. 3, 1992, pp.229-246

10. Y. W. Park, P. H. Cohen and C. O. Ruud, *"The Development of a Mathematical Model for Pridicting the Depth of Plastic Deformation in a Machined Surface"*, Materials & Manufacturing Processes, Vol. 8, 1993, No 6 , pp. 703-715.

11. E. Usui and A. Hirota, *"An Energy Approach to Mechanics of Three-Dimensional Metal Machining"*, Proc. Int. Conference on Production Engineering, Tokyo, 1974, pp. 541.

12. K. Nakayama and M. Arai, *"On the storage of Data on Metal Cutting Forces"*, Annals of the CIRP, Vol. 25, No. 1, 1976, pp. 13-18

13. W. Grzesik, *"The Mechanics of Continuous Chip Formation in Oblique Cutting with Single-Edge Tool-Part II, Experimental Verification of the Theory"*, Int. J. Mach. Tools Manufact., Vol. 30, No. 3, 1990, pp. 373-388.

14. S. D. J. A. Arescularatne, G. Barrow and S. Hinduja, *"Prediction of the Radial Force in Turning using Feed Force Data"*, Int. J. Mach. Tools Manufact., Vol. 33, No. 6, 1992, pp. 827-839.

15. A. H. Cottrel, *"The Mechanical Properties of Matter"*, John Willey and Sons Inc., New York, 1964, pp.269.

16. D. W. Wu and Y. Matsumoto, *"The Effect of Hardness on Residual Stresses in Orthogonal Machining of AISI 4340 Steel"*, Journal of Engineering for Industry, Transactions of the ASME, Vol. 112, 1990, pp. 245-252.

17. J. T. Black, *"Mechanics of Chip Formation"*, Metals Handbook, 9th Edition, ASM, Vol. 16, 1989, pp. 7-12.

18. S. Kobayashi and E. G. Thomsen, *"Some Observations on the Shearing Process in Metal Cutting"*, Journal of Engineering for Industry, Transactions of the ASME, Vol. 81, 1959, pp. 251.

19. N. N. Zorev, *"Interrelationship Between Shear Processes Occurring Along Tool Face and on Shear Plane in Metal Cutting"*, International

Research in Production Engineering, Presented at International Production Engineering Reseaarch Conference, 1963, pp. 42-49.

20. D. R. Olberts, *"A Study of the Effects of Tool Flank Wear on Tool Chip Interface Temperature"*, Journal of Engineering for Industry, Transactions. of the ASME, Vol. 81, 1959, pp. 152-158.

21. S. B. Rao, *"Tool Wear Monitoring Through the Dynamics of Stable Turning"*, Journal of Engineering for Industry, Transactions of the ASME, Vol. 108, 1986, pp. 183-190.

22. M. Masuda, Y. Kuroshima and Y. Chujo, *"Failure of Tungsten Carbide-Cobalt Alloy Tools in Machining of Carbon Materials"*, Wear, Vol. 169, 1993, pp. 135-140.

23. D. A. Dorndeld and E. Kannatey-Asibu JR, *"Acoustic Emission During Orthogonal Metal-Cutting"*, Int. J. Mech. Sci., Vol. 22, 1979, pp. 285-296.

24. E. Kannatey-Asibu JR and D. A. Dorndeld, *"Quantitative Relationships for Acoustic Emission from Orthogonal Metal Cutting"*, Journal of Engineering for Industry, Transactions of the ASME, Vol. 103, Aug. 1981, pp 330-334

25. T. Hodgson, *"Cubic Boron Nitride Machining with Particular Reference to Cutting Forces When Machining With Tool Steel"*, The Institution of Engineers, Australia, 1981.

26. L. De Chiffre, *"What we can do about Chip Formation"*, Int. J. Mach. Tool Des. Res., 1977, pp. 225.

27. E. G. Thomsen, S. Kobayashi and C. T. Yang *"Mechanics of Plastic Deformation in Metal Processing"*, Macmillan, New York, 1967, pp. 451.

28. Dimitri Kececioglu and Wis Milwaukee, *"Shear-Strain Rate in Metal Cutting and Its Effects on Shear-Flow Stress"*, Journal of Engineering for Industry, Transactions of the ASME, Vol. 80, 1958, pp. 158-168.

29. B. F. Von Turkovich, *"Dislocation Theory of Shear Stress and Strain Rate in Metal Cutting"*, Proc. 8th I.M.T.D.R. Conference, 1967, pp.534.

30. E. H. Lee and B. W. Shaffer, *"The Theory of Plasticity Applied to a Problem of Machining"*, Journal of Engineering for Industry, Transactions of the ASME, Vol. 73, 1951, pp. 405-413.

31. H. Hücks, *"Plastizitätsmechaniche Grundlagen und Kenngrössen der Zerspannung"*, Dissertation, Technische Hochschule, Aachen, Germany, 1951.

32. G. V. Stabler, *"Fundamental Geometry of Cutting Tools"*, Proceeding Institution of Mechanical Engineers, Vol. 165, No. 63, 1951, pp.14-23.

33. P. L. B. Oxley, *"An Analysis for Orthogonal Cutting with Restricted Tool-Chip Contact "*, Int. J. Mech. Sci., Pergamon Press Ltd, Vol. 4, 1962, pp. 129-135.

34. T. Sata, *"Friction Process on Cutting Tool and Cutting Mechanism"*, International Research in Production Engineering, ASME, New York, 1963, pp. 18

35. G. Boothroy, *"Effect of Surface Slope on the Shear Angle in Metal Cutting"*, Journal of Engineering for Industry, Transaction of ASME, Vol. 89, 1970, pp. 115-118.

36. R. N. Mittal and B. L. Juneja, *"Effect of Stress Distribution on the Shear Angle in the Controlled Contact Orthogonal Cutting"*, Int. J. Mach. Tool Des., Vol. 22, No. 2, 1982, pp. 87-96.

37. W. H. Robert, *"Numerical Method"*, Quantum Plublishers Inc., 1987, pp. 121-129.

38. P. Albrecht, *"Analysis of the Mechanics of the Cutting When machining Cylindrical Surfaces"*, Annals of CIRP, Vol. 13, 1987, pp.263-271.

39. J. S. Lin and C. I. Weng, *"Non Linear Dynamics of the Cutting Process"*, Int. J. Mech. Sci. Vol. 33, No. 8, 1991, pp. 645-657.

40. G. W. Rowe and P. J. Spick, *"A New Approach to Determination of the Shear-Plane Angle in Machining"*, Journal of Engineering for Industry, Transactions of ASME, Vol. 89, 1967, pp. 530.

41. M. Y. Friedman and E. Lenz, *"Investigation of the Tool-Chip Contact Length in Metal Cutting"*, Int. J. Mach. Tool Des. Res., Vol. 10, 1970, pp. 401-416.

42. A. B. Sadat and M. Y. Reddy, *"Surface Integrity of Inconel-718 Nickel-base Superalloy Using Controlled and Natural Contact Length Tools. Part I : Lubricated"*, Experimental Mechanics, sep. 1992, pp. 282-288.

43. R. S. Hahn, Discussion of Paper by M.C. Shaw, N. H. Cook and I. Finnie, *"The Shear Angle Relationship in Metal Cutting"*, Transaction of ASME, Vol. 83, 1953, pp. 273.

44. M. I. Klushin, *"Determination of the Contact Zone Between Chip and Rake Face and the Pressure in this Zone"*, Stankii Instruminent, Vol. 31, 1960.

45. P. L. B. Oxley, *"An Analysis for Orthogonal Cutting with Restricted Tool-Chip Contact "*, Int. J. Mech. Sci., Pergamon Press Ltd, Vol. 4, 1962, pp. 129-135.

46. C. Rubenstein, *"A Simple Theory of Orthogonal Cutting"*, Int. J. Mach. Tool Des., Res., Vol. 4, 1965, pp. 123.

47. N. N. Zorev, *"Metal Cutting Mechanics"*, Pergamon Press, Oxford, 1962.

48. T. N. Abuladze-Loladze, *"Prochnost i Iznosotojkost Rechzushego Instrumenta"* Moscow, Machinostroenie, 1982.

49. G. S. Gad, E. J. A. Armarego and A. J. R. Smith, *"Tool-Chip contact length in orthogonal machining and its importance in tool temperature predictions"*, Int. J. Prod. Res., Vol. 30, No. 3, 1992, pp. 485-501.

50. M. Shiraishi and S. Sato, *"Dimensional and Surface Roughness controls in a Turning Operation"*, Journal of Engineering for Industry, Transaction of ASME, Vol. 112, 1990, pp. 78-83.

51. J. Colgan, H. Chin, K. Danai and S. R. Hayashi, *"On-Line Tool Breakage Dection in Turning: A Multi-Sensor Method"*, Journal of Engineering for Industry, Transactions of the ASME, Vol. 116, 1994, pp. 117-123.

52. G. F. Micheletti, W. Koening, H. R. Victor, *"In process Tool Wear Sensors for Cutting Operations"*, Annal of CIRP, Vol 25, No 2, 1976, pp483-496

53. T. Moriwaki, *"Sensing and Prediction of Cutting Tool Failure"*, Bull. Japan Soc. of Prec. Engg., Vol. 18, No. 2, 1984, pp 90-96.

54. E. H. Frost-Smith, et. al., *"Optimisation of the Machining Process and Overall System Concepts"*, Proc. MTIRA Conference on A. C. of Machining Tools, April 1970.

55. G. Rutelli and D. Cuppini, *"Development of Wear Sensor for Tool Management System"*, Journal of the Engineering Material Technology, Vol. 110, 1988, pp. 59-62.

56. K. Uehara, *"New Attempts for Short Time Tool-Life Testing"*, Annals of the CIRP, Vol. 22, No. 1, 1973.

57. Y. Nakazawa, *"Detection Method of Abnormal State of Tool in Turning"*, Preprints of Spring Annual Meeting of the Japan Soc. of Prec. Engg., 1980, pp. 106-108.

58. N. H. Cook, *"Tool Wear Sensors"*, Wear, Vol. 62, 1980, pp. 49-57.

59. S. M. Arsovski, *"Wear Sensors in Adaptive Control Systems of Machine Tools"*, International Journal of Production Research, Vol. 21, 1983, pp. 347-356.

60. T. Sata, *"Rapid Tool-Life Tests By means of Irradiated Carbide Cutting Tools"*, Bull. Japan Soc. of Prec. Engg., Vol. 24, 1958, pp. 453.

61. N. H. Cook, K. Subramanian and S. Basile, *"Micro-isotope Tool Wear Sensing Method"*, ,Annals of the CIRP, Vol. 27, 1978, pp. 73-78.

62. S. Jetly, *"Measuring CuttingTool Wear On-Line: Some Practical Considerations"*, Manufacturing Engineering, July 1984, pp. 55-60.

63. B. Colding and A. Novak, *"Sensing of Workpiece Diameter, Vibration and Out-off-Roundness by Laser-way to Automate Quality Control"*, Annals of the CIRP, Vol. 30, 1981, pp. 473-476.

64. J. L. El. Gomayel and K. D. Bregger, *"On-Line Tool Wear Sensing for Turning Operations"*, Journal of Engineering for Industry, Transactions of the ASME, Vol. 108, 1986, pp. 44-47.

65. H. Takeyama, Y. Doi, T. Mitsuoka and H. Sekiguchi, *"Sensors of Tool-Life for Optimisation of Machining"*, Journal of Mech. Lab. of Japan, Vol. 14, No. 2, 1968.

66. G. Spur and F. Leonards, *"Kontinuierlich Arbeitende Verschleisssenoren fur AW-Syteme Beider Drehbear Beitung"*, ZWF, Vol.68, No. 10, 1973.

67. T. H. Stoferle and B. Bellmann, *"Continuous Measuring of Flank Wear"*, Proc. 16th Int. Machine Tool Design and Research Conference, 1975, pp. 573-578.

68. H. Suzuki and K. J. Weinamann, *"An On-Line Tool Wear Sensor for Straight Turning Operations"*, Journal of Engineering for Industry, Transactions of the ASME, Vol. 107, 1985, pp. 397-399.

69. Y. Kashimura, *"In-Process Detection of Tool Failure by Making use of Force Ratios"*, Transactions of the JSME, Vol. 49, No. 441, 1983, pp. 835-842.

70. G. F. Micheletti, A. DeFilippi and R. Ippolito, *"Tool Wear and Cutting Forces In Steel Turning"*, Annals of the CIRP, Vol. 16, 1986, pp.353-360.

71. K. Danai A. G. Ulsoy, *"A Dynamic State Model for On -Line Tool Wear Estimation in Turning"*, Journal of Engineering for Industry, Transactions of the ASME, Vol. 109, 1987, pp. 396-399.

72. H. V. Ravindra, Y. G. Srinivasa and R. Krishnamurthy, *"Modelling of Tool Wear Based on Cutting Forces in Turning"*, Wear, Vol. 169, 1993, pp 25-32.

73. S. M. Pandit and S. Kashou, *"Vibration in Friction Coefficient with Tool Wear"*, Wear, Vol. 84 , 1983, pp 65-79.

74. C. Jiang, Y. Zhang and H. Xu, *"In-Process Monitoring of Tool Wear Stage by the Frequency Band energy Method"*, Annals of the CIRP, Vol. 36, 1987, pp 45-48.

75. L. C. Lee, *"A Study of Noise Emission for Tool Failure Prediction"*, International Journal of Machine Tool Design Research, Vol. 26, 1986, pp. 205-215.

76. D. Sprugeon and R. A. C. Slater, *"In Process Indication of Surface Roughness using a Fibre Optics Transducer"*, Proc. of 15th MTDR Conference, 1974, pp. 339.

77. H. Murray, *"Exploratory Investigation of Laser Method for Grinding Research"*, Annals of the CIRP, Vol. 22, No. 1, 1973, pp. 137.

78. Y. Nakazawa, *"Detection Method of Abnormal State of Tool in Turning"*, Preprints of Spring Annual Meeting of JSPE, 1980, pp. 106-108.

79. S. R. Hayashi, C. E. Thomas and D. G. Wildes, *"Tool Break Detection by Monitoring Ultrasonic Vibrations"*, Annals of the CIRP, Vol. 37, No. 1, 1988, pp. 61-64.

80. E. Usui and T. Shirakashi, *"Analytical Prediction of Cutting Tool Wear"*, Wear, Vol. 100, 1984, pp. 129-151.

81. D. A. Stephenson *"Assessment of Steady-State Metal Cutting Temperature Models Based on Simultaneous Infrared and*

Thermocouple Data", Journal of Engineering for Industry, Transactions of the ASME, Vol. 114, 1992, pp. 127-136.

82. D. A. Stephenson and A. Ali, *"Tool Temperatures in Interrupted Metal Cutting"*, Journal of Engineering for Industry, Transactions of the ASME, Vol. 114, 1992, pp. 127-136.

83. K. Ide and K. Hironaka, *"Detection of Tool Failure by Ratio of Motor loads"*, Preprints of Spring Annual Meeting of JSPE, 1983, pp. 607-608.

84. J. W. Youn, M. Y. Yang and H. Y. Park, *"Detection of Cutting Tool Fracture by Dual Signal Measurements"*, Int. J. Mach. Tools Manufact., Pergamon, Vol. 34, No. 4, 1994, pp. 507-525.

85. J. Tlusty and G. C. Andrews, *"A Critical Review of Sensors for Unmanned Machining"*, Annals of the CIRP, Vol. 32, No. 2, 1983, pp. 1-10.

86. G. Chryssolouris and M. Guillot, *"A Comparison of Statistical and AI Approaches to the Selection of Process Parameters in Intelligent Machining"*, Journal of Engineering for Industry, Transactions of the ASME, Vol. 112, 1990, pp. 122-131.

87. L. Fucich, K. Obermiller, A. Shuster and M. C. Shaw, *"Use of Manual Adaptive Control in the Evaluation of New Metal Cutting Tools "* American Machinist, Vol. 121, No. 5, 1977, pp. 81-84.

88. M. C. Shaw, *"Optimisation of Metal Cutting Processes On the Art of Cutting Metals - 75 Years Later"*, PED- Vol. 7, 1982, pp. 149-157.

89. D. A. Gall, *"Adaptive control of the abrasive cut-off operation"*, Annals of the CIRP, Vol. 17, 1969, pp. 395-399.

90. C. L. Wu, P. K. Haboush, D. R. Lymburner and G. H. Smith, *"Closed-Loop Machining Control for Cylindrical Turning"*, Ford Motor Company, Dearborn, Michigan, 1987, pp. 189-204.

91. Y. D. Chen, J. Ni and S. M. Wu, *"Real-Time CNC Tool Path Generation for Machining IGES Surfaces"*, Journal of Engineering for Industry, Transactions of the ASME, Vol. 115, Nov. 1993, pp. 480.

92. Jong-Jin Park and A. Galip Ulsoy, *"On-Line Flank Wear Estimation Using an Adaptive Observer and Computer Vision, Part I Theory"*, Journal of Engineering for Industry, Transactions of the ASME, Vol. 115, Feb. 1993, pp. 30-43.

93. Jong-Jin Park and A. Galip Ulsoy, *"On-Line Flank Wear Estimation Using an Adaptive Observer and Computer Vision, Part II: Experiment"*, Journal of Engineering for Industry, Transactions of the ASME, Vol. 115, Feb. 1993, pp. 44-55.

94. K. B. Pederson, *"A Computer Vision System for Wear Measurement of Cutting Tools"*, 3rd International Conference on Computer-Aided Production Engineering, 1988, pp. 421-427.

95. E. N. Diei and D. A. Dornfeld, *"A Model of Tool Fracture Generated Acoustic Emission During Machining"*, Journal of Engineering for Industry, Transactions of the ASME, Vol. 109, Aug. 1987, pp. 227-233.

96. J. M. Lee, D. K. Choi and C. N. Chu, *"Real Time Tool Breakage Monitoring for NC Turning and Drilling"*, Annals of the CIRP, Vol. 43, No. 1, 1994, pp. 81-84.

97. R. G. Liptai, D. O. Harris and C. A. Tarto, *"An Introduction to Acoustic Emission"*, Acoustic Emission, ASTM STP 505, American Society for Testing and Maerials, 1972, pp. 3-10.

98. J. Kaiser, *"Untersuchungen über das auftreten Geräuschen beim Zugversuch"*, Arkiv für das Eisenhuttenwesen, AREIA, Vol. 24, No. 1/2, 1953, pp. 43-45.

99. B. H. Schofield, R. A. Bareiss and A. A. Kyrala, *"Acoustic Emission Under Applied Stress"*, ASTIA Document AD 155674, WADC Technical Report, 1958, pp. 58-194.

100. C. A. Tatro, *"Sonic Techniques in the Detection of Crystal Slip in Metals"*, Status Report, Division of Engineering Research, College of Engineering, Michigan State University, East Lansing, Mich., 1959.

101. H. L. Dunegan, D. O. Harris and C. A. Tatro, *"Acoustic Emission Research"*, Report UCID-4868, Revision 1, Lawrence Radiation Laboratory, Livermore, Calif., 1964.

102. H. R. Hardy, *"Acoustic Emission/Microseismic Activity in Geologic Structures and Materials"*, Proceedings of 3rd Conference, Pennsylvania, Oct. 1981, Trans. Tech. Publication, Huston, Gulf, 1984.

103. R. A. Muenow, *"Uses of Acoustic Emission in Construction"*, Presented at Symposium on Acoustic Emission, Bal Harbour, Fla., 7-8 Dec. 1971.

104. H. L. Dunegan and A. T. Green, *"Factors Affecting Acoustic Emission Response From Materials"*, Acoustic emission, ASTM stp 505, 1972, pp. 100-113.

105. P. Souquet, N. Gsib, M. Deschamos, J. Roget, J. C. Tanguy, *"Tool Monitoring with Acoustic Emission Industrial Results and Future Prospects"*, Annals of the CIRP, Vol. 36, No. 1, 1987, pp. 57-60.

106. M. Lee, D. G. Wildes and S. R. Hayashi and B. Keramati, *"Effect of Tool Geometry on Acoustic Emission Intensity"*, Annals of the CIRP, Vol. 37, No. 1, 1988, pp. 57-60.

107. R. Teti and D. Dornfeld, *"Modelling and Experimental Analysis of Acoustic Emission from Metal Cutting"*, Journal of Engineering for Industry, Transactions of the ASME, Vol. 111, 1989, pp. 229-237.

108. D. V. Hutton and Qinghuan Yu, *"On Effect of a Built-Up Edge on Acoustic Emission in Metal Cutting"*, Journal of Engineering for Industry, Transactions of the ASME, Vol. 112, 1990, pp. 184-189.

109. T. Blum and I. Inasaki, *"A Study on Acoustic Emission from Orthogonal Cutting Process"*, Journal of Engineering for Industry, Transactions of the ASME, Vol. 112, 1990, pp. 203-210.

110. C. L. Jiaa and D. A. Dornfeld, *"Experimental Studies of Sliding Friction and Wear Via Acoustic Emission Signals Analysis"*, Wear, Vol. 139, 1990, pp. 403-424.

111. S. Rangwala D. Dornfeld *"A Study of Acoustic Emission Generated During Orthogonal Metal Cutting - 1 : Energy analysis"*, Int. J. Mech. Sci., Pergamon Press Plc., 1991, pp 471-487.

112. R. J. Boness and S. L. McBride, *"Adhesive and Abrasive Wear Studies Using Acoustic Emission Techniques"*, Wear, Vol. 149, 1991, pp. 41-53.

113. D. A. Dornfeld and V. Lisiewicz,*"Acoustic Emission Feedback for Precision Deburring"*, Annals of the CIRP, Vol. 41, No. 1, 1992, pp. 93-100.

114. A. E. Diniz, J. J. Liu and D. A. Dornfeld, *"Correlating Tool Life, Tool Wear and Surface Roughness by Monitoring Acoustic Emission in Finish Turning"*, Wear, Vol. 152, 1992, pp. 395-407.

115. K. Matsuoka, D. Forrest and M. K. Tse, *"On-Line Wear Monitoring using Acoustic Emission"*, Wear, Vol. 162, 1993, pp. 605-610.

116. R. Teti and G. F. Micheletti, *"Tool Wear Monitoring Through Acoustic Emission"*, Annals of the CIRP, Vol. 38, No. 1, 1989, pp. 99-102.

117. S. Lingard and K. K. Ng, *"An Investigation of Acoustic Emission in Sliding Friction and Wear of Metals"*, Wear, Vol. 130, 1989, pp. 367-379.

118. R. Teti, U. and La Commare, *"Cutting Conditions and Work Material State Identification Through Acoustic Emission Methods"*, Annals of the CIRP, Vol. 41, 1992, pp 89-92.

119. S. Lingard, C. W. Yu and C. F. Yau, *"Sliding Wear Studies using Acoustic Emission"*, Wear, Vol. 162-164, 1993, pp. 597-604.

120. S. Rangwala D. Dornfeld *"A Study of Acoustic Emission Generated During Orthogonal Metal Cutting - 2 : Spectral analysis"*, Int. J. Mech. Sci., Pergamon Press Plc., 1991, pp 489-499.

121. S. Y. Liang, and D. A. Dornfeld, *"Detection of Cutting Tool Wear Using Time Series Analysis of Acoustic Emission Signals"*, Journal of Engineering for Industry, Transactions of the ASME, Vol. 111, 1989, pp. 199-205.

122. J. A. Rice and S. M. Wu, *"Acoustic Emission Source and Transmission Path Characterization Through Homomorphic Processing"*, Journal of Engineering for Industry, Transactions of the ASME, Vol. 116, 1994, pp. 32-41.

123. J. A. Rice and S. M. Wu, *"On the Feasibility of Catastrophic Cutting Tool Fracture Prediction Via Acoustic Emission"*, Transactions of the ASME, Vol. 115, Nov. 1993, pp. 390-397.

124. E. Emel and E. Kannatey-Asibu Jr, *"Tool Failure Monitoring in Turning by Pattern Recognition Analysis of AE Signals"*, Journal of Engineering for Industry, Transactions of the ASME, Vol. 110, 1988, pp. 137-145.

125. T. Moriwaki and M. Tobito, *"A New Approach to Automatic Detection of Life of Coated Tool Based on Acoustic Emission Measurement"*, Journal of Engineering for Industry, Transactions of the ASME, Vol. 112, 1990, pp. 212-218.

126. S. Damodarasamy and S. Raman, *"An Inexpensive System for Classifying Tool Wear States using Pattern Recognition"*, Wear, Vol. 170, 1993, pp. 149-160.

127. S. M. Pandit and S. M. Wu, *"Time Series and System Analysis with Applications"*, Wiley, New York, 1983.

128. T. M. Romberg, A. G. Cassar and R. W. Harris, *"A Comparison of Traditional Fourier and Maximum Entropy Methods for Vibration Analysis"*, ASME Journal of Vibration, Acoustic, Stress, and Reliability in Design, Vol. 106, 1984, pp. 36-39.

129. T. Uematsu and N. Mohri, *"Prediction and Detection of Cutting Tool Failure by Modified Group Method of Data Handling"*, Int. J. Mach. Tools Des. Res. Vol. 26, No. 1, 1986, pp. 69-80.

130. S. Rangwala and D. Dornfeld *"Sensors Integration Using Neural Networks for Intelligent Tool Condition Monitoring"*, Journal of Engineering for Industry, Transactions of the ASME, Vol. 112, 1990, pp. 219-228.

131. D. Dornfeld and M. F. Devries, *"Neural Network Sensor Fusion for Tool Condition Monitoring"*, Annals of the CIRP, Vol. 39, No. 1, 1990, pp. 101-105.

132. H. H. (Tom) Huang and H. P. (Ben) Wang, *"Machine Fault Classification Using an ART 2 Neural Network"*, Int. J Adv Manuf. Technol., Springer-Verlag London Limited, Vol. 8, 1993, pp. 194-199

133. M. F. Devries and D. Dornfeld, *"A Step towards Intelligent Manufacturing : Modelling and Monitoring of Manufacturing Processes through Artificial Neural Network"*, Annals of the CIRP, Vol. 42, No. 1, 1993, pp. 485-488.

134. Jun Wang, *"Multiple-Objective Optimisation of Machining Operations Based on Neural Networks"*, Int. J Adv Manuf. Technol., Springer-Verlag London Limited, Vol. 8, 1993, pp. 235-243

135. P. G. Li and S. M. Wu, *"Monitoring Drilling Wear States by a Fuzzy Pattern Recognition Technique"*, Journal of Engineering for Industry, Transactions of the ASME, Vol. 110, 1988, pp. 297-300.

136. T. J. Jo and D. W. Cho, *"Fuzzy Pattern Recognition for Tool Wear Monitoring in Diamond Turning"*, Annals of the CIRP, Vol. 41, No. 1, 1992, pp. 125-129.

137. B. T. Chao and K. J. Trigger, *"Controlled Contact Cutting Tools"*, Journal of Engineering for Industry, Transactions of the ASME, Vol. 81, 1959, pp. 139-151.

138. M. J. Schmenk, *"Acoustic Emission and The Mechanics of Metal Cutting"*, Acoustic Emission Monitoring and Analysis in Manufacturing, The Winter Annual Meeting of The ASME, PED-Vol. 14, 1984, pp. 95-105.

139. Lan Ming-Shong and D. A. Dornfeld, *"Acoustic Emission and Machining-Process analysis and Control"*, Advance Manufacturing Processes, Marcel Dekker Inc., Vol. 1, No. 1, 1986, pp. 6-11.

140. K. Iwata and T. Moriwaki, *"An application of Acoustic Emission Measurement to In-Process Sensing of Tool Wear"*, Annuals of CIRP, Vol. 26, No 1, 1977, pp. 21-26.

141. E. Paul DeGramo, J. T. Black and Ronard A. Kohser, *"Meterial and Processes in Manufacturing"*, 7th Edition, 1988.

142. Sadik, Ibrahim Mushin and Bo Lindstroem, "Role of Tool-Chip Contact Length in Metal Cutting", Journal of Materials Processing Technology, Vol.137, No.1-4, 1993, pp.613 - 627.

143. G. Lankford and M. Cohen, *"Strain Hardening of Iron by Severe Plastic Deformation"*, Transactions of American Society for Materials, Vol. 62, 1969, pp. 623-638.

144. S. Ramalingham and K. J. Trigger, in Advances in Machine Tool Design and Research, Pergamon Press, 1971.

145. Y. J. Park and D. P. Saini, *"A New Model for Prediction of Acoustic Emissions in Orthogonal Cutting Operations "*, 3rd ICCM/AUTOFACT-ASIA'95, July 1995, pp. 1077-1088.

146. H. Kato and K. Yamaguchi, *"Stress Distribution at the Interface Between Tool and Chip in Machining"*, Transactions of the ASME, Vol. 94, 1972, pp. 683-689.

147. M. C. Shaw, *"New Mechanism of Plastic Flow"*, Int. J. Mech. Sci., Vol. 22, pp. 673-686.

148. Paul H. Cohen, *"Forces, Power, and Stresses in Machining"*, Metals Handbook, 9th Edition, ASM, Vol. 16, 1989, pp. 13-18.

149. G. F. Micheletti, A. Defilippi and R. Ippolito, *"Tool Wear and Cutting Forces in Steel Turning"*, Annal of CIRP, Vol 16, 1968, pp 353-360.

150. S. Kobayashi and E. G. Thomsen, *"The Role of Friction in Metal Cutting"*, Journal of Engineering for Industry, Transactions of the ASME, Vol. 103, 1960, pp. 324-332.

151. X. Li, *"Modelling the Joint of Tool-Work Interface Friction and Work Material Bulk Deformation in Metalworking Processes"*, Journal of Manufacturing Systems, Vol. 12, No. 3, 1993, pp. 229-238.

152. E. M. Kopalinsky, X. Li and P. L. B. Oxley, *"Modelling Tool-Work Interface Friction in Metal Working Processes"*, Tribological Aspects in Manufacturing, New York : American Society of Mechanical Engineers, PED-Vol. 54/TRIB-Vol. 2, 1991, pp. 217-235.

153. E. Kannatey-Asibu JR and D. A. Dornfeld, *"A Study of Tool Wear Using Statistical Analysis of Metal Cutting Acoustic Emission"*, Wear, Vol. 76, No. 2, 1982, pp 247-261.

154. M. Y. Lee, E. Thomas and D. G. Wildes,*"Review Prospects for In-Process Diagnosis of Metal Cutting by Monitoring Vibration Signals"*, Journal of Materials Science, No. 22, 1987, pp. 3821-3830.

155. T. Moriwaki, *"Application of Acoustic Emission Measurement to Sensing of Wear and Breakage of Cutting-Tool"*, Bull. Japan Soc. of Prec. Engg., Vol. 17, No. 3, Sept. 1983, pp 154-160.

156. V. Messaritis and W. K. D. Borthwic, *"Processing Acoustic Emission Signal Data for Characterising Cutting Tool Wear and Chip Management* ", Proc. 1st Int. Conf. on Computer-Aided Production Engineering, Edinburgh, 1984, pp 261-268.

157. Ichiro Inasaki, Shuhei AIDA and Shinichiro Fukuoka, *"Monitoring System for Cutting Tool Failure Using an Acoustic Emission Sensor"*, International Journal of the JSME, Vol. 30, No. 261, 1987, pp.523-528.

158. I. Inasaki and S. Yonetsu, *"In-Process Detection of Cutting Tool Damage by Acoustic Emission Measurement"*, Proc. 22nd MTDR Conference, 1981, pp. 261-268.

159. D. A. Dornfeld and C. S. Pan, *"A Study of Continuous/Discontinuous Chip Formation Using Acoustic Emission"*, J. Applied Metal Working, Vol. 4, No. 1, July 1985, pp. 18-29.

160. I. M. Minis, E. B. Magrab and I. O. Pandelidis,*"Improved Methods for the Prediction of Chatter in Turning, Part 1 : Determination of structural Response Parameters ; Part 2 : Determination of Cutting Process Parameters ; Part 3 : A Generlized Linear Theory"*, Journal of Engineering for Industry, Transactions of the ASME, Vol. 112, 1990, pp. 12-20, 21-27, 28-35.

161. A. S. Tetelman and A. G. Evans, *"Failure Prediction in Brittle Materials Using Fracture Mechanics and Acoustic Emission"*, 1976, pp. 895-925.

162. Paul A. Tipler, *"Physics for Scientists and Engineers"*, Worth Publishers Inc., 3rd Edition, 1991, pp.900 -905.

163. M. A. Hamstad, *"On Energy Measurement of Continuous Acoustic Emission"*, Laurence Livermore Laboratory Report No. UCRL-76286, 1974.

164. Brüel and Kjar, *"Measuring Vibration"*, Denmark, 1982, pp. 5

165. J. M. Gere and S. P. Timoshenko, *"Mechanics of Materials"*, Chapman & Hall, London, 1991.

166. V. C. Venkatesh and H. Chandrasekaran, *"Experimental Techniques in Metal Cutting"*, Rev. Ed., Prentice-Hall, New Delli, 1987.

167. SAS Institute Inc., *"SAS/STAT User's Guide"*, 1988 Edition, SAS Institute Inc., Cary, NC, 1988.

168. Y. Yao and X. D. Fang, *"Modelling of Multivariate Time Series For Tool Wear Estimation in Finishing -Turning"*, Int. J. Mach. Tools Manufact., Vol. 32, No. 4, 1992, pp. 495-508.

169. M. S. Lan and Y. Naerheim, *"Application of Acoustic Emission Monitoring in Machining"*, Proc North American Manufacturing Research Conference, 1985, pp. 310-313.

170. D. C. Montgomery, *"Design and Analysis of Experiments"*, John Wiley and Sons, 2th Edition, New York, 1984, pp. 387-433.

171. G. E. P. Box, W. H. Hunter and J. S. Hunter, *"Statistics for Experimenters : An Introduction to Design Data Analysis and Model Building"*, John Wiley and Sons, 10th Edition, New York, 1987, pp. 165-240.

APPENDICES

Appendix A : Basic Equations for Theoretical Values

The predicted AE_{RMS} voltages with the variation of cutting process parameters were calculated using the fundamental equations. These were taken into consideration to be general among the many equations that were available.

1. Shear plane angle (ϕ), shear force (F_s) and shear stress (τ_s) generated on the shear plane can be expressed as :

$$\phi = \tan^{-1}\frac{r\cos\alpha}{1-r\sin\alpha} \tag{A-1}$$

$$F_s = F_c\cos\phi - F_t\sin\phi \tag{A-2}$$

$$\tau_s = \frac{F_s\sin\phi}{bt} \tag{A-3}$$

2. Friction angle (ϕ) and chip contact length (l) on the tool-chip interface can be expressed as :

$$\beta = \tan^{-1}\frac{F}{N} \tag{A-4}$$

$$l = m\frac{t\sin(\phi+\beta-\alpha)}{\sin\phi\cos\beta} \tag{A-5}$$

Where, the coefficient of the chip contact length, m is equal to be 2 for carbon steel.

Appendix B : Experimental Data for Theoretical Models

Table B.1 The Design Matrix and Measurements of Experimental Stage One

(As used in Chapter 4)

No.	Cutting Process Parameters				Experimental Measurements			
	f	V	α	b	V_{RMS}	F_c	F_t	t_c
	mm/rev	m/mim	deg.	mm	V	N	N	mm
1	0.15	150	-5	2.5	2.204	622	532	0.48
2	0.15	175	-5	2.5	2.250	643	579	0.46
3	0.15	200	-5	2.5	2.294	687	626	0.45
4	0.15	225	-5	2.5	2.373	750	692	0.44
5	0.15	250	-5	2.5	2.459	733	623	0.42
6	0.15	150	0	2.5	2.200	532	415	0.46
7	0.15	175	0	2.5	2.209	631	526	0.45
8	0.15	200	0	2.5	2.251	665	555	0.43
9	0.15	225	0	2.5	2.391	699	589	0.42
10	0.15	250	0	2.5	2.405	721	618	0.41
11	0.15	150	5	2.5	2.200	539	374	0.45
12	0.15	175	5	2.5	2.273	599	492	0.43
13	0.15	200	5	2.5	2.173	639	489	0.42
14	0.15	225	5	2.5	2.322	715	525	0.41
15	0.15	250	5	2.5	2.399	704	512	0.40
16	0.20	150	-5	2.5	2.208	825	732	0.60
17	0.20	175	-5	2.5	2.251	817	761	0.58
18	0.20	200	-5	2.5	2.343	1117	734	0.56
19	0.20	225	-5	2.5	2.430	1048	847	0.55
20	0.20	250	-5	2.5	2.499	1028	828	0.53
21	0.20	150	0	2.5	2.217	778	613	0.58
22	0.20	175	0	2.5	2.188	885	706	0.56
23	0.20	200	0	2.5	2.221	945	751	0.54
24	0.20	225	0	2.5	2.410	998	734	0.53
25	0.20	250	0	2.5	2.486	1020	776	0.51
26	0.20	150	5	2.5	2.180	733	623	0.56
27	0.20	175	5	2.5	2.183	867	639	0.54
28	0.20	200	5	2.5	2.385	964	816	0.52
29	0.20	225	5	2.5	2.278	937	623	0.51
30	0.20	250	5	2.5	2.378	1025	674	0.49
31	0.25	150	-5	2.5	2.211	1056	914	0.72
32	0.25	175	-5	2.5	2.213	1123	927	0.69
33	0.25	200	-5	2.5	2.240	1198	919	0.67
34	0.25	225	-5	2.5	2.378	1279	985	0.65

35	0.25	250	-5	2.5	2.475	1285	931	0.63
36	0.25	150	0	2.5	2.135	1023	806	0.69
37	0.25	175	0	2.5	2.066	1088	848	0.67
38	0.25	200	0	2.5	2.219	1180	871	0.64
39	0.25	225	0	2.5	2.248	1202	817	0.62
40	0.25	250	0	2.5	2.447	1182	839	0.61
41	0.25	150	5	2.5	2.115	978	705	0.67
42	0.25	175	5	2.5	2.100	1001	662	0.64
43	0.25	200	5	2.5	2.102	1172	751	0.62
44	0.25	225	5	2.5	2.292	1134	681	0.60
45	0.25	250	5	2.5	2.368	1182	975	0.59
46	0.30	150	-5	2.5	2.170	1067	923	0.83
47	0.30	175	-5	2.5	2.326	1282	1033	0.80
48	0.30	200	-5	2.5	2.328	1439	1059	0.77
49	0.30	225	-5	2.5	2.413	1510	1004	0.75
50	0.30	250	-5	2.5	2.495	1336	890	0.73
51	0.30	150	0	2.5	2.116	1039	870	0.80
52	0.30	175	0	2.5	2.155	1146	955	0.77
53	0.30	200	0	2.5	2.277	1208	985	0.74
54	0.30	225	0	2.5	2.409	1407	1018	0.72
55	0.30	250	0	2.5	2.460	1487	1052	0.70
56	0.30	150	5	2.5	2.106	1001	662	0.77
57	0.30	175	5	2.5	2.106	1087	744	0.74
58	0.30	200	5	2.5	2.263	1183	715	0.72
59	0.30	225	5	2.5	2.322	1382	769	0.69
60	0.30	250	5	2.5	2.392	1281	826	0.68
61	0.35	150	-5	2.5	2.251	1531	1112	0.93
62	0.35	175	-5	2.5	2.359	1558	1045	0.90
63	0.35	200	-5	2.5	2.396	1623	1067	0.87
64	0.35	225	-5	2.5	2.330	1770	1073	0.84
65	0.35	250	-5	2.5	2.474	1838	1047	0.82
66	0.35	150	0	2.5	2.101	1458	1218	0.90
67	0.35	175	0	2.5	2.222	1496	1160	0.86
68	0.35	200	0	2.5	2.315	1612	1171	0.84
69	0.35	225	0	2.5	2.346	1670	1123	0.81
70	0.35	250	0	2.5	2.442	1755	1136	0.79
71	0.35	150	5	2.5	2.210	1409	932	0.87
72	0.35	175	5	2.5	2.223	1469	890	0.83
73	0.35	200	5	2.5	2.193	1578	862	0.81
74	0.35	225	5	2.5	2.328	1404	743	0.78
75	0.35	250	5	2.5	2.372	1633	792	0.76
76	0.40	150	-5	2.5	2.186	1703	1219	1.04
77	0.40	175	-5	2.5	2.147	1664	1027	1.00
78	0.40	200	-5	2.5	2.282	1830	1145	0.96
79	0.40	225	-5	2.5	2.423	2000	1148	0.93

80	0.40	250	-5	2.5	2.483	2063	1123	0.91
81	0.40	150	0	2.5	2.210	1458	1218	1.00
82	0.40	175	0	2.5	2.264	1776	1277	0.96
83	0.40	200	0	2.5	2.254	1820	1252	0.93
84	0.40	225	0	2.5	2.389	1879	1212	0.90
85	0.40	250	0	2.5	2.360	1946	1204	0.88
86	0.40	150	5	2.5	2.051	1543	993	0.96
87	0.40	175	5	2.5	2.148	1594	904	0.93
88	0.40	200	5	2.5	2.185	1777	943	0.89
89	0.40	225	5	2.5	2.315	1763	844	0.87
90	0.40	250	5	2.5	2.322	1831	836	0.85
91	0.45	150	-5	2.5	2.128	1627	1259	1.13
92	0.45	175	-5	2.5	2.348	1969	1352	1.09
93	0.45	200	-5	2.5	2.359	1931	1192	1.06
94	0.45	225	-5	2.5	2.443	2257	1202	1.02
95	0.45	250	-5	2.5	2.580	2377	1319	1.00
96	0.45	150	0	2.5	2.146	1554	1246	1.09
97	0.45	175	0	2.5	2.242	1893	1238	1.05
98	0.45	200	0	2.5	2.382	1834	1227	1.02
99	0.45	225	0	2.5	2.260	2000	1204	0.99
100	0.45	250	0	2.5	2.503	2157	1384	0.96
101	0.45	150	5	2.5	2.173	1585	950	1.05
102	0.45	175	5	2.5	2.212	1934	1056	1.01
103	0.45	200	5	2.5	2.274	1731	877	0.98
104	0.45	225	5	2.5	2.334	2001	915	0.95
105	0.45	250	5	2.5	2.453	1780	830	0.93

Table B.2 The Design Matrix and Measurements of Experimental Stage Two

(As used in Chapter 4)

No	Cutting Process Parameters				Experimental Measurements				
	f	V	α	b	l_{fw}	V_{RMS}	F_c	F_t	t_c
	mm/rev	m/mim	deg.	mm	mm	V	N	N	mm
1	0.15	150	- 5	2.5	0.000	2.204	622	532	0.48
2	0.15	200	- 5	2.5	0.000	2.294	687	626	0.45
3	0.15	250	- 5	2.5	0.000	2.459	733	623	0.42
4	0.30	150	- 5	2.5	0.000	2.170	1067	923	0.83
5	0.30	200	- 5	2.5	0.000	2.328	1439	1509	0.77
6	0.30	250	- 5	2.5	0.000	2.495	1336	890	0.73
7	0.45	150	- 5	2.5	0.000	2.128	1627	1259	1.13
8	0.45	200	- 5	2.5	0.000	2.359	1931	1192	1.06
9	0.45	250	- 5	2.5	0.000	2.580	2377	1319	1.00

10	0.15	150	- 5	2.5	0.289	2.454	824	553	0.48
11	0.15	200	- 5	2.5	0.289	2.495	924	623	0.45
12	0.15	250	- 5	2.5	0.289	2.681	886	579	0.42
13	0.30	150	- 5	2.5	0.289	2.345	1514	905	0.83
14	0.30	200	- 5	2.5	0.289	2.377	1584	814	0.77
15	0.30	250	- 5	2.5	0.289	2.715	1549	792	0.73
16	0.45	150	- 5	2.5	0.289	2.489	2228	1204	1.13
17	0.45	200	- 5	2.5	0.289	2.539	2131	1131	1.06
18	0.45	250	- 5	2.5	0.289	2.647	2055	1075	1.00
19	0.15	150	- 5	2.5	0.493	2.540	893	651	0.48
20	0.15	200	- 5	2.5	0.493	2.608	1148	837	0.45
21	0.15	250	- 5	2.5	0.493	2.834	1083	795	0.42
22	0.30	150	- 5	2.5	0.493	2.495	1330	957	0.83
23	0.30	200	- 5	2.5	0.493	2.707	1411	959	0.77
24	0.30	250	- 5	2.5	0.493	2.826	1439	782	0.73
25	0.45	150	- 5	2.5	0.493	2.627	2271	1340	1.13
26	0.45	200	- 5	2.5	0.493	2.688	2194	1279	1.06
27	0.45	250	- 5	2.5	0.493	2.869	1967	831	1.00
28	0.15	150	- 5	2.5	0.687	2.712	1126	776	0.48
29	0.15	200	- 5	2.5	0.687	2.895	1336	890	0.45
30	0.15	250	- 5	2.5	0.687	3.095	1247	818	0.42
31	0.30	150	- 5	2.5	0.687	2.643	1387	872	0.83
32	0.30	200	- 5	2.5	0.687	2.830	1510	904	0.77
33	0.30	250	- 5	2.5	0.687	2.973	1583	832	0.73
34	0.45	150	- 5	2.5	0.687	2.659	2306	1257	1.13
35	0.45	200	- 5	2.5	0.687	2.857	2057	1304	1.06
36	0.45	250	- 5	2.5	0.687	3.157	1963	871	1.00
37	0.15	150	5	2.5	0.000	2.200	539	374	0.45
38	0.15	200	5	2.5	0.000	2.173	639	489	0.42
39	0.15	250	5	2.5	0.000	2.399	704	512	0.40
40	0.30	150	5	2.5	0.000	2.106	1001	662	0.77
41	0.30	200	5	2.5	0.000	2.263	1183	715	0.72
42	0.30	250	5	2.5	0.000	2.392	1281	826	0.68
43	0.45	150	5	2.5	0.000	2.173	1585	950	1.05
44	0.45	200	5	2.5	0.000	2.274	1731	877	0.98
45	0.45	250	5	2.5	0.000	2.453	1780	830	0.93
46	0.15	150	5	2.5	0.289	2.387	704	599	0.45
47	0.15	200	5	2.5	0.289	2.464	823	614	0.42
48	0.15	250	5	2.5	0.289	2.641	817	577	0.40
49	0.30	150	5	2.5	0.289	2.330	1425	965	0.77
50	0.30	200	5	2.5	0.289	2.374	1503	877	0.72
51	0.30	250	5	2.5	0.289	2.596	1421	838	0.68
52	0.45	150	5	2.5	0.289	2.471	2069	1203	1.05
53	0.45	200	5	2.5	0.289	2.504	1903	1197	0.98
54	0.45	250	5	2.5	0.289	2.579	1838	1047	0.93

55	0.15	150	5	2.5	0.493	2.440	873	648	0.45
56	0.15	200	5	2.5	0.493	2.597	959	754	0.42
57	0.15	250	5	2.5	0.493	2.753	1039	870	0.40
58	0.30	150	5	2.5	0.493	2.402	1230	852	0.77
59	0.30	200	5	2.5	0.493	2.505	1365	952	0.72
60	0.30	250	5	2.5	0.493	2.795	1423	914	0.68
61	0.45	150	5	2.5	0.493	2.535	2078	1197	1.05
62	0.45	200	5	2.5	0.493	2.612	1995	1096	0.98
63	0.45	250	5	2.5	0.493	2.822	1812	790	0.93
64	0.15	150	5	2.5	0.687	2.673	1011	755	0.45
65	0.15	200	5	2.5	0.687	2.803	1285	826	0.42
66	0.15	250	5	2.5	0.687	2.941	1092	704	0.40
67	0.30	150	5	2.5	0.687	2.596	1364	933	0.77
68	0.30	200	5	2.5	0.687	2.792	1372	881	0.72
69	0.30	250	5	2.5	0.687	2.996	1486	987	0.68
70	0.45	150	5	2.5	0.687	2.728	2150	1426	1.05
71	0.45	200	5	2.5	0.687	2.847	1907	1379	0.98
72	0.45	250	5	2.5	0.687	3.011	1853	943	0.93

Appendix C : Experimental Data for Empirical Models

Table C.1 Cutting Process Parameters and Limits for Sharp Cutting Edge Tools (As used in Chapter 5)

Items		Ranges				
Input Variables	Units	Low		Middle		High
Feed rate (f)	mm/rev	0.15		0.30		0.45
Rake angle (α)	degree	-5		0		+5
Cutting speed (V)	m/min	150	175	200	225	250

Table C.2 Cutting Process Parameters and Limits for Worn Cutting Edge Tools

(As used in Chapter 5)

Items		Ranges		
Input Variables	Units	Low	Intermediate	High
Feed rate (f)	mm/rev	0.15	0.30	0.45
Cutting speed (V)	m/min	150	200	250
Flank wear land (l_{fw})	mm	0.289	0.493	0.687
Rake angle (α)	degree	-5		+5

Table C.3 Factorial Design and Measurements of Experiments for Sharp Tools

(As used in Chapter 5)

Number of trial	**Cutting Process Parameters**			**Measurements**
	Feed rate	Cutting speed	Rake angle	AE_{RMS} voltages
1	0.15	150	- 5	2.204
2	0.15	175	- 5	2.250
3	0.15	200	- 5	2.294
4	0.15	225	- 5	2.373
5	0.15	250	- 5	2.459
6	0.15	150	0	2.200
7	0.15	175	0	2.209
8	0.15	200	0	2.251
9	0.15	225	0	2.391
10	0.15	250	0	2.405
11	0.15	150	5	2.200
12	0.15	175	5	2.273
13	0.15	200	5	2.173
14	0.15	225	5	2.322
15	0.15	250	5	2.399
16	0.30	150	- 5	2.170
17	0.30	175	- 5	2.326
18	0.30	200	- 5	2.328
19	0.30	225	- 5	2.413
20	0.30	250	- 5	2.495
21	0.30	150	0	2.116

22	0.30	175	0	2.155
23	0.30	200	0	2.277
24	0.30	225	0	2.409
25	0.30	250	0	2.460
26	0.30	150	5	2.106
27	0.30	175	5	2.106
28	0.30	200	5	2.263
29	0.30	225	5	2.322
30	0.30	250	5	2.392
31	0.45	150	- 5	2.128
32	0.45	175	- 5	2.348
33	0.45	200	- 5	2.359
34	0.45	225	- 5	2.443
35	0.45	250	- 5	2.580
36	0.45	150	0	2.146
37	0.45	175	0	2.242
38	0.45	200	0	2.382
39	0.45	225	0	2.260
40	0.45	250	0	2.503
41	0.45	150	5	2.173
42	0.45	175	5	2.212
43	0.45	200	5	2.274
44	0.45	225	5	2.334
45	0.45	250	5	2.453

Table C.4 Factorial Design and Measurements of Experiments for Worn Tools

(As used in Chapter 5)

No.	**Cutting Process Parameters**				**Measurements**
	Feed rate	Cutting speed	Wear land	Rake angle	AE_{RMS} voltages
1	0.15	150	0.289	- 5	2.454
2	0.15	200	0.289	- 5	2.495
3	0.15	250	0.289	- 5	2.681
4	0.30	150	0.289	- 5	2.345
5	0.30	200	0.289	- 5	2.377
6	0.30	250	0.289	- 5	2.715
7	0.45	150	0.289	- 5	2.489
8	0.45	200	0.289	- 5	2.539
9	0.45	250	0.289	- 5	2.647
10	0.15	150	0.493	- 5	2.540
11	0.15	200	0.493	- 5	2.608

12	0.15	250	0.493	- 5	2.834
13	0.30	150	0.493	- 5	2.495
14	0.30	200	0.493	- 5	2.707
15	0.30	250	0.493	- 5	2.826
16	0.45	150	0.493	- 5	2.627
17	0.45	200	0.493	- 5	2.688
18	0.45	250	0.493	- 5	2.869
19	0.15	150	0.687	- 5	2.712
20	0.15	200	0.687	- 5	2.895
21	0.15	250	0.687	- 5	3.095
22	0.30	150	0.687	- 5	2.643
23	0.30	200	0.687	- 5	2.830
24	0.30	250	0.687	- 5	2.973
25	0.45	150	0.687	- 5	2.659
26	0.45	200	0.687	- 5	2.857
27	0.45	250	0.687	- 5	3.157
28	0.15	150	0.289	5	2.387
29	0.15	200	0.289	5	2.464
30	0.15	250	0.289	5	2.641
31	0.30	150	0.289	5	2.330
32	0.30	200	0.289	5	2.374
33	0.30	250	0.289	5	2.596
34	0.45	150	0.289	5	2.471
35	0.45	200	0.289	5	2.504
36	0.45	250	0.289	5	2.579
37	0.15	150	0.493	5	2.440
38	0.15	200	0.493	5	2.597
39	0.15	250	0.493	5	2.753
40	0.30	150	0.493	5	2.402
41	0.30	200	0.493	5	2.505
42	0.30	250	0.493	5	2.795
43	0.45	150	0.493	5	2.535
44	0.45	200	0.493	5	2.612
45	0.45	250	0.493	5	2.822
46	0.15	150	0.687	5	2.673
47	0.15	200	0.687	5	2.803
48	0.15	250	0.687	5	2.941
49	0.30	150	0.687	5	2.596
50	0.30	200	0.687	5	2.792
51	0.30	250	0.687	5	2.996
52	0.45	150	0.687	5	2.728
53	0.45	200	0.687	5	2.847
54	0.45	250	0.687	5	3.011